

To  
J. Courtney  
Best regards  
Charles

**A MONTE CARLO METHOD  
IN CONTRIBUTION RESPONSE TRANSPORT**

A dissertation

Submitted to the Graduate Faculty of the  
Louisiana State University and  
Agricultural and Mechanical College  
in partial fulfillment of the  
requirements for the degree of  
Doctor of Philosophy

in

The Interdepartmental Programs in Engineering

by  
Charles H. Aboughantous  
IEA, Institut Technique Professionnel, 1973  
M.S. in N.E. University of Cincinnati, 1979  
May 1993

DOCTORAL EXAMINATION AND DISSERTATION REPORT

Candidate: Charles H. Aboughantous

Major Field: Engineering Science

Title of Dissertation: A Monte Carlo Method in Contribution Response  
Transport

Approved:


  
Major Professor and Chairman

  
Dean of the Graduate School

EXAMINING COMMITTEE:

  
\_\_\_\_\_

  
\_\_\_\_\_

  
\_\_\_\_\_

  
\_\_\_\_\_

  
\_\_\_\_\_

  
\_\_\_\_\_

Date of Examination:

December 12, 1992

---

© Copyright 1993  
Charles H. Aboughantous  
All rights reserved

## ACKNOWLEDGMENTS

The author wishes to express his gratitudes to the many people who cooperated in various capacities to conclude this dissertation. First thanks go to Mark L. Williams. As a teacher, he introduced the author to the Monte Carlo method with rare a devotion and a remarkable dedication. He served as major advisor on this dissertation. Numerous discussions with him as well as his comments helped refining ideas investigated in this research project. Thanks are extended to John Courtney, Arthur Sterling and Jabo Tang for having reviewed the original manuscript. Their comments are most appreciated. Also thanks are extended to all the members of the committee and to those from afar, D. Ray Edwards and Nick Tsoulfanidis. Their encouragements will also be remembered.

This work was partially supported by a research grant from the U.S. Department of Energy, under the University Nuclear Engineering Research Program (Grant No. DE-FG02-89ER12899).

## TABLE OF CONTENTS

	page
<b>Acknowledgments</b> .....	iii
<b>List of tables</b> .....	vi
<b>List of figures</b> .....	vii
<b>Abstract</b> .....	xii
<b>Introduction</b> .....	1
<b>Prologue</b> .....	3
<b>CHAPTER 1 Contributon response governing equations</b> .....	12
1.1 Introduction .....	12
<i>A. SPECTRAL EQUATIONS</i> .....	13
1.2 Contributon response transport equations .....	13
1.3 Perturbation contributon response equations .....	17
1.4 Existence and uniqueness of solutions to contributon transport equation .....	23
<i>B. MULTIGROUP EQUATIONS</i> .....	25
1.5 Derivations of contributon response transport equations .....	25
<b>CHAPTER 2 The contributon Monte Carlo method</b> .....	29
2.1 Time independent integral equations for contributon response transport .....	29
2.2 The CMC method .....	31
<i>A. ANALOG CMC</i> .....	32
<i>B. NONANALOG CMC</i> .....	34
2.3 Practicle use of response $\bar{\mathfrak{N}}$ .....	37
2.4 Probability functions for CMC method .....	39
<i>A. SOURCE PDFs</i> .....	39
(a) <i>The c-pdf</i> .....	41
(b) <i>The g-pdf</i> .....	42
(c) <i>The <math>\mu</math>-pdf</i> .....	42

	(d) <i>The <math>\varphi</math>-pdf</i> .....	43
	<i>B. TRANSPORT PDF</i> .....	43
	<i>C. SCATTERING PDFs</i> .....	46
	(a) <i>The <math>g</math>-pdf</i> .....	46
	(b) <i>The <math>\mu</math>-pdf</i> .....	47
	(c) <i>The <math>\varphi</math>-pdf</i> .....	47
	2.5 The CMC method and importance biasing .....	48
<b>CHAPTER 3</b>	<b>Spherical harmonics representation of CMC probability functions</b>	<b>50</b>
	3.1 Introduction .....	50
	3.2 Positive definite pdfs .....	53
	3.3 Maxima of positive definite pdfs .....	58
	3.4 Working pdfs for the CMC method .....	60
	<i>A. SOURCE PDFs</i> .....	61
	<i>B. TRANSPORT PDF</i> .....	63
	<i>C. SCATTERING PDFs</i> .....	64
	3.5 Sampling the S and the E pdfs .....	66
<b>CHAPTER 4</b>	<b>A shielding sample problem</b> .....	<b>68</b>
	4.1 Geometry .....	68
	4.2 Adjoint and forward DOT calculations .....	71
	4.3 Monte Carlo calculations .....	72
<b>CHAPTER 5</b>	<b>Sample problem and analysis of the CMC method</b> .....	<b>73</b>
	5.1 The $\eta$ -test criterion .....	73
	5.2 Application of $\eta$ -test to the sample problem .....	74
	5.3 Analysis of source pdfs of CMC .....	76
	5.4 Analysis of the scattering pdfs .....	86
<b>CHAPTER 6</b>	<b>Results from CMC calculations and recommendations</b> .....	<b>94</b>
	6.1 Results .....	94
	6.2 Recommendations for further investigations .....	97
<b>References</b> .....		<b>101</b>
<b>Vitae</b> .....		<b>105</b>

## LIST OF TABLES

- TABLE 5.1 Multigroup discrete pdf  $E(g)$  for the selection of the emergent energy group at cell (60,100), in % units. Empty spaces to the right in the table are magnitudes of  $E(g)$  less than 1% ..... 86
- TABLE 6.1 Comparison of detector response calculated with nonanalog CMC and with DOT code for **steel** perturbation of variable thickness  $H$ . The ratio of Monte Carlo to DOT calculations is also shown. The fractional standard deviations and the CPU time are for Monte Carlo calculations only. Scoring surface is  $h=10$  cm above the perturbation. 95
- TABLE 6.2 Comparison of detector response calculated with nonanalog and with analog CMC and with DOT code for **water** perturbation of variable thickness  $H$ . The ratio of Monte Carlo to DOT calculations is also shown. The fractional standard deviations and the CPU time are for Monte Carlo calculations only. Scoring surface is at  $h=10$  cm above the perturbation ..... 95
- TABLE 6.3 Numerical verification of Williams-Engle's theorem where the scoring surface (enclosure) is paced  $h$  centimeters from the top of the perturbation. The detector response is calculated with analog CMC for 20 cm water perturbation ..... 96

## LIST OF FIGURES

FIGURE 1.1	An illustration of a system of a medium with free surface boundary hosting a neutron source and a detector. The closed surface $\sigma$ (dotted line) is an enclosure . . . . .	14
FIGURE 1.2	A neutron source-detector arrangement in a medium as a shield with free surface boundary and a perturbation of material different than medium. The domain is everything inside the free surface boundary. $\sigma$ is a Williams-Engle's enclosure . . . . .	19
FIGURE 2.1	Coordinates of neutron trajectory in convex medium where $\sigma$ is the free surface boundary, $\hat{\Omega}$ is the direction of travel of neutron, $\mathbf{r}$ is the current position of neutron and $\mathbf{r}'$ the position where the neutron comes from. A dummy variable $R$ takes on the value 0 at $\mathbf{r}$ , the value $R_{\sigma}^-$ at $\mathbf{r}_{\sigma}$ in direction $-\hat{\Omega}$ and $R_{\sigma}^+$ in direction $\hat{\Omega}$ . . . . .	30
FIGURE 2.2	A segment of the random walk showing one generation of nonregenerative collisions. An $\mathfrak{R}$ value represents the response at the end of one generation of collisions and a $\varpi$ is the regenerated response value of a response particle of the next generation of collisions. The tip of an arrow is a collision site of a response particle within the perturbation region . . . . .	36
FIGURE 2.3	An illustration of a contribution response emission from a source cell $\delta V$ centered at $\mathbf{r}$ within the volume $V$ of the source of emission density $\tilde{S} \mathbf{r} u$ in the approximate geometry. $\hat{\Omega}$ is the direction and $E$ is the energy of the emitted response . . . . .	40
FIGURE 2.4	Segmentation of the trajectory of a response particle near the saturation cell in the R-Z plane. Point P is the new collision site where the optical track length $\beta$ saturates by the sum of all segments $\Delta S$ mfp equivalent . . . . .	45



FIGURE 3.1	Angular representation of polar and azimuthal angles in a local cartesian coordinates system with origin coinciding with the pole at 0. The new polar axis is z-axis .....	52
FIGURE 3.2	An illustration of converting a properly normalized pdf $f(x)$ which takes negative values on some interval $\delta = [a, b]$ to a positive definite pdf $F(x)$ always positive on its domain by multiplying the mother pdf by a scaling factor $\gamma$ .....	55
FIGURE 3.3	Numerical evaluation of the maximum of a pdf by the method of segmentation. The interval of definition of the random variable $x$ is divided into equal intervals $\Delta x$ . The maximum value of a pdf shown as a thick continuous curve is at point $c$ in this case .....	59
FIGURE 3.4	A flow chart for the sampling of the S and the E pdfs represented by $X(x)$ where $x$ is a dummy variable which espouses the identity of any of the random variables of S and E .....	66
FIGURE 4.1	Cross sectional view in the R-Z plane of the cylindrical shield showing the relative positions of source, detector, perturbation and scoring surface (the enclosure $\sigma$ ). The thickness $H$ of the perturbation and the distance $h$ from the top of perturbation to scoring surface are variable .....	69
FIGURE 4.2	Discretization of the R-Z plane of the cylinder shield as used in DOT calculations. Each rectangle represents a cross section of an axisymmetric ring which is a cell in DOT geometry and in Monte Carlo geometry. Field properties and contribution response cross sections are uniform in each cell .....	70
FIGURE 5.1	A surface plot for the emission ratio of vacuum perturbation in concrete shield and a neutron source, for scattering from group 1 to group 2 at cell index (40,53). Angular cosine $\mu$ and azimuthal angle $\varphi$ (in radians) are incident parameters .....	75

FIGURE 5.2	A surface plot for the emission ratio of steel perturbation in concrete shield and a neutron source, for scattering in group 1 at cell index (40,53). Angular cosine $\mu$ and azimuthal angle $\varphi$ (in radians) are incident parameters . . . . .	77
FIGURE 5.3	A surface plot for the emission ratio of steel perturbation in concrete shield and a neutron source, for scattering from group 7 to group 8 at cell index (40,53). Angular cosine and azimuthal angle $\varphi$ (in radians) are incident parameters . . . . .	78
FIGURE 5.4	A surface plot for the emission ratio of water perturbation in concrete shield and a neutron source, for scattering in group 1 at cell index cell index (40,53). Angular cosine and azimuthal angle $\varphi$ (in radians) are incident parameters . . . . .	79
FIGURE 5.5	A surface plot for the emission ratio of water perturbation in concrete shield and a neutron source, for scattering from group 1 to group 2 at cell index (40,53). Angular cosine and azimuthal angle $\varphi$ (in radians) are incident parameters . . . . .	80
FIGURE 5.6	Graphs for contributon response pdf (thick line) for the selection of emission cell, due to a plane isotropic neutron source and a ring detector of sample problem. The neutron source pdf is shown in thin line. The source is at the bottom of the concrete cylinder with inner radius of 10 cm and outer radius of 76 cm . . . . .	82
FIGURE 5.7	Graphs for contributon response pdf (thick line) for the selection of the angular cosine $\mu$ , of an emitted response particle from source radial cell 41 and for groups 1 and 2. The isotropic pdf for selection source neutron is shown at 0.5 (thin line). The neutron source and the ring detector are those of the sample problem in concrete shield . .	84

FIGURE 5.8 Polar graph for response particles pdfs (solid lines curves) for the selection of the azimuthal angle  $\varphi$  of an emitted response particle from response source radial cell 41 and for group 1. Curves a, b, c correspond to emergent directional cosines  $\mu=0.1, 0.5, 0.9$  respectively. Dotted line circle (curve d) is the isotropic pdf for neutron emission ..... 85

FIGURE 5.9 Graphs for response particles scattering pdfs in concrete shield, for the selection of emergent directional cosine  $\mu$ , from group 1 to group 1 scattering, at cell index (40,53) and for incident azimuthal angle  $\varphi'=\pi/4$  and incident directional cosines  $\mu'=0.9, 0.5, 0.1$  corresponding to curves a, b, and c respectively. Neutron source and ring detector are those of sample problem ..... 88

FIGURE 5.10 Polar graphs for the response particle scattering pdfs in concrete shield for the selection of emergent azimuthal angles  $\varphi$ , from group 1 to group 1 scattering, at cell index (40,53), for incident directional cosine  $\mu'=0.5$  and incident azimuthal angles  $\varphi'=\pi, \pi/2$  and 0 radian corresponding to curves a, b, and c respectively. Neutron source and detector are those of sample problem ..... 89

FIGURE 5.11 Graphs for response particles scattering pdfs in concrete shield, for the selection of emergent directional cosines  $\mu$ , for scattering from group 7 to group 9, at cell index (40,53), for incident azimuthal angle  $\varphi'=\pi/4$  and for incident directional cosines  $\mu'=0.9, 0.5, 0.1$  corresponding to curves a, b and c respectively. Neutron source and detector are those of sample problem ..... 90

FIGURE 5.12 Graphs for response particles scattering pdfs in concrete shield, for the selection of emergent directional cosines  $\mu$ , for scattering in group 6, at cell index (78,100), for incident azimuthal angle  $\varphi'=\pi$  and for two sets of incident directional cosines:  $\mu'<0$  (dotted lines) and  $\mu'>0$  (solid lines) of values  $|\mu'|=0.9, 0.5, 0.1$  corresponding to curves a, b and c respectively ..... 91

FIGURE 5.13 Graphs for response particles scattering pdfs in concrete shield, for the selection of emergent directional cosines  $\mu$ , for scattering in group 10, at cell index (40,148), for incident azimuthal direction  $\varphi'=\pi$  and for two sets of incident directional cosines:  $\mu'<0$  (dotted lines) and  $\mu'>0$  (solid lines) of values  $|\mu'|=0.9, 0.5, 0.1$  corresponding to curves a, b and c respectively . . . . . 93

## ABSTRACT

A contribution response Monte Carlo method is developed and successfully applied to a sample deep penetration shielding problem. The random walk is simulated in most of its parts like in conventional M.C. by introducing the concept of a fictitious response particle. The scoring is peculiar to the proposed method and it need not be made at the detector itself so that computing time can be reduced by an order of magnitude or more depending on the geometry of the problem. The probability density functions are natural. They possess properties not encountered in conventional M.C. methods currently in use. The selection of all random variables from any pdf depends on all defining parameters of the system, namely, the geometry of the problem, relative position of source-detector, volume of detector, nature and magnitude of the detector response function and the material of the shield. The source and the scattering pdfs are continuous functions of the directional cosine and the azimuthal angle random variables. The selection of the parameters of the emergent particle from the scattering pdf is affected by the past history of the particle. The transport pdf is an unusual exponential kernel strongly dependent on the path followed by the particle between collisions. One thousand particles are sufficient to reproduce the same answer obtained using DOT discrete ordinates two dimensional code with a very small fractional standard deviation and with less than five minutes CPU time on a 3090 IBM main frame system. Analog and nonabsorption biasing Monte Carlo were considered.

## INTRODUCTION

The Monte Carlo method has proven to be a powerful tool in many engineering problems where the deterministic methods are not up to simulate the physical process of interest in real three dimensional geometry. Among these problems is the deep penetration shielding problem in particle transport, a problem of prime relevancy to the final objective of this research project. The efficiency of the method has been improved by biasing the random walk of the particles in favor of a more favorable transport to the terminus station, i.e., the particle detector for our purpose. In this respect, numerous types of biasing have been proposed and tested under realistic environments. Some limited success has been recorded, but not enough to assert a general biasing technique which will prevail in all conceivable shielding problems. Continuous efforts are devoted to develop a theoretical model for the particle transport, with the expectations that it is likely to succeed where its predecessors have demonstrated various degrees of inadequacy. Upon manipulating the neutron transport equation and its adjoint equation in a similar way to the derivation of the reciprocity relation in neutron transport, Williams has recently obtained a governing deterministic equation for a *contributon response field* and suggested in his theoretical development an application of the Monte Carlo method<sup>1</sup>.

Williams' contributon field is a mapping of a neutron (or any neutral particle) field (a  $\psi$ -field) characterized by the neutron flux  $\psi$  onto the new *contributon response field* (a C-field) defined by  $C = \psi\psi^*$ , where C is a contributon response flux and  $\psi^*$  is an adjoint function often called adjoint flux. In reactor theory applications, it is also given the meaning of an importance function. The resulting contributon response governing equation to be solved by Monte Carlo possesses its own expressions for the contributon *response source*, the *response scattering* and the *response transport* probability density functions (pdfs). The formal expressions for the first two pdfs appear very similar to

those obtained in particle transport for an importance biased Monte Carlo where the adjoint function is elected to be the importance function. This apparent similarity is merely semiotic, for the pdfs in Williams' work pertain to C-field, whereas all the pdfs obtained with importance biasing techniques are conceptually  $\psi$ -field operations. In a C-field, contributions are not lost from the system. They terminate only at the detector, whether the detector is within the medium or at its boundary. All source particles sampled by Monte Carlo contribute to the response of interest, thus improving the efficiency of the Monte Carlo calculations.

The suggested Monte Carlo method<sup>1</sup> simulates contribution response as a neutral particle which behaves in a C-field much like a neutron does in a  $\psi$ -field. The object of the present work is to construct and to test a contribution response Monte Carlo based on a perturbation form of the contribution transport equation proposed by Williams<sup>1</sup>.

## PROLOGUE

Monte Carlo methods can be grouped in two types: Analog and nonanalog. The analog method is simple and reliable when it can produce an answer and, when it does, it is the least efficient method in general. On the other hand, in most realistic engineering problems it is simply impractical. By contrast, the nonanalog Monte Carlo may be far more efficient than the analog one especially when used in conjunction with *importance* biasing. It can be applied to a broad range of realistic engineering problems, but in many cases the reliability of the answers is not very assuring. In some specialized problems, such as deep penetration in shielding design, the method may not produce reliably accurate answers. The new *Contributon Monte Carlo* method developed in this thesis benefits from the simplicity of analog Monte Carlo and can be extended to nonabsorption biasing of nonanalog Monte Carlo. From results obtained with a sample problem, the method appears to produce reliable answers in some cases where importance biased methods fail and with quite great an efficiency.

The importance biasing was introduced initially as a way of optimizing the sampling probability density function (pdf). In an early work by Kahn<sup>2</sup> (1954), the importance sampling is described as a concept derived (at some earlier time) from the theoretical zero-variance estimates and its corresponding generalization to integral equations. He discusses a general formalism to obtain the optimum sampling pdf from what he called the *measure* of the importance of a point in the domain of the given pdf. The pdf thus obtained is in fact a biased pdf which minimizes the scoring variance without necessarily reducing it to zero. The underlying idea presented in Kahn's work found its way to neutron transport applications where it espouses a variety of forms that suit the structure of the Monte Carlo models devised by various investigators.



Coveyou et al.<sup>3</sup> followed the formalism previously described by Kahn and defined an importance function as the measure of an event in a neutron field at a phase space coordinate. After pointing out that this class of functions is not that of importance functions of reactor theory, the authors selected what they termed the *value function* to form the basis for optimizing the importance function. That value function turned out to be the optimal pdf previously defined in Kahn's work. The value function here is the solution of an adjoint form of the transport equation with the detector response function as an inhomogeneous source term. The selection of the value function by Coveyou et al. for the purpose just indicated was based on what the authors perceived as *reasonable*. Following this choice, a formal expression for the optimal importance function was obtained by minimizing the variance of the effect of interest using variational techniques. Unfortunately, the importance function thus obtained appears to be of little direct value, using the authors' own assessment, because it is overly complex for practical use. The result of these efforts provided enough reasons for the authors to *suspect* that the importance function in fact *might* be a good choice if elected to be a function proportional to the value function. Unfortunately, they were unable to determine how far their choice is away from the optimal one. They recognized that this importance function requires a priori knowledge of the value function which, if known, solves the original problem without further labor. They suggested rather a judicial choice, understandably within the criteria set forth by Kahn. They credited Kahn in this endeavor and Goertzel and Kalos<sup>4</sup> for being most responsible for the implementation of the adjoint formulation in Monte Carlo biasing.

Burgart and Stevens<sup>5</sup> (1970) followed the path of their predecessors in the selection of the importance function. They used it to bias the transport kernel and the collision kernel. This approach utilizes an adjoint solution to a one dimensional discrete ordinate problem from which they derived two importance functions, one to bias the

transport kernel and another one to bias the collision kernel. These importance functions are dependent on the direction of the incident particle and the direction of the emergent particle. It was recognized by Burgart and Stevens that other investigators<sup>6-8</sup> had also used the adjoint function for an importance function in Monte Carlo biasing. More recent publications<sup>9,10</sup> also use this general type of biasing. The use, generation, and implementation of the adjoint function in the biasing process vary with the needs and the modeling pursued by the individual group of investigators.

In the case of Burgart and Stevens the adjoint function was obtained from a one dimensional multigroup discrete ordinate code, (thus independent of the azimuthal scattering angle,) and then was manipulated to suit the desired application. A grid of 30 fixed directions was defined in the laboratory system and particles were allowed to travel in these discrete directions only. A best exponential fit was obtained from the discrete ordinates adjoint functions over a number of mean free paths, for each energy group and for each of the fixed directions on the grid. That exponential fit was taken for the importance function to bias the transport kernel; the latter is dependent on energy (of the incoming particle) and on position by material zone. The product of the two exponentials synthesizes the biased transport kernel. The adjoint function was manipulated differently for the biasing of the collision kernel. It was averaged over spatial regions, and the results thus obtained were used for importance biasing functions. The energy of the outgoing particle at the collision site was calculated by an expression derived from the kinematics of collision. It was used to obtain the importance function for collision kernel biasing. The authors provide no specific prescription for the source biasing. They used monoenergetic sources: a point, isotropic source for one set of applications and a parallel beam as a boundary source for another set. In the former case the grid of fixed directions was used to select the direction of the source particle.

Tang et al.<sup>9</sup> devised a Monte Carlo importance biasing model with several distinct importance functions, one for each of the scattering and transport kernels and two for the source biasing. The first function is a two dimensional adjoint function known as the *point value*, obtained using the DOT<sup>11</sup> discrete ordinates code. The second importance function, the *event value*, was constructed from the point value function. These two value functions were volume averaged over finite regions of the neutron field, for all energy groups and for all directions, before they were used to construct the desired pdfs. Tang et al. proposed that the point value seems to be the appropriate importance function for the scattering kernel and the event value the appropriate function to bias the transport kernel. The importance biased pdfs obtained in this manner were used to sample for the direction of the emergent particle from a collision and the distance it will travel to the next collision. The energy group of the emergent particle was obtained by sampling the marginal pdf obtained from the scattering kernel before biasing. In this approach the energy group selection is independent of any direction. The sampling for the outgoing direction is made from a well defined discrete pdf defined over a finite number of polar angles of the scattered particle. The pdf for the azimuthal angle is assumed isotropic. All possible outgoing directions must be known so that the corresponding point value functions can be identified. This discrete sampling requires the selection of the azimuthal angles for each of the available set of discrete directions before proceeding to select the cosine of the polar angle.

Tang et al.'s approach to bias the scattering and the transport kernels could be extended very easily to a large class of problems. The source biasing however, is particular to the geometry and the material composition of the specific problem the authors analyzed. This was a concrete cylinder with an axial shaft and a monoenergetic isotropic planar source at the bottom of the cylinder. They considered two importance functions. The first one favors the emission of source particles in a way to encourage

more particles to stream through the shaft by selecting some arbitrary step function for biasing. The second importance function was obtained from a DOT R-Z adjoint problem with a linear uniform isotropic source at the axis of the cylinder, for energy group 1. The discrete numerical adjoint function in R was used to obtain a set of best fit functions. They were used as importance functions to bias the radial location of the emitted particle. The azimuthal angle pdf was isotropic in the two cases.

In a relatively recent investigation on discrete angle biasing, Cramer<sup>12</sup> extracted from TRIPOLI<sup>13</sup> code the essence of importance biasing without the recourse to running discrete ordinates multigroup codes to obtain adjoint functions. He obtained an analytic expression for the importance function, a parametric homographic function in the cosine of the polar angle of the emergent direction relative to the most important direction from the collision site. The parameter is a user's choice and may possibly be problem dependent. Cramer recognized the origin of this function in earlier works by Goertzel and Kalos<sup>4,14</sup>. This importance function is energy independent and was implemented in the biasing of (a) the transport pdf, (b) the marginal pdf for the discrete directions implemented in MORSE<sup>15</sup> code, and (c) the pdf for the azimuthal angle. The source is also biased for the direction of the emitted particle with the same importance function employed in the collision angular biasing. Energy biasing was not an objective in Cramer's investigation.

An instructive conclusion that can be drawn from the previous investigations, and from many others not cited here, is that the selection of the importance function and the way it is implemented in the biasing process is still an unresolved problem. It is possible to concede that an optimum choice of an importance function is eventually a zero variance choice, leaving aside for the moment the computing economy. Then we must address the question, how should we select an approximation of that ideal function, by intuition or by auxiliary calculations? Having settled on a choice, will that function be

equally good for all the kernels involved in the Monte Carlo calculations? Shall its implementation in the biasing of one kernel be same as in the biasing of the other kernel? And finally, what calculation burdens are inflicted on sampling the transport and collision kernels, and the source as well. There is little in the reported investigations which suggests that these questions have been addressed consistently, at least in the context of adjoint functions. Most investigators in importance biasing share the opinion that a properly selected *exact* adjoint function is a zero variance importance function, but this consensus is constrained to Kahn's criteria. (An anomalous case was reported by Carter and McCormick<sup>16</sup> where they stated that the neutron scalar flux  $\Phi(\mathbf{r})$  is a zero-variance. Hoogenboom<sup>17</sup> has shown that this assertion is unlikely.)

In the midst of continuous efforts to find the most efficient importance function, Williams and Engle presented their deterministic *Spatial Channel Theory* early in 1976. It is directed primarily toward evaluating the response of source particles deep in a shield or on its boundary. They recognized, for the first time, the existence of a peculiar source particle which espouses the identity of a *response* instantly as it is created by the source, a response that propagates in the system through preferred *channels* ending at the detector. Because of this deterministic behavior of the particle, it was given the name *contributon*<sup>18</sup>, a particle which contributes to the detector all the response it acquires at the source. The *disappearance* of a contributon as a particle in the medium should be perceived as a mathematical transformation of the physical corpuscle to a response quantity in the entire domain. The C-field is the functional interpreter of a corpuscle (contributon) to a response. This concept is the basis of Williams and Engle's contributon *response flux* and *response current*<sup>18</sup>. The latter lead to the fundamental theorem of contributon response theory which plays an important role in the reduction of CPU time of the Monte Carlo method object of this dissertation.

The concept of contribution immediately attracted the attention of Monte Carlo developers. By the turn of 1977, Dubi et al.<sup>19</sup> presented the first attempt to model Williams and Engle's contribution response transport in a Monte Carlo play. Their attempt has merits with respect to the difficult task of constructing a Monte Carlo method, but it hardly can be credited a success as a contribution Monte Carlo method. First, on the computing speed of the method, the authors reported a reduction in computing time by nearly half what it took an analog Monte Carlo to solve the same problem, presumably on the same computing system. They did not report how much was the actual computing time

Dubi et al. presented an experimental validation of their method using a homogeneous medium with a point source and provided data of fluence estimates from a contribution Monte Carlo and from a conventional analog Monte Carlo. The estimate with a half million contributions is no better than the estimate with eighty thousand conventional particles, in a statistical sense. Thus their conclusion that the method is superior to conventional analog Monte Carlo is not justified. The authors used Williams-Engle's theorem as a fluence estimator in a homogeneous medium. In this medium, the fundamental theorem of contribution theory predicts an exact answer with only one source contribution. Sampling one and a half million contributions to obtain an estimate with a fractional standard deviation of 47% is unwarranted labor. Williams and Engle defined a contribution as a source particle and everywhere in the medium they used *contribution flux* invariably for *response flux*, and same for current. It is apparent from Dubi et al.'s article that the authors did not properly implement this concept of contribution response in their Monte Carlo method. They stated expressly that contributions contribute with certainty to the response of the detector and sampled the contribution as a particle, a physical corpuscle, everywhere in the medium. Yet they

allowed a contributon to deplete in response as it progresses in the medium without counting the depleted response toward detector response, contrary to the very definition of a contributon. They also allowed contributons to emit secondary particles which are free to escape out of the medium at random.

The foregoing reveals that Dubi et al.'s model by no means can be characterized as a *contributon* Monte Carlo method. Despite the claim by the authors that they used analog Monte Carlo, judging by substance of the article, their model is likely some sort of biasing technique. The apparent inability of the method to compete efficiently with conventional importance biasing suggests that its linkage to importance biasing is unlikely. The importance biasing methods cited earlier, (ref. 5, 9, 10, 12, 13) produced much more efficient results.

In a recent work, M.L. Williams presented his *Generalized Contributon Response Theory* and derived for the first time a *perturbation* contributon response governing equation which appears to be pertinently suited for Monte Carlo applications. The *Contributon Monte Carlo* (CMC) method of this dissertation extracts its probability density functions (pdf) from Williams' equation. The contributon response is modeled as a response *corpuscle* which behaves in a C-field much like a neutron does in a  $\psi$ -field, except that a response particle does not leak out of the medium. Scattering and absorption cross sections are defined to suite this purpose. The contributon response absorption cross section has an unusual character. It takes positive or negative values depending on a number of parameters. When positive, it is an absorption coefficient in the common definition of absorption; when negative, it is interpreted as a *multiplication coefficient*<sup>1</sup>. The object of this dissertation is to develop a CMC method which can utilize Williams' concept of response production. Analog and nonanalog Monte Carlo with nonabsorption biasing are considered. A numerical model is developed to meet the expectations of the theory and is encoded as a computer program in cylindrical geometry.

Validity and efficiency of the model are demonstrated by comparing the estimates obtained for a two-dimensional model with calculated responses using DOT computer code in axisymmetric geometry.

*Primum Vivere. . .*

*Deinde Philosophari.*

---

---



## CHAPTER ONE

### CONTRIBUTON RESPONSE GOVERNING EQUATIONS

#### 1.1 Introduction

A comprehensive contributon response theory was recently developed by Williams<sup>1</sup>. Its underlying hypothesis is the existence of a source particle which, unlike other source particles, is included in the exclusive set of particles that contribute to the response of the detector in integral sense. This is true whether the detector is within the medium or at its boundary. The particle was given the name *contributon*<sup>18</sup>. As it will be shown shortly, a mathematical transformation will mask the corpuscular nature of a contributon and translates it to a *contributon response* everywhere in the system, including the source itself. Its field prescription is a *contributon response field* which will be designated thereafter by C-field.

There is a fundamental distinction between a contributon and a contributon response<sup>1</sup>. A contributon is a fully pledged particle which preserves its corpuscular identity and it is recognized as such everywhere in the system: in the source, in the medium and at the detector. It is simply a response carrier destined to reach the detector where it encounters the one-time fatal interaction in the system and terminates there. A contributon response is *the measure of the effect of the contributon on the detector*. The contributon response needs not necessarily be a result of an actual interaction with the detector. It is simply a flow field in a contributon response continuum. The physical interpretation of this mathematical model of a C-field was first presented by Williams and Engle. Abu-Shumays et al.<sup>21</sup> introduced later a contributon stream line in a two

dimensional C-field, and recently Williams discussed some aspect of contribution *response potential flow*. He indicated that in nonsource/nonsink regions in realistic shield configurations this flow is rotational<sup>1</sup>. This response flow interpretation is implied by the striking similarity between the contribution response current in a C-field and the governing continuity equations of a flow field in mathematical physics. The flow in a C-field is from the source to the detector, a sink, which plays the role of a *meter* in Lewins' sense<sup>20</sup>.

## A. SPECTRAL EQUATIONS

### 1.2 Contribution response transport equations

A contribution response field, or a C-field, can be obtained from the neutron transport equation, also known as the forward equation:

$$\nabla \cdot \hat{\Omega} \psi(\mathbf{r}, \tau) + \Sigma_t(\mathbf{r}, E) \psi(\mathbf{r}, \tau) = \int_{\tau'} \Sigma(\mathbf{r}, \tau' \rightarrow \tau) \psi(\mathbf{r}, \tau') d\tau' + Q(\mathbf{r}, \tau) \quad (1.1)$$

defined over a convex spatial domain and subject to the vacuum boundary condition  $\psi=0$  for all inward directions, and its adjoint equation:

$$-\nabla \cdot \hat{\Omega} \psi^*(\mathbf{r}, \tau) + \Sigma_t(\mathbf{r}, E) \psi^*(\mathbf{r}, \tau) = \int_{\tau'} \Sigma(\mathbf{r}, \tau \rightarrow \tau') \psi^*(\mathbf{r}, \tau') d\tau' + Q^*(\mathbf{r}, \tau) \quad (1.2)$$

defined over the same convex domain of Eq(1.1) and subject to the vacuum boundary condition  $\psi^*=0$  for all outward directions. The function  $\psi$  is the directional neutron flux due to a neutron source  $Q$  and  $\psi^*$  is the expected response contribution function per particle due to a detector defined by its response function  $Q^*$ . The domain of definition of  $\psi$  and  $\psi^*$  has a total and a scattering cross sections  $\Sigma_t$  and  $\Sigma_s$ , respectively as illustrated

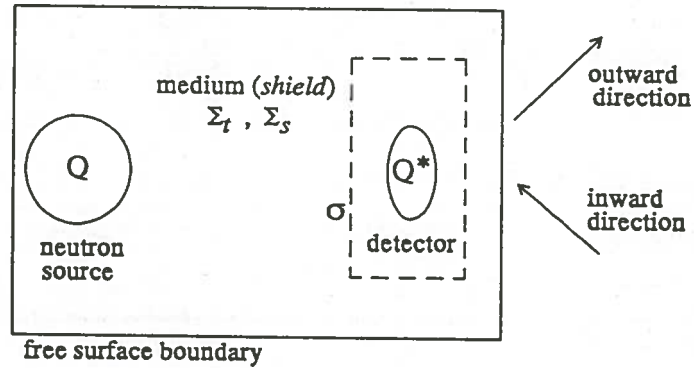


**Figure 1.1.** An illustration of a system of a medium with free surface boundary hosting a neutron source and a detector. The closed surface  $\sigma$  (dotted line) is an enclosure.

in Figure 1.1. The function  $\psi^*$  is often called adjoint flux, or adjoint function, interpreted as an importance function in neutron field applications<sup>20,22,23</sup>. Bell and Glasstone<sup>22</sup> indicated that  $\psi^*$  can also be interpreted as the expected value of a quantity of interest such as count rate, electric charge, . . .etc. depending on the nature of  $Q^*$ . Their remark, however, did not go beyond the extent of a footnote. The other terms in equations (1.1) and (1.2) are defined as follow:

$\Sigma_t(\mathbf{r}, E)$  = neutron total cross section

$\Sigma(\mathbf{r}, \tau' \rightarrow \tau)$  = neutron double differential scatter cross section

$(\mathbf{r}, \tau)$  = a phase space of six degrees of freedom

$\mathbf{r}$  = a position vector defining a three dimensional geometric space

$\tau \equiv (E, \hat{\Omega})$  = an energy-direction space of three degrees of freedom:  $E$  for the particle energy and  $\hat{\Omega}$  for the particle direction of motion defined by a polar angle  $\theta$  and an azimuthal angle  $\varphi$

In the above equations and in all equations to follow, the unprimed variables will refer to postcollision, or emergent values, and the primed variables will refer to precollision, or

incident values; an exception is the double differential scatter where the arrow points always to the emergent variable. Inclusion of all variables in every function will produce unduly cumbersome expressions; therefore they will be omitted for notational convenience whenever their omission produces no confusion; the functions of primed variables will be primed instead, e.g.,  $\psi(\mathbf{r}, \tau')$  will be presented simply by  $\psi'$ .

An additional simplification to writing the transport equation and its adjoint is the use of operator notation. Define the operator  $\mathbf{B}$  and its adjoint  $\mathbf{B}^*$  by:

$$\mathbf{B}(\bullet) = \Sigma_t(\bullet) - \int_{\tau'} \Sigma(\tau' \rightarrow \tau)(\bullet)' d\tau' \quad (1.3)$$

$$\mathbf{B}^*(\bullet)^* = \Sigma_t(\bullet)^* - \int_{\tau'} \Sigma(\tau \rightarrow \tau')(\bullet)^*' d\tau' \quad (1.4)$$

Then the forward equation (1.1) and the adjoint equation (1.2) take the forms:

$$\nabla \cdot \hat{\Omega} \psi + \mathbf{B} \psi = Q \quad (1.5)$$

$$-\nabla \cdot \hat{\Omega} \psi^* + \mathbf{B}^* \psi^* = Q^* \quad (1.6)$$

Multiply the forward equation by  $\psi^*$  and the adjoint equation by  $\psi$  and subtract the second resulting equation from the first one and rearrange. Case<sup>24</sup> obtained the equation:

$$\nabla \cdot \hat{\Omega} \psi \psi^* + \psi^* \mathbf{B} \psi - \psi \mathbf{B}^* \psi^* = \psi^* Q - \psi Q^* \quad (1.7)$$

from which he proved the optical reciprocity theorem in neutron transport in the one velocity approximation. Williams and Engle defined the contribution *response flux*:

$$C \equiv C(\mathbf{r}, \tau) = \psi(\mathbf{r}, \tau) \psi^*(\mathbf{r}, \tau) \quad (1.8)$$

which has the unit of response rate per unit area, per unit energy and per steradian, and manipulated Case's equation (1.7) to obtain the spectral contribution response transport equation:

$$\nabla \cdot \hat{\Omega} C + \theta_s C = \int_{\tau'} \theta(\tau' \rightarrow \tau) C' d\tau' + \Gamma \quad (1.9)$$

where:

$$\theta_s = \int_{\tau'} \theta(\tau \rightarrow \tau') d\tau' \quad (1.10)$$

$$\theta(\tau \rightarrow \tau') = \Sigma(\tau \rightarrow \tau') \frac{\psi^{*'}}{\psi^*} \quad (1.11)$$

$$S = \psi^* Q \quad (1.12)$$

$$\mathfrak{R} = \psi Q^* \quad (1.13)$$

$$\Gamma = S - \mathfrak{R} \quad (1.14)$$

where  $S$  is the *contributon response source* and  $\mathfrak{R}$  is the *detector response function* in the  $C$ -field, not to be confused with the detector response function  $Q^*$  in  $\psi$ -field. The designators  $\mathfrak{R}$  or  $Q^*$  will always be used to avoid any confusion between response functions. The  $\theta$  coefficients defined by Eq(1.10) and by Eq(1.11) were recognized as *contributon response scattering cross section* and *contributon response double differential scattering cross section* respectively<sup>1</sup>.

The ultimate goal of solving Eq(1.9) is to obtain the value of the response at the detector due to the source strength  $Q$ . In general, the response source density rate  $S$  is not equal to the detector density rate  $\mathfrak{R}$ . However, the integrals over their respective volumes are equal<sup>18,22</sup>:

$$\bar{\mathfrak{R}} = \iiint_{\mathbf{r}\tau} S d\mathbf{r} d\tau = \iiint_{\mathbf{r}\tau} \mathfrak{R} d\mathbf{r} d\tau \quad (1.15)$$

where  $\bar{\mathfrak{R}}$  is the response of the detector due to the source  $Q$ . The simplicity of this expression is quite misleading. It infers that the answer to the problem can be obtained without the need of performing Monte Carlo calculations. This is true if a complete

description of the flux  $\psi$  or the adjoint function  $\psi^*$  are known. In realistic engineering problems neither of these descriptions is often known in general three dimensional geometry. Fortunately, there is another expression to calculate the response  $\bar{\mathfrak{R}}$  particularly useful for Monte Carlo calculations. It enables the calculation of the response  $\bar{\mathfrak{R}}$  from the integral<sup>18</sup>:

$$\bar{\mathfrak{R}} = - \int_{\sigma} d\sigma \int_{\tau} \mathbf{n} \cdot \hat{\Omega} C d\tau \quad (1.16)$$

which expresses the Williams-Engle theorem:

*if an arbitrary closed surface  $\sigma$  contains exclusively the detector in a contribution response field, then the response of the detector is equal to the integral contribution response flow rate crossing the enclosure in the inward direction.*

In Expression (1.16), the vector  $\mathbf{n}$  is the outward normal to the enclosure  $\sigma$ , and  $\hat{\Omega}$  is the direction of propagation of contribution response crossing  $\sigma$ . A remarkable property of this theorem is that  $\sigma$  is any arbitrary surface. It can be of any shape anywhere in the medium with only one condition: It completely separates the detector from the source (see Figure 1.1 supra). It can be deformed to enclose the source  $Q$  itself and tend asymptotically to join its surface. The outward normal  $\mathbf{n}$  in this case points the natural direction of response flow out of the source. It will be shown in Chapter 2 that the exact flux  $C$  need not be known to benefit from this theorem.

### 1.3 Perturbation contribution response equations

The merit of the equations of the preceding section is that they enjoy all the rigor of mathematical physics and they are general. Unfortunately, in the form they are presented they do not lend themselves to actual numerical computations. Their

application requires a priori knowledge of the exact adjoint function  $\psi^*$  which, if known and used in Eq(1.12), will give the answer to the problem from Eq(1.15) without further needs to invoke Monte Carlo calculations. This function is not accessible to users in general and to shielding designers in particular. To this effect, the potential of the method cannot be exploited in realistic engineering problems. Williams<sup>1</sup> devised a perturbation method pertinently suited to contribution response Monte Carlo calculations in realistic engineering problems.

Williams' perturbation method is based on the assumption that the exact adjoint function  $\psi^*$  solution to Eq(1.6) can be replaced by some approximate adjoint function  $\tilde{\psi}^*$  which can be obtained by accessible means. Before continuing further in exploring what this approximate function might be, it is instructive to review some definitions of the components of the problem.

The *domain* is the volume of a convex space contained inside the free surface boundary. This includes the *medium*, the *perturbation*, the *source* and the *detector* shown in Fig(1.2). For our purpose, the components of the domain may be defined by materials. In this case the medium is the material - not necessarily uniform - which fills the domain and defined by the neutronic cross sections  $\bar{\Sigma}$ . It could include source and detector volumes as well. The perturbation is a chunk of material of arbitrary shape and extent implanted within the medium and can be defined by its neutronic cross sections  $\Sigma$ . The source of neutrons, designated by  $Q$ , emits neutral particles of any kind such as neutrons, photons or like. It can be isotropic or otherwise, volumetric or boundary source. The detector, designated by  $Q^*$ , can be volumetric, such as a foil or a vial, or a surface, such as the free boundary of the medium, or a fictitious surface within the medium (Fig. 1.2).

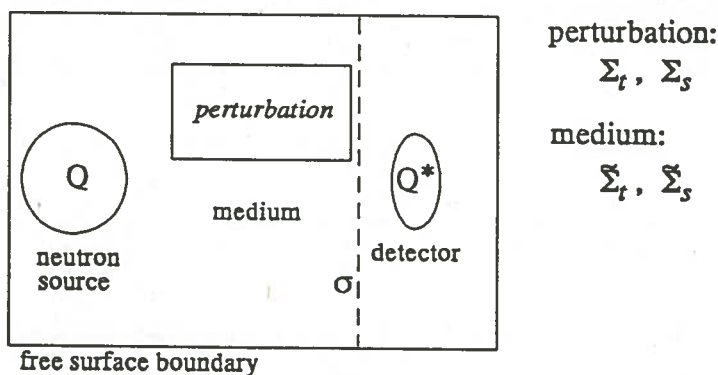


**Figure 1.2.** A neutron source-detector arrangement in a medium as a shield with free surface boundary and a perturbation of material different than medium. The domain is everything inside the free surface boundary.  $\sigma$  is a Williams-Engle enclosure.

The components of the domain may also be defined by geometric regions, mainly perturbed and unperturbed regions. The perturbed region is that portion of space of the domain which is designated to host the perturbation material. When the perturbation is physically in place, the neutronic cross section of the perturbed region is  $\Sigma$ , and perturbed region and perturbation may be used interchangeably. When the perturbation is removed from the system, the perturbed region is filled with material of medium of neutronic cross section  $\bar{\Sigma}$ , the same cross sections used in adjoint calculations. The unperturbed region is the space outside the perturbed region and is filled with material of medium of neutronic cross section  $\bar{\Sigma}$ . By these definitions, the *exact* adjoint function  $\psi^*$  prevails everywhere in the domain with the perturbation in place. The *perturbed* adjoint function  $\tilde{\psi}^*$  prevails everywhere in the domain with the perturbation removed. The domain in this case becomes an approximate geometry to the problem. For this reason,  $\tilde{\psi}^*$  will also be referred to as *approximate* adjoint function to the exact function  $\psi^*$ .

The choice of  $\tilde{\psi}^*$ , however arbitrary it may be, should be consistent with the problem in hand and should not infringe any of the requirements which validate Eq(1.6).



Williams' perturbation equations require that one fundamental condition must be satisfied: The governing equation in  $\tilde{\psi}^*$  must obey the same boundary conditions of the governing equation in  $\psi^*$ . The consequence to this condition is that the two functions must have the same degrees of freedom in space, that is, if  $\psi^*$  is three dimensional,  $\tilde{\psi}^*$  must also be three dimensional. A symmetry condition, however, need not be strictly conserved. The approximate solution  $\tilde{\psi}^*$  can be obtained from a symmetry problem in one or in two-dimensional convex geometry while  $\psi^*$  is intrinsically a three dimensional function. In this class of problems we have the one-dimensional spherical geometry and the two-dimensional axisymmetric cylindrical and ellipsoidal geometries. These requirements leave relatively limited options to work with to compute the approximate adjoint function. One option is to use the two dimensional discrete ordinates DOT code to generate the approximate solution  $\tilde{\psi}^*$  in the R-Z plane in cylindrical geometry.

In the preceding paragraphs we discussed the approximate adjoint function but said nothing about the neutron flux  $\psi$ . There is no need to define an approximate flux  $\tilde{\psi}$ . It is always exact. It appears only in the defining expressions of the contributon response fluxes, but will take no explicit part in any CMC calculations. Williams' perturbed contributon response flux is then defined by:

$$\tilde{C} = \psi \tilde{\psi}^* \quad (1.17)$$

and the governing transport equation in  $\tilde{C}$  takes the form<sup>1</sup>:

$$\nabla \cdot \hat{\Omega} \tilde{C} + \tilde{\theta}_t \tilde{C} = \int_{\tau'} \tilde{\theta}(\tau' \rightarrow \tau) \tilde{C}' d\tau' + \tilde{\Gamma} \quad (1.18)$$

where  $\tilde{\Gamma} = \tilde{S} - \mathfrak{R}$ ,  $\tilde{S} = Q\tilde{\psi}^*$ , the contributon response source in the approximate geometry and  $\mathfrak{R}$  is the detector response function defined by Eq(1.13), an invariant quantity under perturbation of Williams' contributon response field. The coefficient  $\tilde{\theta}_t$  was recognized as the *total contributon response cross section* defined by<sup>1</sup>:

$$\tilde{\theta}_t = \tilde{\theta}_s + \tilde{\theta}_a \quad (1.19)$$

where  $\tilde{\theta}_s$  is a scattering cross section in the approximate geometry, always positive, and is defined same as by Eq(1.10) with all terms of Eq(1.11) now tilded, and  $\tilde{\theta}_a$  is a *contributon response amorphous cross section*. It is amorphous because it alternates signs with position, energy and direction, i.e., at a given position  $\mathbf{r}$  and for a given energy  $E$ , it may be positive in one direction and negative in another one. Williams interpreted  $\tilde{\theta}_a > 0$  as a response absorption coefficient and  $\tilde{\theta}_a < 0$  as a response production coefficient, and derived the expression<sup>1</sup>:

$$\begin{aligned} \tilde{\theta}_a &= (\Sigma_t - \tilde{\Sigma}_t) - \int_{\tau'} \Sigma(\tau \rightarrow \tau') \frac{\tilde{\psi}^{*'}}{\tilde{\psi}^*} d\tau' + \tilde{\theta}_s \\ &= \Delta\Sigma_t - \tilde{\theta}'_s + \tilde{\theta}_s \end{aligned} \quad (1.20)$$

One exception to the rule of primed quantities is that  $\tilde{\theta}'_s \equiv \tilde{\theta}'_s(\tau)$ , i.e., it is not function of the primed parameter  $\tau'$ . This primed coefficient is evaluated from the perturbation cross section  $\Sigma$ , the unprimed coefficient is evaluated from  $\tilde{\Sigma}$ . Equation (1.18) and its companion equations (1.17), (1.19) and (1.20) are all the extent of the contributon Monte Carlo method initially suggested by Williams<sup>1</sup> and implemented in this dissertation. Past this point, all hypothesis, concepts, derivations, formulation and the implementation of these developments in the proposed Monte Carlo method are the product of the author efforts devoted to this dissertation.

Insertion of  $\tilde{\theta}_a$  from Eq(1.20) into Eq(1.19) results:

$$\tilde{\theta}_t = \Delta\Sigma_t - \tilde{\theta}'_s + 2\tilde{\theta}_s \quad (1.21)$$

An observation of merit is that  $\tilde{\theta}_a$  can be positive or negative as a result of competitive contributions from its defining parameters contained in Eq(1.20), namely,

directions, energies, scattering cross sections and total cross sections. These contributions are emissions from scattering and absorptions as shown in Eq(1.21) where absorption is contained in  $\Delta\Sigma_t$ . As  $\bar{\theta}_a$  grows negative,  $\bar{\theta}_t$  as defined by Eq(1.19) decreases in magnitude and eventually becomes undesirably negative. In the case of  $\bar{\theta}_t < 0$ , it is not clear whether a solution to Eq(1.18) exists or not, and if it does, under what conditions. The sampling algorithm implemented in this dissertation is constructed to work only with  $\bar{\theta}_t > 0$  by imposing a lower bound to  $\bar{\theta}_a$  such that:

$$\bar{\theta}_a + \bar{\theta}_s = \bar{\theta}_t > 0 \implies \bar{\theta}_a > -\bar{\theta}_s, \quad \forall(\mathbf{r}, \tau)$$

This condition may be represented in a more suitable form as a continuous function:

$$\eta = \frac{\bar{\theta}_s}{\bar{\theta}_t} > 0 \tag{1.22}$$

It is the author's hypothesis that this definition of  $\eta$  represents the amount of response emitted per interaction. For this reason it will be called *response emission ratio*. Its interval of definition is said a *confined spectrum* if  $\eta \in (0, 1)$ , an *extended spectrum* if  $\eta > 0$  and its upper limit is larger than one, and a *mixed spectrum* if  $\eta$  takes positive and negative values. The emission ratio is *neutral* if  $\eta = 1$ . This is the case when response transport occurs in the unperturbed region. One obscure situation could occur when  $\eta = |\infty|$ . There is no physical interpretation at this time which could explain the meaning of this singularity. Williams<sup>1</sup> suggested that *negative absorption* has the significance of response *production* within the perturbation. It follows that  $\bar{\theta}_a$  may assume two meanings depending on the magnitude of  $\eta$ . When  $\eta < 1$ ,  $\bar{\theta}_a$  may be interpreted as an absorption coefficient and  $\eta$  is the *nonabsorption probability*. When  $\eta > 1$ ,  $\bar{\theta}_a$  may be interpreted as a response *regeneration* coefficient and  $\eta$  is the *amplitude of regeneration*. In the latter case,  $\bar{\theta}_a$  plays a role in a  $\check{C}$ -field somewhat similar to the fission cross section  $\nu\Sigma_f$  in  $\psi$ -field.

#### 1.4 Existence and uniqueness of solutions to contribution transport equation

It was indicated earlier that Eq(1.18) is a *premier* in the scientific literature, not as a mathematical equation as much as it is a governing equation of a specific physical process. It is appropriate at this point to address the question of existence and uniqueness of its solution. The worth of the efforts in addressing this problem is to give a merit to the answers obtained by solving contribution response transport equations with the Monte Carlo method. The same question was previously addressed in neutron transport. Davison<sup>25</sup> approached the problem of existence and uniqueness of solutions to the equations of neutron transport for the time dependent problem. Case and Zweifel<sup>26</sup> examined the same problem more thoroughly and extended their work jointly with Olhoeft<sup>27</sup> to time independent neutron transport equations (Eqs 1.5, 1.6). Among the conditions for a positive solution to exist is that  $0 < \eta < 1$  and  $\bar{\Gamma} > 0$ . In that case, Case and Zweifel's theorems apply rigorously to Eq(1.18) confirming the existence of the solution under these restrictive conditions. The authors recognized that they made no attempt to be comprehensive in their treatment to the problem. They imposed restrictions on cross sections and sources under which the theorems are true, and recognized that for certain other restrictions it may be impossible to prove anything. The restrictions other than confined spectrum and positive source that can be imposed on Eq(1.18) are likely to be of the type of conditions with which it is impossible to prove anything.

Suppose for the moment that we impose Olhoeft's condition on the source term expressed by Eq(1.14). Then require that

$$\bar{\Gamma} \geq 0 \Rightarrow \bar{S} \geq \mathfrak{R} \quad (1.23)$$

which is a sufficient condition to obtain a physically sound solution, i.e.,  $\bar{C} > 0$  if and when it exists. By integrating  $\bar{\Gamma}$  over the largest possible volume which contains the source volume and the detector volume, and over all directions and all energies, we get:

$$\iint_{\mathbf{r}\tau} \tilde{\Gamma} \, d\mathbf{r}d\tau \geq 0 \Rightarrow \iint_{\mathbf{r}\tau} \tilde{\mathfrak{S}} \, d\mathbf{r}d\tau \geq \iint_{\mathbf{r}\tau} \mathfrak{R} \, d\mathbf{r}d\tau \Leftrightarrow \tilde{\mathfrak{R}}_s \geq \bar{\mathfrak{R}} \quad (1.24)$$

where  $\tilde{\mathfrak{R}}_s$  is the response of the detector due to the source  $\tilde{\mathfrak{S}}$  in the approximate geometry without perturbation, and  $\bar{\mathfrak{R}}$  is the exact response, the final objective of this Monte Carlo method. Clearly, condition (1.23) is too stringent to obtain condition (1.24). The function  $\tilde{\Gamma}$  may take negative values at some points in the phase space  $(\mathbf{r},\tau)$  and its integral can still be positive. We are interested in this integral value.

We learn from inequality (1.24) that a positive solution to Eq(1.18) exists if the perturbation material is of the kind to result in a response reading by the detector at most equal to the reading of the detector in the approximate geometry without perturbation. This happens when  $\eta \leq 1$  for all  $\tau$  at all positions within the perturbation. In this case, an analog or a nonabsorption biasing Monte Carlo solution to Eq(1.18) is a Neumann series and the proposed algorithm discussed in Chapter 2 performed very smoothly. It is possible, however, that adjoint calculations in the approximate geometry of a given problem produces an underestimated  $\tilde{\mathfrak{R}}_s$  for some perturbation materials. This happens when  $\eta > 1$  for some  $\tau$  and  $\eta < 1$  for others. This observation suggests that a strict Neumann series solution to Eq(1.18) does not exist. An alternate algorithm is proposed. The underlying hypothesis, the validity and the implementation of this alternate algorithm in the random walk of the proposed Monte Carlo are discussed in detail in Chapter 2. However, the general outlines of the method are presented here.

The solution to the problem is *Segmented* into *successive* Neumann series solutions. The first solution *segment* starts with an initial guess equal to the source strength and the series grows as long as  $\eta \leq 1$ . The first time  $\eta$  takes a value larger than one, the series is terminated and a new one starts with a new initial guess equal to  $\eta$  now larger than one. The succession of these *segments* solutions is proposed here to be the

solution to the problem. As to whether such a solution is *the* solution to the problem and whether it is unique, perhaps the best answer to this question at this time is Case and Zweifel's statement that it may be impossible to rigorously prove anything! All that can be said at this point with respect to the validity of this segmented series solution is that it performed well with the sample problem of Chapter 4 and produced very acceptable data.

## B. MULTIGROUP EQUATIONS

### 1.5 Derivation of contribution response multigroup equations

The equations of the previous section are expressed in terms of continuous energy variable  $E$ . In actual numerical calculations, the practice is to work with energy groups instead, if for any reason, the neutronic cross sections are available in multigroup structured libraries. Bell and Glasstone, and Henry<sup>23</sup>, among many others, describe the methods of obtaining neutronic multigroup constants and the derivations of the neutron transport multigroup equations from spectral equations. With no upscattering, the multigroup forms of Eqs(1.1 & 1.2) are respectively:

$$\nabla \cdot \hat{\Omega} \psi_g + \Sigma_{tg} \psi_g = \sum_{g'=1}^g \int_{\hat{\Omega}'} \Sigma_{g' \rightarrow g}(\mu_0) \psi_{g'}' d\hat{\Omega}' + Q_g \quad (1.25)$$

$$-\nabla \cdot \hat{\Omega} \psi_g^* + \Sigma_{tg} \psi_g^* = \sum_{g'=g}^G \int_{\hat{\Omega}'} \Sigma_{g \rightarrow g'}(\mu_0) \psi_{g'}^{*'} d\hat{\Omega}' + Q_g^* \quad (1.26)$$

where:  $\psi_g \equiv \psi_g(r, \hat{\Omega}) =$  multigroup flux

$\psi_g^* \equiv \psi_g^*(r, \hat{\Omega}) =$  multigroup adjoint function

$Q_g \equiv Q_g(r, \hat{\Omega}) =$  multigroup neutron source

$Q_g^* \equiv Q_g^*(r, \hat{\Omega}) =$  multigroup detector response function in  $\psi$ -field

$\Sigma_{tg} \equiv \Sigma_{tg}(\mathbf{r})$  = multigroup total cross section

$\Sigma_{g' \rightarrow g}(\mu_0) \equiv \Sigma_{g' \rightarrow g}(\mathbf{r}, \mu_0)$  = group to group differential scattering  
cross section

Multiply Eq(1.25) by  $\psi_g$  and Eq(1.26) by  $\psi_g^*$ , subtract the resulting equations and rearrange to obtain the multigroup response transport equation:

$$\nabla \cdot \hat{\Omega} C_g + \theta_{sg} C_g = \sum_{g'=1}^G \int_{\hat{\Omega}'} \theta_{g' \rightarrow g}(\hat{\Omega}' \rightarrow \hat{\Omega}) C_{g'} d\hat{\Omega}' + S_g - \mathfrak{R}_g \quad (1.27)$$

where:  $C_g \equiv \psi_g \psi_g^*$  = multigroup contribution response flux (1.28)

$S_g \equiv Q_g \psi_g^*$  = multigroup contribution response source (1.29)

$\mathfrak{R}_g \equiv Q_g^* \psi_g$  = Multigroup detector response function in C-field (1.30)

and the multigroup contribution cross sections are defined formally by:

$$\theta_{sg} = \sum_{g'=g}^G \int_{\hat{\Omega}'} \theta_{g \rightarrow g'}(\hat{\Omega} \rightarrow \hat{\Omega}') d\hat{\Omega}' \quad (1.31)$$

$$\theta_{g \rightarrow g'}(\hat{\Omega} \rightarrow \hat{\Omega}') = \Sigma_{g \rightarrow g'}(\mu_0) \frac{\psi_{g'}^*}{\psi_g} \quad (1.32)$$

where G is the index of the lowest energy group such that:  $g=1,2,\dots,G$ .

Comparison of expression (1.28) for the definition of multigroup flux  $C_g$  with definition (1.8) for spectral flux C shows that to obtain  $C_g$  from C it simply requires exchanging the energy variable E with the group index g. However, application of this rule to convert Eq(1.9) to a multigroup equation is not sufficient. An additional operation must be applied as it can be learned from Eq(1.27). The integral over energy in Eq(1.9)

must be converted to a summation over the group index. An appropriate choice of the running index must be made with care to coincide the group index with the energy integration variable with no upscattering. Application of this rule to Eq(1.18) converts that equation to the multigroup form of the contribution response transport equation in the  $\bar{C}$ -field:

$$\nabla \cdot \hat{\Omega} \bar{C}_g + \bar{\theta}_{tg} \bar{C}_g = \sum_{g'=1}^g \int_{\hat{\Omega}'} \bar{\theta}_{g' \rightarrow g}(\hat{\Omega}' \rightarrow \hat{\Omega}) \bar{C}'_{g'} d\hat{\Omega}' + \bar{S}_g - \bar{\mathfrak{R}}_g \quad (1.33)$$

This is the governing equation for the *working contribution field*  $\bar{C}_g$  in which the Monte Carlo simulation will be performed. It follows that:

$$\left. \begin{aligned} \bar{\theta}_{tg} &= \bar{\theta}_{ag} + \bar{\theta}_{sg} \\ &= \Delta \Sigma_{tg} - \bar{\theta}'_{sg} + 2 \bar{\theta}_{sg} \end{aligned} \right\} \quad (1.34)$$

$$\bar{\theta}_{sg} = \sum_{g'=g}^G \int_{\hat{\Omega}'} \bar{\theta}_{g \rightarrow g'}(\hat{\Omega} \rightarrow \hat{\Omega}') d\hat{\Omega}' \quad (1.35)$$

$$\bar{\theta}_{g \rightarrow g'}(\hat{\Omega} \rightarrow \hat{\Omega}') = \Sigma_{g \rightarrow g'}(\mu_0) \frac{\tilde{\psi}_{g'}^*}{\tilde{\psi}_g^*} \quad (1.36)$$

$$\bar{\theta}'_{sg} = \sum_{g'=g}^G \int_{\hat{\Omega}'} \Sigma_{g \rightarrow g'}(\mu_0) \frac{\tilde{\psi}_{g'}^*}{\tilde{\psi}_g^*} d\hat{\Omega}' \quad (1.37)$$

$$\bar{\mathfrak{R}} = - \sum_{g=1}^G \int_{\sigma} d\sigma \int_{\hat{\Omega}} \mathbf{n} \cdot \hat{\Omega} C_g d\hat{\Omega} \quad (1.38)$$



$$\eta_g = \frac{\bar{\theta}_{sg}}{\bar{\theta}_{tg}} \quad (1.39)$$

Expressions (1.34) through (1.37) are the multigroup forms of contribution response cross sections in  $\bar{C}$ -field, expression (1.38) is the statement of Williams-Engle's theorem in the multigroup approximation and the multigroup emission ratio is defined by Eq(1.39).

## CHAPTER TWO

### THE CONTRIBUTION MONTE CARLO METHOD

#### 2.1 Time independent integral equations for contribution response transport

In the previous Chapter we obtained the time independent governing equations for contribution response transport and we assumed that the equations are properly balanced and are completely defined. Of interest to the analysis in this Chapter is Eq(1.18), an integro-differential equation in  $\tilde{C}$ . Two probability functions needed for Monte Carlo sampling can be extracted directly from this equation, namely, the source pdf and the scattering pdf. A third pdf, the response transport pdf is also needed for a complete Monte Carlo sampling. It is lurking invisible in Eq(1.18) but can be obtained from a time independent integral equation of contribution response transport in  $\tilde{C}$ . It flows naturally that the search for the missing pdf begins by first obtaining a physically sound integral equation in  $\tilde{C}$ .

In general, a time dependent integral equation for neutron transport is first obtained, either from basic principles<sup>25</sup> or by integrating the time dependent form of Boltzmann transport equation, which is the same as Eq(1.5) with the time derivative term  $\frac{1}{v} \dot{\psi}$  in the LHS. Various mathematical techniques are used for these derivations<sup>25,28-31</sup>. A time independent integral equation is then obtained at the limit as  $t \rightarrow \infty$ . Instructional derivations of the time independent integral equation were also obtained by integrating Eq(1.5) along a trajectory of the travel of a neutron<sup>22,29</sup> from its current position to the boundary of the medium and in the direction where it came from, i.e., in direction  $-\hat{\Omega}$  as illustrated in Figure 2.1. Using the notations shown in Figure 2.1, we have for the forward equation:

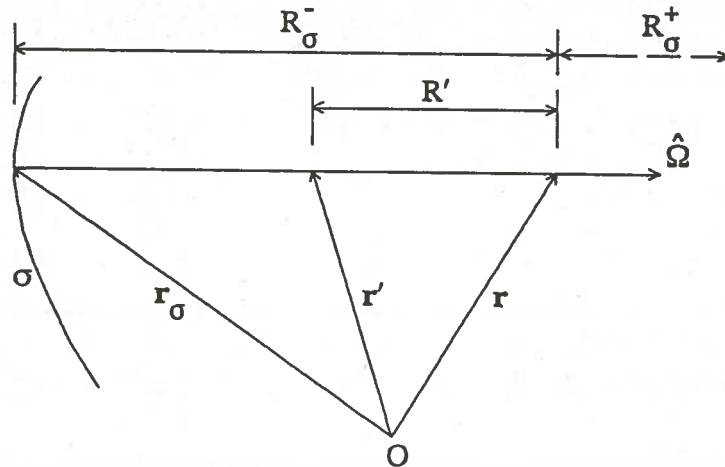


**Figure 2.1.** Coordinates of neutron trajectory in a convex medium where  $\sigma$  is the free surface boundary,  $\hat{\Omega}$  is the direction of travel of neutron,  $\mathbf{r}$  the current position of neutron and  $\mathbf{r}'$  the position where the neutron comes from. A dummy variable  $R$  takes on the value 0 at  $\mathbf{r}$ , the value  $R_{\sigma}^{-}$  at  $\mathbf{r}_{\sigma}$  in direction  $-\hat{\Omega}$  and  $R_{\sigma}^{+}$  in direction  $\hat{\Omega}$ .

$$\psi(\mathbf{r}) = \int_0^{R_{\sigma}^{-}} e^{-\beta(\mathbf{r},R)} q(\mathbf{r}-R\hat{\Omega}) dR \quad (2.1)$$

$$\beta(\mathbf{r},R) = \int_0^R \Sigma_t(\mathbf{r}-R'\hat{\Omega}) dR' \quad (2.2)$$

$$q(\mathbf{r}-R\hat{\Omega}) = \int_{\tau'} \Sigma(\mathbf{r}-R\hat{\Omega},\tau' \rightarrow \tau) \psi'(\mathbf{r}-R\hat{\Omega}) d\tau' + Q(\mathbf{r}-R\hat{\Omega}) \quad (2.3)$$

with boundary condition  $\psi(R_{\sigma}^{\pm})=0$  for reentrant neutrons and  $q$  is the neutron emission density<sup>25</sup>. We recognize that Eq(1.18) is formally identical to Eq(1.5) except that Eq(1.18) defines a different boundary value problem:  $\tilde{C}(R_{\sigma}^{\pm}) = \tilde{C}(R_{\sigma}^{\pm}) = 0, \forall \hat{\Omega}$ , where  $R_{\sigma}^{\pm}$

are distances from position  $\mathbf{r}$  to the boundary along direction  $\hat{\Omega}$  (Fig. 2.1). That does not prevent us, however, from proceeding to obtain the integral equation in  $\tilde{C}$  same way as the integral equation in  $\psi$  was obtained. This will result in:

$$\tilde{C}(\mathbf{r}) = \int_0^{R_0^-} e^{-\beta(\mathbf{r},R)} \varphi(\mathbf{r}-R\hat{\Omega}) dR \quad (2.4)$$

$$\beta(\mathbf{r},R) = \int_0^R \tilde{\theta}_t(\mathbf{r}-R'\hat{\Omega}) dR' \quad (2.5)$$

$$\varphi(\mathbf{r}-R\hat{\Omega}) = \int_{\tau'} \tilde{\theta}(\mathbf{r}-R\hat{\Omega},\tau' \rightarrow \tau) \tilde{C}'(\mathbf{r}-R\hat{\Omega}) d\tau' + \tilde{\Gamma}(\mathbf{r}-R\hat{\Omega}) \quad (2.6)$$

where  $\beta$  is the optical distance between two consecutive collisions of *response particles* in  $\tilde{C}$ -field (the concept of response particle will be introduced in the next section) and  $\varphi$  the contributon response emission density; the variable  $\tau$  is implied in all functions. Equation (2.4), like Eq(2.1), is a Fredholm integral equation of the second kind<sup>30,32</sup> and it has same solution of Eq(1.18), when it exists. The exponential term of Eq(2.4) will be used for the transport pdf of the proposed CMC method. It is indicated that, in some cases, an integral equation like Eq(2.4) does not have a Neumann series solution yet the solution may exist and if it does, it can be obtained by other methods<sup>32</sup>.

## 2.2 The CMC method

Monte Carlo methods of neutron transport can be utilized in contributon response transport. For this purpose we discretize contributon response emission from source  $\tilde{S}$  by defining a discrete response entity, a *response particle*, which is destined to behave in a

$\bar{C}$ -field exactly same as a neutron does in a  $\psi$ -field, except that a response particle does not leak out of the system. The *response value* of this pseudo particle is one response unit (1ru) at the source. A Monte Carlo method based on this concept will be referred to as *Contributon Monte Carlo* (CMC) method.

A response particle is allowed to collide, scatter and be absorbed in a  $\bar{C}$ -field, the same as a neutron does in a neutron field. Collisions occur everywhere in the domain, but absorption is allowed only in the perturbation materials in accordance with Eq(1.20). A response particle is also *regenerative* in accordance with Williams<sup>1</sup> multiplication hypothesis. It assumes a new response value every time  $\eta > 1$ . These properties distinguish a response particle from a contributon, which by definition cannot be absorbed, does not multiply, and carries its response faithfully from the source to the detector without alteration. Different contributons could carry different response values at the source, and a contributon is a physical source particle, e.g., a neutron, while a response particle is a discrete characterization of the response continuum introduced to suit the Monte Carlo random walk. An immediate consequence to this concept of a response particle is that the random walk can be modeled with a pure analog Monte Carlo or with nonabsorption biasing, nonanalog Monte Carlo. In the latter case a response value correction is made with nonabsorption probability  $\eta$ . In all of what follows, a particle should always be understood to be a response particle and that should introduce no confusion since there are no other particles involved.

#### A. ANALOG CMC.

In the case of analog Monte Carlo, a particle begins its random walk at the source with response value of 1ru and everywhere in the domain  $\eta \leq 1$ . In the unperturbed region it always emerges from a collision with the same response value. In the perturbed region,

Russian Roulette is played at every collision to decide survival or termination of the particle. For this purpose, a random number  $\xi$  is selected on the interval  $(0, 1)$  and compared with the nonabsorption probability  $\eta$ . If  $\xi > \eta$  the particle will be terminated and a new source particle will be sampled, otherwise the particle will be allowed to continue its journey at least to the next collision site without alteration of its response value. In actual computations, the scoring need not be made at the detector itself. Instead, Williams-Engle's theorem of §1.2 is used with surface  $\sigma$  a few centimeters from the perturbation. This way, substantial amount of computing time can be saved.

For some isolated points in the perturbed region, it is possible that, when  $\eta=0$ , for some energies and directions  $\tau'$  and  $\tau$ ,  $\eta < 0 \Rightarrow \bar{\theta}_t < 0$ . This can be expected to happen as a result of truncation of a finite spherical harmonics series representing fluxes and cross sections. This is no real worry since a solution  $\bar{C}$  always exists for perturbations with confined  $\eta$ -spectrum. The user should use his judgement to introduce an effective treatment to this anomalous behavior of the function  $\eta$ . A remedy is proposed here by way of illustration. When this happens, reset  $\eta=1 \Rightarrow \bar{\theta}_t = \bar{\theta}_s$ , and let the particle continue its journey toward the next collision site. This is equivalent to leave the response value of the particle unchanged until the next collision site. A new direction and energy will have to be sampled for. Other remedies of users' preference can be implemented as well. It is emphasized here that this anomalous behavior of  $\eta$  is invoked at this point as a possibility. It is not intended to confirm its occurrence or to deny it, and it is not known at this time how frequently it will occur, when it does. A few experiments with the sample problem, using water and steel perturbation materials, were not conclusive, suggesting that the occurrence of this phenomenon is likely to be rare.

If  $N$  source particles are sampled with analog Monte Carlo, and only  $n$  particles make it to the detector, or past the scoring surface, the average response per source particle will be simply:

$$\bar{\mathfrak{R}} = \frac{n}{N} ru \quad (2.7)$$

It can be shown that the fractional standard deviation (fsd) in this case reduces to:

$$\text{fsd} = \sqrt{\frac{1}{n} - \frac{1}{N}} \iff \sigma = \bar{\mathfrak{R}} \cdot \text{fsd} \quad (2.8)$$

where  $\sigma$  here is the standard deviation.

### B. NONANALOG CMC.

The analog CMC just described demonstrated an excellent performance in a sample problem (see chap. 4) for a *nonregenerative* perturbation, i.e., for  $\eta \leq 1$  for all energies and directions and everywhere in the domain. If it is desired to work with nonanalog Monte Carlo, nonabsorption biasing is an option for nonregenerative perturbations but it is the only option available at this time in problems with *regenerative* perturbations, i.e., for  $\eta \geq 1$ . It produced the same answers as analog CMC for the same nonregenerative perturbation and same number of source particles with significantly improved fsd at the expense of additional CPU time which can be as high as twice the analog CPU time, depending on the volume of the perturbation.

In the unperturbed region, the random walk is identical to that of the analog CMC, and that whether the perturbation is regenerative or nonregenerative. At each collision, the particle emerges with the same response value it carried before the collision, but with new energy and direction selected from the scattering pdfs. If the particle reaches the scoring site without interactions in the perturbed region, it scores the response it carried at the source. The particle is said to be *unbiased*. Many particles are expected to follow random walks exclusively in the unperturbed region without colliding in the perturbed region.

In the perturbed region, the random walk is always biased against absorption whenever  $\eta < 1$ . If the perturbation is nonregenerative and the  $k$ th particle encountered  $v_k$  collisions within the perturbed region before it reaches the scoring site, then the particle will score the response:

$$\bar{\mathfrak{R}}_k = \bar{\omega} \prod_{i=1}^{v_k} \eta_{ki} \quad (2.9)$$

where  $\bar{\omega}$  is the response value of the particle at the source, and  $\eta_{ki}$  is the nonabsorption probability of the  $k$ th particle at the  $i$ th collision within the perturbation region. If the perturbation is regenerative,  $\eta$ -spectrum is extended and nonabsorption biasing applies as long as  $\eta \leq 1$ . When  $\eta > 1$ , the author made the trial hypothesis to correct the response value of the particle by *regeneration*. Although lacking theoretical rigor, this method performed well for the sample problem considered.

Suppose that the  $k$ th particle started its journey with a response value  $\bar{\omega}$ . This response value remains unchanged until the particle's first collision in the perturbed region. Suppose further that for the first, second, . . . up to the  $v_k$ th collision within the perturbation region, all  $\eta_{ki}$  are less than 1 and for the  $v_k+1$ st collision  $\eta_{k,v+1} > 1$ . The response value of the particle up to the  $v_k$ th collision inclusive is going to be  $\bar{\mathfrak{R}}_k$  of Eq(2.9). The response correction by regeneration is to discard the response  $\bar{\mathfrak{R}}_k$  and reassign a response value  $\bar{\omega} = \eta_{k,v+1}$  to the particle at the  $v_k+1$ st collision site. The next collision will be labeled  $i=1$  and a new generation of collisions begins from there. Several generations of collisions may succeed before the particle scores the response value from Eq(2.9) from the last generation of collisions. Every time the particle is *refreshed* by regeneration, it will be allowed to move to the next collision site with the same incident energy and direction at the current collision site. The hypothesis that the emergent direction is the same as the incident direction is proposed in another contest to the author by M.L. Williams and was adopted for this approach.



As indicated, refreshing the response value of a particle by regeneration is a trial hypothesis. It is emphasized here that this approach is not a deduction from the fundamental equation of contribution response theory. It was introduced earlier (§1.4) to construct the segmented solution to Eq(1.18) from successive Neumann series when condition (1.24) is not satisfied. The score value from the last generation of collisions, however, can be proved if the validity of this hypothesis is accepted. The proof begins by first defining a *generation of collisions* as a number of  $\nu$  consecutive nonregenerative collisions, i.e., the emission ratio of all of these collisions is  $\eta \leq 1$ . Suppose that a response particle completes the  $(i-1)$ th generation of  $\nu'$  collisions and is incident at collision site  $i$  with a response value  $\bar{\mathfrak{R}}_{i-1}$  as illustrated in Figure 2.2; the response ratio at this collision site is  $\eta_i > 1$ . (The index  $k$  for the  $k$ th particle is omitted for notational convenience.) By our hypothesis, the particle's response value  $\bar{\mathfrak{R}}_{i-1}$  will be discarded and the particle emerges from the collision with a new response value  $\omega_i = \eta_i$ . A new generation of collisions, the  $i$ th generation, begins departing from the  $i$ th collision site and terminates at

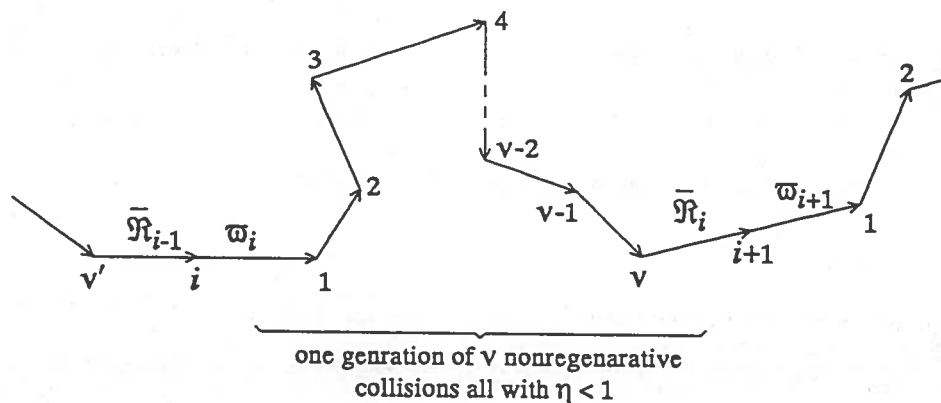


**Figure 2.2.** A segment of the random walk showing one generation of nonregenerative collisions. An  $\mathfrak{R}$  value represents the response at the end of one generation of collisions and a  $\omega$  is the regenerated response value of a response particle of the next generation of collisions. The tip of an arrow is a collision site of a response particle within the perturbation region.

the collision site  $i+1$  with a response value  $\bar{\mathfrak{R}}_{i+1}$  that can be calculated from Eq(2.9). At this collision site the response ratio is  $\eta_{i+1} > 1$ . Here too, the response value  $\bar{\mathfrak{R}}_{i+1}$  of the particle will be scraped and the new value  $\bar{\omega}_{i+1} = \eta_{i+1}$  will be assigned to the particle. By repeating this sequence of contiguous generations of collisions, we conclude that the response the particle scores comes only from the last generation of collisions. The number  $\nu$  of collisions in a generation can be zero or any random integer.

If  $N$  particles are sampled and  $n$  of them score their response unbiased, the detector average response (in ru) per source particle becomes:

$$\bar{\mathfrak{R}} = \frac{1}{N} \left\{ \sum_{k=1}^{N-n} \bar{\mathfrak{R}}_k + n \right\} \quad (2.10)$$

and the standard deviation becomes:

$$\sigma = \frac{1}{N} \sqrt{\sum_{k=1}^{N-n} (\bar{\mathfrak{R}} - \bar{\mathfrak{R}}_k)^2 + n (\bar{\mathfrak{R}} - 1)^2} \Rightarrow \text{fsd} = \frac{\sigma}{\bar{\mathfrak{R}}} \quad (2.11)$$

### 2.3 Practical use of response $\bar{\mathfrak{R}}$

The detector response  $\bar{\mathfrak{R}}$  as calculated with expression (2.7), or alternatively with expression (2.10), represents a number of response units per response particle created at the source with response value of 1ru. Such a particle, as defined in the previous section (§2.2), does not have a physical existence. From this situation arises the need to find a systematic way to evaluate the exact response of the detector per source neutron knowing the detector response  $\bar{\mathfrak{R}}$  per response particle from CMC calculations.

Consider the general case where all response particles are emitted at the source with same response value  $\varpi$  ru. The response  $\bar{\mathcal{R}}$  of the detector will have to be calculated with an expression equivalent to (2.7) in response units per response particle. Define a *fractional detector response* (fdr) by the ratio:

$$\text{fdr} = \frac{\bar{\mathcal{R}}}{\varpi} \quad (2.12)$$

Both  $\varpi$  and  $\bar{\mathcal{R}}$  are in response units per response particle. Obtain an approximate response  $\tilde{\mathcal{R}}_{\text{neut}}$  in response units per neutron in the approximate geometry and for a neutron source Q. Define  $\bar{\mathcal{R}}_{\text{neut}}$  as the exact response of the detector in response units per neutron. Then we have:

$$\text{fdr} = \frac{\bar{\mathcal{R}}}{\varpi} = \frac{\bar{\mathcal{R}}_{\text{neut}}}{\tilde{\mathcal{R}}_{\text{neut}}} \implies \bar{\mathcal{R}}_{\text{neut}} = \frac{\bar{\mathcal{R}}}{\varpi} \tilde{\mathcal{R}}_{\text{neut}} \quad (2.13)$$

The value of  $\varpi$  is users' choice. It is convenient to set  $\varpi = 1$  ru/particle so that the simple statistics of Eq(2.8) or Eq(2.11) can be used. Then Eq(2.13) simplifies to:

$$\bar{\mathcal{R}}_{\text{neut}} = \bar{\mathcal{R}} \tilde{\mathcal{R}}_{\text{neut}} \quad (2.14)$$

where the fdr is now  $\bar{\mathcal{R}}$ . It is dimensionless and it represents the magnitude of the detector response from CMC calculations. The explicit expression of  $\tilde{\mathcal{R}}_{\text{neut}}$  can be obtained from Eq(1.15) in the approximate geometry:

$$\tilde{\mathcal{R}}_{\text{neut}} = \frac{\int \tilde{\mathcal{S}} d^3\mathbf{r} d\tau}{\int Q d^3\mathbf{r} d\tau} = \frac{\int \tilde{\psi}^* Q d^3\mathbf{r} d\tau}{\int Q d^3\mathbf{r} d\tau} \quad (2.15)$$

where the spatial integrals are over the volume  $V_s$  of the neutron source Q. It can be shown that if the neutron source is isotropic, Eq(2.15) simplifies to:

$$\tilde{\mathcal{R}}_{\text{neut}} = \frac{1}{V_s} \sum_g \int_{V_s} \chi_g \tilde{\Phi}_g^*(\mathbf{r}) d^3\mathbf{r}$$

where  $\chi_g$  is the fraction of source neutrons appearing in group  $g$  and  $\tilde{\Phi}_g^*(\mathbf{r})$  is the multigroup scalar adjoint flux in the approximate geometry. By inserting the response conversion factor  $\tilde{\mathcal{R}}_{\text{neut}}$  from this last expression into Eq(2.14), we obtain the actual response reading of the detector in  $\psi$ -field, the final objective of the Monte Carlo calculations.

## 2.4 Probability functions for CMC method

Now we turn to the probability density functions for the proposed CMC method. In this section the pdfs will be stated in their general forms. Complete expressions for numerical computation will be developed in the next Chapter consistently with the internal structure of DOT code. Since all actual calculations will be performed in conjunction with multigroup structured cross sections libraries, all pdfs will be cast in the multigroup approximation. They can be adapted to the internal structure of any operational computer code of users' choice.

### A. SOURCE PDFs.

Consider the general case of a volumetric contribution response source in an approximate geometry such as the one depicted in Figure 2.3. The emission density rate of this source is described by a density function  $\tilde{S}$  expressed in response units per unit energy and per steradian and defined by Eq(1.12) in the approximate geometry, that is,  $\tilde{S} = Q\tilde{\psi}^*$ . For computational expediency it is convenient to divide the volume  $V$  of the source into smaller cells  $\delta V$  such that  $V = \sum \delta V$  and assume that the neutron source  $Q$ , the

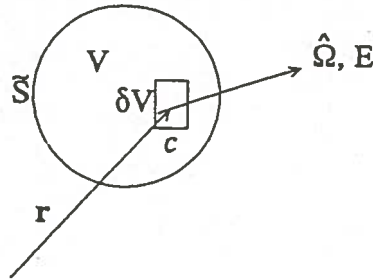


**Figure 2.3.** An illustration of a contribution response emission from a source cell  $\delta V$  centered at  $r$  within the volume  $V$  of the source of emission density rate  $\tilde{S}$  in the approximate geometry.  $\hat{\Omega}$  is the direction and  $E$  is the energy of the emitted response.

adjoint function  $\tilde{\psi}^*$  and hence  $\tilde{S}$  itself are uniform within every cell. An emitted response at  $r$  within the source volume can then be examined as a response particle emitted from cell  $c$  of volume  $\delta V$ , with energy  $E$  and in direction  $\hat{\Omega}$  as illustrated in Figure 2.3. In the special case of a planar source or a linear source, the source cell will continue to be represented by the symbol  $\delta V$  with the understanding that each cell type should be implemented in its defining geometry. Therefore, the source probability function  $S$  will be function of at least three independent parameters:  $c$ ,  $\hat{\Omega}$  and  $E$ . Direction  $\hat{\Omega}$  is completely determined by two parameters: a polar angle  $\vartheta$  between direction  $\hat{\Omega}$  and the polar axis and an azimuthal angle  $\phi$ . The polar angle enters in all calculations as an argument of cosine function  $\mu \equiv \cos\vartheta$  which is commonly known as *directional cosine*; it will also be referred to as the *polar direction* relative to a polar axis of users' choice, generally problem dependent. It follows that the source particle probability function is the joint pdf  $S(c, E, \mu, \phi)$  in continuous energy variable, or equivalently  $S(c, g, \mu, \phi)$  in multigroup approximation. It will be sampled for each of these parameters one at a time from properly normalized marginal and conditional pdfs. For computational efficiency

tied to the internal structure of DOT code, the sequence of selection of the source particle parameters is of the order shown in  $S$ : Cell index  $c$ , group index  $g$ , polar direction  $\mu$ , azimuthal angle  $\varphi$ .

(a) *The c-pdf.* An expression for a properly normalized source cell pdf, or  $c$ -pdf, can be obtained from its basic definition: The ratio of integral response emitted from cell  $c$  of volume  $\delta V$  to the integral response emitted from the volume  $V$  of the source; an integral response should be understood in energy and direction. This ratio translates into the expression:

$$S(\delta V) = \frac{\int_{\delta V} d^3r \int_E dE \int_{\hat{\Omega}} d\hat{\Omega} Q(r, E, \hat{\Omega}) \tilde{\psi}^*(r, E, \hat{\Omega})}{\int_V d^3r \int_E dE \int_{\hat{\Omega}} d\hat{\Omega} Q(r, E, \hat{\Omega}) \tilde{\psi}^*(r, E, \hat{\Omega})} \quad (2.16)$$

where the integrand is the contribution response source  $\tilde{S}$ . With the assumption that neutron source  $Q$  and adjoint function  $\tilde{\psi}^*$  are uniform in  $\delta V$ , the positional parameter  $r$  can be replaced by the corresponding cell index  $c$  of volume  $V_c = \delta V$  and Eq(2.16) can be rearranged to cast the form

$$S(c) = \frac{V_c \int_E dE \int_{\hat{\Omega}} d\hat{\Omega} Q_c(E, \hat{\Omega}) \tilde{\psi}_c^*(E, \hat{\Omega})}{\sum_c V_c \int_E dE \int_{\hat{\Omega}} d\hat{\Omega} Q_c(E, \hat{\Omega}) \tilde{\psi}_c^*(E, \hat{\Omega})} \quad (2.17)$$

For an isotropic neutron source,  $Q$  is independent of  $\hat{\Omega}$  and the index  $c$  can be omitted from  $Q(E)$  which now represents the number of neutrons emitted in  $dE$  at  $E$ . With this assumption the multigroup representation of Eq(2.17) can be obtained by replacing the energy variable  $E$  by the group index  $g$  in accordance with the convention discussed earlier (§1.5):

$$S(c) = \frac{V_c \sum_g Q_g \int_{\hat{\Omega}} \tilde{\psi}_{cg}^*(\hat{\Omega}) d\hat{\Omega}}{\sum_c V_c \sum_g Q_g \int_{\hat{\Omega}} \tilde{\psi}_{cg}^*(\hat{\Omega}) d\hat{\Omega}} \quad (2.18)$$

where  $Q_g$  now represents the fraction of neutrons emitted in group  $g$  and  $c \in \{1, \dots, N_c\}$  is the cell index;  $N_c$  is the number of source cells, usually a users' choice and problem dependent parameter. Also, if the source has a uniform thickness,  $V_c$  represents the area of cell  $c$ .

(b) *The g-pdf.* This is a conditional pdf  $S(g:c)$  for the selection of emission energy group  $g$  knowing the cell index  $c$ , where  $g \in \{1, \dots, G_s\}$  and  $G_s$  is the last energy group of source particles or equivalently source contribution response. It is the ratio of the response emitted from cell  $c$  in group  $g$  and in all directions  $\hat{\Omega}$  to the response emitted from the same cell in all groups and in all directions. It can be obtained directly from Eq(2.18):

$$S(g:c) = \frac{Q_g \int_{\hat{\Omega}} \tilde{\psi}_{cg}^*(\hat{\Omega}) d\hat{\Omega}}{\sum_g Q_g \int_{\hat{\Omega}} \tilde{\psi}_{cg}^*(\hat{\Omega}) d\hat{\Omega}} \quad (2.19)$$

(c) *The  $\mu$ -pdf.* This is a conditional pdf  $S(\mu:c,g)$  for the selection of the polar direction  $\mu \in (-1, 1)$  of a source particle knowing the emission cell  $c$  and the energy group  $g$ . It is defined as the ratio of the response emitted in all azimuthal angles from cell  $c$  and in group  $g$  to the response emitted from same cell in same energy and in all directions. To explicit the expression for this pdf, direction  $\hat{\Omega}$  is broken into its components  $\mu$  and  $\varphi$ . Then from Eq(2.19):

$$S(\mu:c,g) = \frac{\int_{\varphi} \tilde{\psi}_{cg}^*(\mu,\varphi) d\varphi}{\int_{\hat{\Omega}} \tilde{\psi}_{cg}^*(\hat{\Omega}) d\hat{\Omega}} \quad (2.20)$$

(d) *The  $\varphi$ -pdf.* This is the conditional pdf  $S(\varphi:c,g,\mu)$  for the selection of the azimuthal angle  $\varphi \in (0, 2\pi)$  of the emitted source particle knowing the emission cell, the energy group and the polar direction. It is defined as the ratio of response emitted from cell  $c$ , group  $g$ , in polar direction  $\mu$  and with azimuthal angle  $\varphi$  to the response emitted in  $c$ ,  $g$ ,  $\mu$  and in all angles  $\varphi$ . Using Eq(2.20) we obtain:

$$S(\varphi:c,g,\mu) = \frac{\tilde{\psi}_{cg}^*(\varphi:\mu)}{\int_{\varphi} \tilde{\psi}_{cg}^*(\varphi:\mu) d\varphi} \quad (2.21)$$

### B. TRANSPORT PDF.

In neutron transport the distance traveled by a neutron between two consecutive collision sites is sampled for from a transport pdf with mnemonic  $t$ -pdf. It represents the trajectory of the particle moving between two collision sites. The  $t$ -pdf for response particles is defined exactly same way as for neutron transport. This pdf is the exponential kernel of Eq(2.4) and is properly normalized in mean free path units. The exponent  $\beta$  is the optical track length between collision sites. Upon sampling for  $\beta$  the usual way, the geometric distance between collision sites may be obtained by solving Eq(2.5) for  $R \in (0, R_{\max})$  where  $R$  is the distance of unknown length units of  $\beta$  mean free paths units, and  $R_{\max}$  is the distance from the current collision site to the boundary along emergent direction  $\hat{\Omega}$ . Carter et al.<sup>33</sup> devised a technique to solve for the track length when the



cross section is continuously varying along the particle trajectory, provided that the maximum of the cross section is known. The method is claimed by the authors to be more efficient than direct numerical integration. That technique does not lead itself to solve Eq(2.5). A variation to numerical integration, the  $\beta$  *progressive saturation* method is devised here to operate in a  $\tilde{C}$ -field geometry passed on to Monte Carlo problem from DOT code or other similar codes which can be used for adjoint calculations.

Consider two consecutive collision sites  $P'$  and  $P$ , the current and the next collision sites respectively, separated by a distance  $R$  which measures  $\beta$  mfp along the direction of flight of a particle. The derivations of the expressions for the progressive  $\beta$  saturation method will be carried out in three-dimensional geometry aided with a Figure in two-dimensional geometry for clarity. A grid of lines in the  $R$ - $Z$  plane discretizes the geometry into *cells* shown as squares in Figure 2.4; the grid lines are surfaces in Monte Carlo geometry. This cellular discretization segments the line  $P'P$  ( $P'$  not shown in the Figure) into *cellular segments*  $\Delta S_i$  shown in Figure 2.4 near the terminus point  $P$ . Each cellular segment can be calculated as the distance between the points of intersections of the line  $P'P$  with the boundaries of the cell, using equations of analytic geometry, and then converted into a cellular optical thickness  $\beta_i = \bar{\theta}_{ii} \Delta S_i$ , where  $\bar{\theta}_{ii}$  is assumed uniform over the volume of the cell. The optical distance  $\beta$  is said saturated when

$$\beta = \sum_{i=1}^{n-1} \beta_i + \bar{\theta}_{in} \Delta S_n \quad (2.22)$$

which is nothing but the integral of Eq(2.5) as a discrete sum. The last cellular segment  $\Delta S_n$  saturates  $\beta$  at the new collision site  $P$  within the *cell of saturation*, and it is always shorter than the distance between the intersection points at the boundaries of this cell. This is because, in Monte Carlo calculations, the selection of the new collision site  $P$  is random and the probability that  $P$  coincides with the boundary of the cell is just zero. Then we will have:

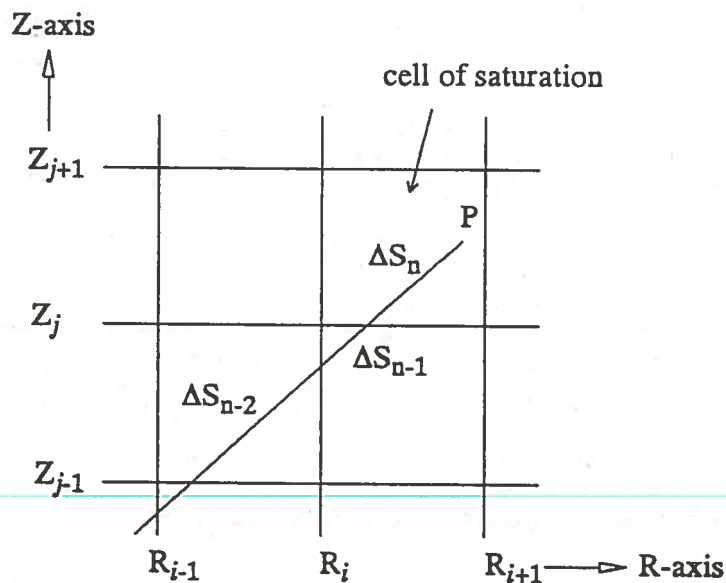


**Figure 2.4.** Segmentation of the trajectory of a response particle near the saturation cell in the R-Z plane. Point P is the new collision site where the optical track length  $\beta$  saturates by the sum of all segments  $\Delta S$  mfp equivalent.

$$\Delta S_n = \frac{\beta - \sum_{i=1}^{n-1} \bar{\theta}_{ti} \Delta S_i}{\bar{\theta}_{tn}} \quad (2.23)$$

The progressive saturation method is to evaluate the sum:

$$\beta_k = \sum_{i=1}^k \beta_i \quad k=1, 2, 3, \dots \quad (2.24)$$

and to check  $\beta_k$  against  $\beta$ . If  $\beta_k < \beta$ , increase  $k$  by 1 and repeat evaluating  $\beta_k$  by Eq(2.24) until  $\beta_k > \beta$ . This happens only one time in the cell of saturation when  $k=n$ . Then the saturation segment  $\Delta S_n$  is evaluated by Eq(2.23) and the distance  $R$  which saturates  $\beta$  becomes:

$$R = \sum_{i=1}^n \Delta S_i \quad (2.25)$$

from which we calculate the coordinates of the new collision site P from  $\mathbf{r} = \mathbf{r}' + \hat{\Omega}R$ .

### C. SCATTERING PDFs.

The scattering pdf  $E(g, \mu, \varphi)$  is a joint probability function which enables the sampling for the emission parameters from a scattering of a response particle at a collision site determined from the  $t$ -pdf. Unless specified otherwise, any probability function with mnemonic  $g$ -pdf,  $\mu$ -pdf or  $\varphi$ -pdf should be understood an emission pdf from scattering, e.g., a  $g$ -pdf for the sampling of energy group of a source response particle will be designated as *source*  $g$ -pdf. An E-pdf is obtained from the coefficient  $\tilde{\theta}(\tau' \rightarrow \tau)$  of the integrand of Eq(2.6), defined in the multigroup approximation. Unless the CMC method is directed toward applications in some specialized crystals, the double differential neutron scattering cross section is assumed rotationally invariant, which is the case in virtually all nuclear engineering applications.

(a) *The g-pdf.* It is a marginal probability function  $E(g)$  from which the energy group  $g \in \{1, \dots, G\}$  of the scattered particle is sampled, where  $G$  is the index of the lowest energy group, generally the thermal group. A  $g$ -pdf is defined as the fraction of the particle energy in all directions to all possible energies that can be emitted in all directions at a collision site. Formally, it can be expressed as the ratio of Eq(1.36) integrated over all directions to same integrated over all directions and summed over all possible energy groups. With no upscattering, we obtain:

$$E(g) = \frac{\int_{\hat{\Omega}} \Sigma_{g' \rightarrow g}(\mu_0) \tilde{\psi}_g^*(\hat{\Omega}) d\hat{\Omega}}{\sum_{g=g'} \int_{\hat{\Omega}} \Sigma_{g' \rightarrow g}(\mu_0) \tilde{\psi}_g^*(\hat{\Omega}) d\hat{\Omega}} \quad (2.26)$$

where  $g'$  is the group index of incident particle, and  $g$  is the group index of the emergent particle at the current collision site; the positional parameter  $r$  should be implied in all terms.

(b) *The  $\mu$ -pdf.* This is a conditional pdf  $E(\mu:g)$  to sample for the polar direction  $\mu \in (-1,1)$  given the energy group  $g$  of the emitted particle by scattering. It is defined as the ratio of the particles emitted in group  $g$ , in direction  $\mu$  and in all azimuthal angles  $\varphi$  to the particles emitted in group  $g$  and in all possible directions  $\hat{\Omega}$ . From Eq(2.26) we obtain:

$$E(\mu:g) = \frac{\int_{\varphi} \Sigma_{g' \rightarrow g}(\mu_0) \tilde{\psi}_g^*(\mu, \varphi) d\varphi}{\int_{\hat{\Omega}} \Sigma_{g' \rightarrow g}(\mu_0) \tilde{\psi}_g^*(\hat{\Omega}) d\hat{\Omega}} \quad (2.27)$$

where the azimuthal angle  $\varphi$  takes all values on  $(0, 2\pi)$ .

(c) *The  $\varphi$ -pdf.* This is the conditional pdf  $E(\varphi:g,\mu)$  from which we sample for the azimuthal angle  $\varphi \in (0, 2\pi)$  given the group  $g$  and the polar direction  $\mu$  of the emitted particle by scattering. It is defined as the fraction of all particles emitted in group  $g$ , in direction  $\mu$  and in azimuthal direction  $\varphi$  to all particles in same  $g$ ,  $\mu$  and in all azimuthal angles  $\varphi$ . From Eq(2.27) we obtain:

$$E(\varphi;g,\mu) = \frac{\Sigma_{g' \rightarrow g}(\mu_0) \tilde{\psi}_g^*(\mu, \varphi)}{\int_{\varphi} \Sigma_{g' \rightarrow g}(\mu_0) \tilde{\psi}_g^*(\mu, \varphi) d\varphi} \quad (2.28)$$

An instructive observation of the foregoing probability functions is that all of them are expressed in terms of parameters pertaining to the approximate geometry, whether the perturbation is in place or removed out of the system.

## 2.5 The CMC method and importance biasing

A visual examination of source and scattering pdfs derived in the previous sections reveals that they *look* the same as their counterparts of importance biasing with  $\tilde{\psi}^*$  as importance function. Despite this apparent similarity, they are conceptually different. The CMC pdfs are defined on the  $\tilde{C}$ -field while the importance biased pdfs are defined on the  $\psi$ -field. Also, the CMC pdfs balance the governing response transport equation, coupled with the forward and the adjoint neutron transport equations, while the importance biased pdfs in  $\psi$ -field do not balance any equation. Therefore, by their definitions the two sets of pdfs are structurally different and functionally different.

First we recognize that the scattering probability per unit length in a  $\psi$ -field is defined by  $\tilde{\psi}^* \Sigma_{g' \rightarrow g}(\mu_0)$ , an importance biased probability density function not properly normalized. The probability character is adhered to this quantity since  $\Sigma_{g' \rightarrow g}(\mu_0)$  is a probability per unit length in differential sense. In a  $\tilde{C}$ -field, the same probability for response scattering is defined by Eq(1.36), also not a properly normalized pdf. It is only in their normalized form that they look alike. Also, sampling biased pdfs require correction of the *statistical weight* of the particle<sup>34</sup>:  $W^*(\text{biased pdf}) = W^*(\text{unbiased pdf})$ ,

where  $W$  is the new weight and  $W'$  the old weight. This weight correction is needed to play biasing by the rules of a fair game. The proposed CMC method works in two modes: (a) in the analog mode no such a weight correction is needed, yet the adjoint function  $\tilde{\psi}^*$  is an integrated part of all the pdfs, (b) in the nonanalog mode the weight correction is introduced as a result of nonabsorption biasing and it is not related to the appearance of the adjoint function in the pdfs. That is, it is not an importance biasing. These observations indicate that the CMC method is unrelated to adjoint biasing in any form. It is just defined in a  $\tilde{C}$ -field the same way as the conventional Monte Carlo method is defined in a  $\psi$ -field without adjoint or importance biasing of any form. The CMC method and the importance biasing are two spurious Monte Carlo method.

## CHAPTER THREE

### SPHERICAL HARMONICS REPRESENTATION OF CMC PROBABILITY FUNCTIONS

#### 3.1 Introduction

Actual transport computations utilize cross sections libraries which contain total cross sections  $\Sigma_{tg}$  needed for the  $t$ -pdf (Eq. 2.27), and the group to group transfer cross sections  $\Sigma_{g' \rightarrow g}(\mu_0)$  stored in terms of their moments in Legendre polynomials expansions. Also, transport codes save adjoint functions  $\tilde{\psi}^*$  as moments in spherical harmonics expansions. Therefore, the general form of the expressions for the pdfs derived in the previous chapter is of little practical use in actual Monte Carlo calculations. In this chapter, they will be rewritten to work specifically with ANISN formatted cross sections libraries such as SAILOR<sup>35</sup>, tied to the axisymmetric two dimensional geometry of DOT code. For other structures of cross sections libraries or codes other than DOT, users will have to rederive their working pdfs starting from the expressions given in Chapter 2.

Insertion of spherical harmonics expansions in the expressions for the pdfs will result in overwhelmingly cumbersome expressions. For the interest of making the expressions look somewhat less complicated, the following unusual notational conventions will be adopted throughout all derivations.

$$\begin{aligned} P_l &\equiv P_{l0}(\mu) & \mu &= \cos\vartheta \\ P_{lm} &\equiv P_{lm}(\mu) & \mu &= \cos\vartheta \\ P'_{lm} &\equiv P_{lm}(\mu') & \mu' &= \cos\vartheta' \end{aligned}$$

where  $P_l$  is the Legendre polynomial of order  $l$ , and  $P_{lm}$  is the associate Legendre function; the primed quantities are descriptive of the precollision directions and the unprimed quantities are descriptive of the postcollision directions. Also, a multiple summation will be represented by one sum with multiple index as follow:

$$\sum_{l=\alpha}^L \sum_{m=\alpha}^l \rightarrow \sum_{lm\alpha}^{Ll}$$

It is important to maintain the order of the indices unaltered because they do not commute, and  $\alpha = 0$  will be omitted in the single sum.

It is a practice to represent transfer cross sections with truncated series in Legendre polynomials of the form<sup>11</sup>:

$$\Sigma_{g' \rightarrow g}(\mu_0) = \frac{1}{4\pi} \sum_{k=0}^K \Sigma_{g' \rightarrow g}^k P_k(\mu_0) \quad (3.1)$$

where  $\Sigma_{g' \rightarrow g}^k$  is the  $k$ th cross section moment,  $K$  is the order of expansion and  $\mu_0 = \hat{\Omega}' \cdot \hat{\Omega}$ . This expression is valid in a polar coordinate system with the pole at the scattering center and polar axis along  $\hat{\Omega}'$ . Equation (3.1) can be expressed in terms of  $\hat{\Omega}'$  and  $\hat{\Omega}$  using the addition theorem of Legendre polynomials<sup>32</sup>:

$$P_k(\mu_0) = P'_k P_k + 2 \sum_{n=0}^k \frac{(k-n)!}{(k+n)!} P'_{kn} P_{kn} \cos n(\varphi - \varphi') \quad (3.2)$$

where the angles  $\vartheta$ ,  $\vartheta'$ ,  $\vartheta_0$ ,  $\varphi$  and  $\varphi'$  relate to the directions  $\hat{\Omega}$  and  $\hat{\Omega}'$  as shown in Figure 3.1. Insertion of Eq(3.2) into Eq(3.1) results the cross section expansion:

$$\Sigma_{g' \rightarrow g}(\mu_0) = \frac{1}{4\pi} \sum_{k=0}^K \Sigma_{g' \rightarrow g}^k \left[ P'_k P_k + 2 \sum_{n=0}^k \frac{(k-n)!}{(k+n)!} P'_{kn} P_{kn} \cos n(\varphi - \varphi') \right] \quad (3.3)$$



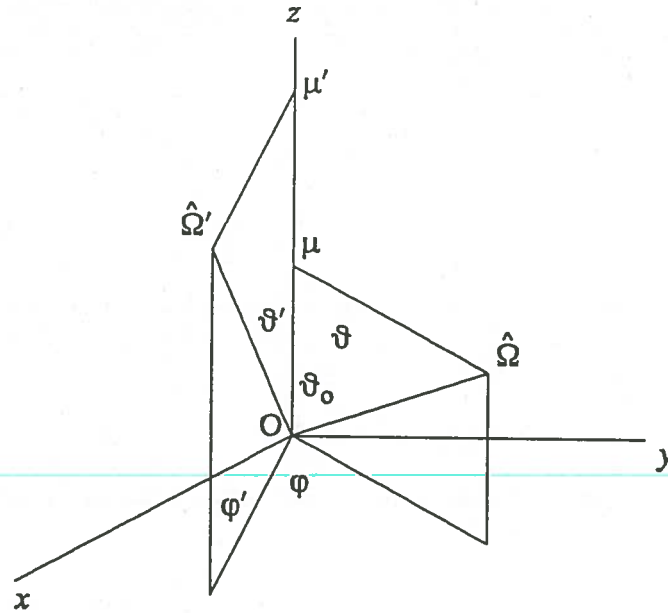


**Figure 3.1.** Angular representation of polar and azimuthal angles in a local cartesian coordinates system with origin coinciding with the pole at O. The new polar axis is z-axis.

Also, the two dimensional adjoint function  $\tilde{\psi}_g^*$  is expanded in a truncated spherical harmonics series of the form<sup>11</sup>:

$$\tilde{\psi}_{cg}^*(\hat{\Omega}) = \sum_{lm}^{Ll} (2l+1) A_{lm} \tilde{\psi}_{cglm}^* P_{lm} \cos m\varphi \quad (3.4)$$

where  $\tilde{\psi}_{cglm}^*$  are the adjoint moments at geometric cell  $c$  in DOT geometry,  $L$  the order of expansion in spherical harmonics usually equal to  $K$ , and the expansion coefficients are defined as:

$$A_{lm} = (-1)^l \sqrt{(2 - \delta_{m0}) \frac{(l-m)!}{(l+m)!}} \quad (3.5)$$

### 3.2 Positive definite pdfs

Insertion of Eq(3.3) and Eq(3.4) into the expressions for the probability density functions of Chapter 2 results expressions which are integrable in closed form over  $\mu$  or  $\varphi$  or both. The resulting functions are properly normalized but are not necessarily always positive for all directions  $\hat{\Omega}$ , a typical symptom of approximating functions with truncated series in Legendre polynomials. We cannot ascribe probability meaning to functions which take on negative values on their respective domains and they are useless for Monte Carlo sampling. To circumvent this difficulty various remedial techniques were proposed.

Coveyou<sup>36</sup> developed a technique for selecting the scattering angles from a set of fixed directions. It was incorporated in O5R<sup>37</sup> and in ESP<sup>38</sup> Monte Carlo codes. Another discrete directions model similar to Coveyou's model but of a more general character is being incorporated in MORSE code. It is based on generalized Gauss quadrature<sup>39</sup>. Whatever the merits of these methods may be, discrete directions sampling is not suitable for contribution Monte Carlo. Carter and Cashwell<sup>34</sup> and Brockmann<sup>40</sup> suggested the possibility of sampling directly from pdfs expressed in truncated Legendre polynomials series. The method requires to take the absolute value of the scattering kernel,  $\theta(\tau' \rightarrow \tau)$  in CMC, and to correct the statistical weight of the particle by the rules of the fair game of conventional biasing, at the risk of obtaining negative weights. The brevity of the discussions on this question by the authors and the lack of citations as to whether the method has ever been adopted for any Monte Carlo code leaves the reader with little faith in the potential of the method to perform successfully in realistic Monte Carlo calculations.

An alternative to the foregoing sampling techniques is to eliminate negative values from the truncated series pdfs without the recourse to a biasing. It is proposed here

to scale such functions with an appropriate *scaling factor* to convert them to properly normalized pdfs never negative on their domains. Probability functions obtained in this manner will be referred to as *positive definite* pdfs. Clearly, properly normalized probability functions which are positive everywhere on their domains need not be redefined.

Consider a real function  $f(x)$  of the independent variable  $x$  defined on a closed domain  $D$ . Assume further that  $f(x)$  alternates sign on  $D$  such that:

$$f(x) < |\infty| \quad \forall x \in D$$

$$f(x) < 0 \quad \forall x \in \delta \subset D$$

$$f(x) > 0 \quad \forall x \in D - \delta$$

and:

$$\int_D f(x) dx = 1 \quad (3.6)$$

To visualize,  $f(x)$  is represented by the curve shown in Figure 3.2 where  $D=[0, c]$  and  $\delta=(a,b)$ . Obviously, condition (3.6) is not sufficient to make  $f(x)$  a probability function because we cannot sample for  $x \in \delta$ . Furthermore, we cannot simply sample for  $x \in D - \delta$  either since now  $f(x)$  is no longer properly normalized on this exclusive domain:

$$\int_{D-\delta} f(x) dx > \int_D f(x) dx = 1$$

It is possible however to construct from  $f(x)$  a *positive definite* pdf denoted by  $F(x)$  by defining a real positive scaling factor  $\gamma$  such that:

$$F(x) = \gamma f(x) > 0 \quad \forall x \in D - \delta \quad (3.7)$$

subject to the normalization:

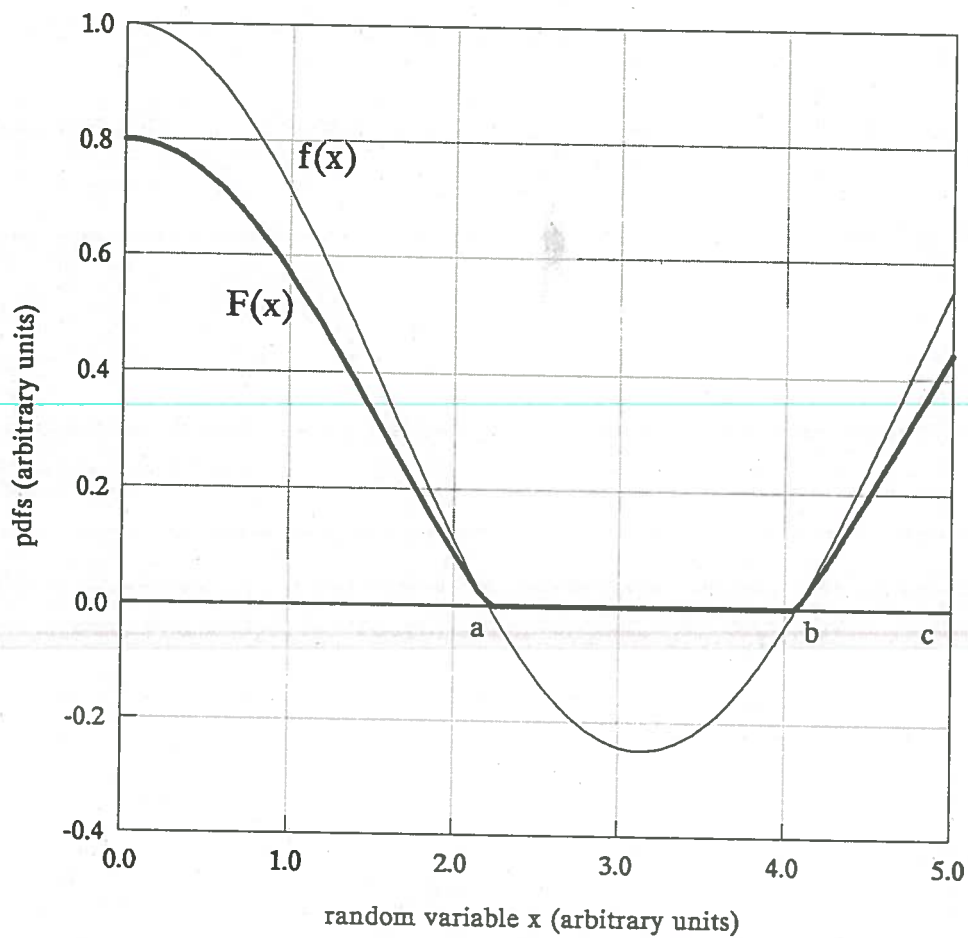


**Figure 3.2.** An illustration of converting a properly normalized pdf  $f(x)$  which takes negative values on some interval  $\delta = [a, b]$  to a positive definite pdf  $F(x)$  always positive on its domain by multiplying the mother pdf  $f(x)$  by a scaling factor  $\gamma$ .

$$\int_{D-\delta} F(x) dx = \gamma \int_{D-\delta} f(x) dx = 1 \quad (3.8)$$

The requirements expressed by Eqs(3.7 & 3.8) are equivalent to redefining  $f(x)$  such that:

$$\left. \begin{aligned} f(x) &\geq 0 \quad \forall x \in D \\ f(x) &= 0 \quad \forall x \in \delta \\ F(x) &= \gamma f(x) \geq 0 \quad \forall x \in D \\ \int_D F(x) dx &= \gamma \int_D f(x) dx = 1 \end{aligned} \right\} \quad (3.9)$$

Now  $F(x)$  is completely defined by Eq(3.9), a properly normalized positive definite probability function. It is expected to give reasonably good description of the random variable  $x$  if the exclusion domain  $\delta$  is small compared to the parent domain  $D$ . We can sample from this pdf if the scaling factor  $\gamma$  is known. Guided by Figure 3.2, we observe that:

$$\frac{1}{2} \int_D [ |f(x)| + f(x) ] dx = \int_0^a f(x) dx + \int_b^c f(x) dx > 1 \quad (3.10)$$

Define a scaling integral  $\mathfrak{S}$ :

$$\mathfrak{S} = \int_D |f(x)| dx \quad (3.11)$$

and choose a scaling factor  $0 < \gamma \leq 1$  which resets integral (3.10) to just unity so that:

$$\gamma \frac{1}{2} \int_D [ |f(x)| + f(x) ] dx = \gamma \frac{\mathfrak{S}}{2} + \frac{\gamma}{2} \int_D f(x) dx = 1 \quad (3.12)$$

Insert Eq(3.6) into Eq(3.12) and rearrange to obtain the relation:

$$\gamma = \frac{2}{1 + \mathfrak{S}} \quad (3.13)$$

Equation (3.11) holds for  $f(x)$  a continuous or discrete function of  $x$ . In the latter case we will have:

$$\mathfrak{S} = \sum_n |f_n| \Delta x_n \quad (3.14)$$

We recognize that Eq(3.11) applies to conditional pdfs for  $\mu$  and  $\varphi$ , and Eq(3.14) applies to the marginal pdf for the energy group  $g$  where  $\Delta x_n = 1$ . One advantage in evaluating  $\gamma$  from Eq(3.13) is that we do not need to determine the interval  $\delta$  where  $f(x) < 0$ . In fact we do not need to know anything about this function other than the assurance that it exists.

The simplicity of the foregoing approach comes with a sacrifice. By setting  $F(x)=0$  on  $\delta$  we artificially made the variable  $x$  equally probable on this interval. By this property,  $F(x)$  becomes isotropic on the exclusion interval when  $x$  represents a direction parameter, while Eq(1.11) and Eq(1.36) indicate otherwise. Avoiding this situation is a simple matter if we sample our pdfs with the rejection technique where no  $x$  values can be selected from  $\delta$ . It remains to justify the exclusion of  $\delta$  from the parent domain  $D$ . We argue in terms of a property of truncated series in Legendre polynomials. They are known to oscillate about zero on intervals where the parent function assumes small amplitudes relative to its maximum value on the domain. It follows that the probability of selecting the variable of interest on these intervals is too small to account for in a random process where statistical variations are unavoidable anyway. Therefore, by avoiding selection of  $x$  on its *exclusion* intervals, we believe that the precision of the final answer is not compromised, at least in statistical sense. The experimental data discussed in a later chapter support this belief.

Finally we address the practical evaluation of the scaling integral  $\mathfrak{S}$ . In the case of Eq(3.14) the summation is simple straightforward operation. When the function  $f(x)$  of

Eq(3.11) is replaced by the pdfs which will be derived shortly, a special care is required to achieve two usually conflicting objectives: Minimizing the computing time and retaining a good accuracy of the integral. A compromise can be achieved by selecting a relatively fast numerical integration method and by relaxing on the accuracy of the integral to a tolerable limit. The accuracy should be understood in the global set of operations involved in the numerical handling of the working pdfs. High accuracy of integral  $\int$  is wasted time in conjunction with the rejection technique to be employed. For our purpose, a reasonable accuracy can be achieved with a fast running Gauss-Legendre (G-L) quadrature with a judicial choice of the order of quadrature. It appeared that order 8 performed with great success in the sample problem.

### 3.3 Maxima of positive definite pdfs

The probability functions  $S$  and  $E$  become nonlinear transcendental functions in the random parameters when expressed in terms of spherical harmonics expansions. That leaves us with but one choice, to sample using the rejection technique. Efficient and expedient sampling with this method requires the knowledge of the maximum of the pdf. There are numerous method to find maxima of functions. The simplest and perhaps the most expedient method is to divide the domain  $D$  into a finite number of small intervals  $\Delta x$  and evaluate the pdf  $F(x)$  at the boundary at each interval. The maximum of these values will be taken for the maximum of  $F(x)$  even though it may not be the actual maximum. A graphical illustration presented in Figure 3.3 demonstrates the justification of this approach.

Suppose that the peak of the maximum  $M$  of the pdf  $F(x)$  lies between delimiters  $a$  and  $b$  of the  $i$ th interval  $\Delta x$  as shown in the figure. Then the calculated maximum  $m$  will have the value at point  $c$  on the curve while  $M$  has its value at point  $d$ . By taking  $m$

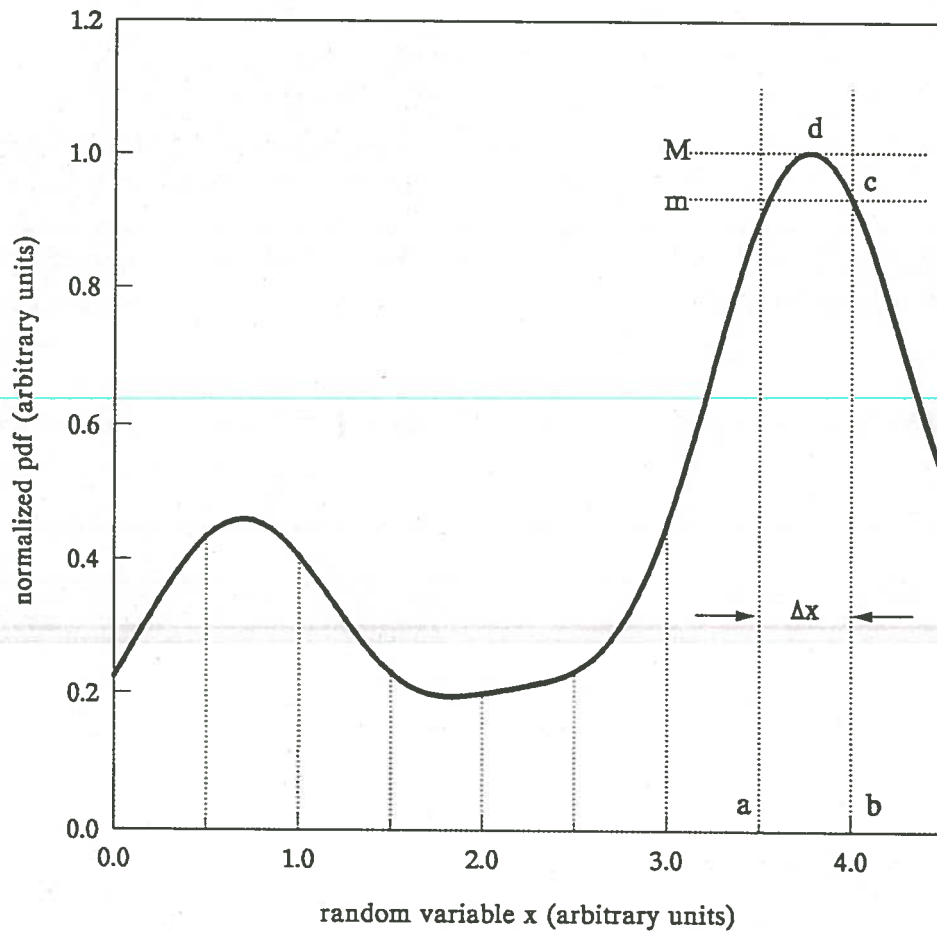


**Figure 3.3.** Numerical evaluation of the maximum of a pdf by the method of segmentation. The interval of definition of the random variable  $x$  is divided into equal intervals  $\Delta x$ . The maximum value of a pdf shown as a thick continuous curve is at point  $c$  in this case.



for maximum of  $F(x)$ , a selection  $F(\xi)$ , from a random number  $\xi$ , which lies under the peak and above line  $m$  will be rejected. However, the rejection of one selection does not prevent that the selection of the next trial will be retained. This reasoning may be expressed quantitatively in terms of the probability  $p$  for a selection  $F(\xi)$  to lie within the area under the peak and above line  $m$ . By assuming that this area is half the area of the rectangle  $(M-m)\Delta x$ , then the probability to reject a selection that otherwise might be retained is just the ratio of this area to the area under the entire curve  $F(x)$  which is unity.

We may write:

$$p = \frac{1}{2} \Delta m \Delta x$$

where  $\Delta m = (M-m)$ . An estimate for the order of magnitude of  $p$  may be obtained by choosing  $\Delta m \sim \Delta x \sim 0.1$ , which is quite reasonable a choice. Then  $p \sim 0.005$ . Considering the randomness of the selection process, the fact that the series are truncated to the 5th order or less, and that broad group cross sections libraries cause virtually no such sharp peaks which would require  $\Delta x$  smaller than 0.1, this order of magnitude of  $p$  is too small to interfere with the precision of the final answer. The results of the sample problem validates the merits of this approach.

### 3.4 Working pdfs for the CMC method

Insertion of Eq(3.3) and Eq(3.4) into the expressions for the probability density functions of Chapter 2 results explicit expressions in  $c$  the cell index in DOT geometry,  $g$  the energy group index,  $\mu$  the polar direction and  $\varphi$  the azimuthal angle. The resulting probability density functions are the working pdfs for the CMC method with response functions  $\tilde{\psi}^*$  from DOT code.

### A. SOURCE PDFs.

One prerequisite for the source pdfs is the precise shape and location of the isotropic source of neutrons. It determines the value of  $V_c$  and the limits of integrations of expressions (2.18), (2.19) and (2.20). For the sample problem described in the next chapter, a plane, isotropic source is placed at the bottom of the cylinder which emits one neutron per unit area and per unit time in the inward direction into the cylinder. That is, neutrons are emitted in  $\mu > 0$  direction only. The area of a cell  $c$ , in DOT geometry, will be represented by:

$$V_c \propto R_c^2 - r_c^2 \quad (3.15)$$

where  $R_c$  is the outer radius and  $r_c$  is the inner radius of cell  $c$ . Now define the parameters:

$$I_l = \int_0^1 P_l(\mu) d\mu \quad (3.16)$$

$$\lambda_{cglm} = (2l + 1) A_{lm} \tilde{\psi}_{cglm}^* \quad (3.17)$$

where  $A_{lm}$  is from Eq(3.5). Then all positive definite S-pdfs of Chapter 2 become expressible in terms of the factors:

$$\tilde{E}_{cg} = Q_g \sum_{l=0}^L I_l \lambda_{cglg} \quad (3.18)$$

$$\tilde{G}_c = V_c \sum_g \tilde{E}_{cg} \quad (3.19)$$

$$\tilde{\Lambda}_{cgl} = \frac{Q_g \lambda_{cglg}}{\tilde{E}_{cg}} \quad (3.20)$$

$$\Gamma_{lm} = \frac{\lambda_{cglm} P_{lm}}{\sum_{l=0}^L \lambda_{cgl0} P_l} \quad (3.21)$$

From these we construct the desired source probability functions:

From Eq(2.18):

$$S(c) = \gamma \frac{\tilde{G}_c}{\sum_c \tilde{G}_c} \quad (3.22)$$

$\gamma$  from Eq(3.13), and:

$$\mathfrak{S} = \frac{\sum_c |\tilde{G}_c|}{\left| \sum_c \tilde{G}_c \right|} \quad (3.23)$$

From Eq(2.19):

$$S(g:c) = \gamma \frac{V_c \tilde{E}_{cg}}{\tilde{G}_c} \quad (3.24)$$

and:

$$\mathfrak{S} = \frac{V_c}{|\tilde{G}_c|} \sum_c |\tilde{E}_{cg}| \quad (3.25)$$

From Eq(2.20):

$$S(\mu:c,g) = \gamma \sum_{l=0}^L \tilde{\lambda}_{cgl} P_l(\mu), \quad \mu \in (0, 1) \quad (3.26)$$

and:

$$\mathfrak{S} = \frac{1}{2} \sum_{q=1}^{N_q} w_q \left| \sum_{l=0}^L \tilde{\lambda}_{cgl} P_l(x_q) \right| \quad (3.27)$$

where  $N_q$  is the order of G-L quadrature,  $w_q$  the weights and  $x_q$  are defined by:

$$x_q = \frac{\mu_q + 1}{2} \quad (3.28)$$

and  $\mu_q \in (-1, 1)$  are Legendre zeros of  $P_{N_q}$ . Finally, from Eq(2.21):

$$S(\varphi:c,g,\mu) = \frac{\gamma}{2\pi} \sum_{lm}^{Ll} \Gamma_{lm} \cos(m\varphi), \quad \varphi \in (0, 2\pi) \quad (3.29)$$

and:

$$\mathfrak{S} = \sum_{q=1}^{N_q/2} w_q \left| \sum_{lm}^{Ll} (-1)^m \Gamma_{lm} \cos(m\pi\varphi_q) \right| \quad (3.30)$$

where  $\varphi_q \in (-1, 1)$  are the Legendre zeros.

### B. TRANSPORT PDFs.

The  $t$ -pdf is defined by the exponential term of Eq(2.4). It is properly normalized and invertible for direct sampling for  $\beta$  the mean free path distance between two consecutive collision sites. However, the actual geometric distance equivalent to  $\beta$  is saturated using the recursion relation of Eq(2.25) where the scattering cross sections  $\bar{\theta}'_{sg}$  and  $\bar{\theta}_{sg}$  need be evaluated at every cell  $i$ , for every group  $g$ , along a direction  $\hat{\Omega}$ , from the current collision site located at cell  $c$ . Clearly, these coefficients are not probability functions nor they are intended to be, but still need be expressed in terms of the expansions (3.3) and (3.4). Insertion of these expansions into Eq(1.35) gives:

$$\bar{\theta}_{sg',i} = \frac{\sum_{g''=g'}^g \sum_{lm}^{Ll} Y_{lm} f_{g' \rightarrow g''}^l \tilde{\Psi}_{ig''lm}^*}{\sum_{lm}^{Ll} (2l+1) Y_{lm} \tilde{\Psi}_{ig'lm}^*} \quad (3.31)$$

where:

$$Y_{lm} = A_{lm} P'_{lm} \cos m\varphi' \quad (3.32)$$

$$f_{g' \rightarrow g''}^l = \begin{cases} \bar{\Sigma}_{g' \rightarrow g''}^l & \text{in the case of } \bar{\theta}_s \\ \Sigma_{g' \rightarrow g''}^l & \text{in the case of } \bar{\theta}'_s \end{cases} \quad (3.33)$$

and  $g'$  is the energy group before emission at cell  $c$ , and  $i$  is the running index shown in Eq(2.23) for all cells crossed along direction  $\hat{\Omega}$  starting from cell  $c$ ; the upper limit of index  $i$  will be determined upon saturating distance  $R_k$  of Eq(2.24) for every emission site tracking.

### C. SCATTERING PDFs.

Insertion of Eq(3.3) and Eq(3.4) into the expressions for E-pdfs of Chapter 2 leads to the following pdfs factors:

$$C_{kn} = A_{kn} P'_{kn} \cos n\varphi' \quad (3.34)$$

$$F_g = \sum_{kn} C_{kn} \bar{\Sigma}_{g' \rightarrow g}^k \tilde{\Psi}_{cgkn}^* \quad (3.35)$$

and, from Eq(2.26):

$$E(g) = \gamma \frac{F_g}{\sum_{g=g'} F_g} \quad (3.36)$$

and:

$$\mathfrak{S} = \frac{\sum_{g=g'} |F_g|}{\left| \sum_{g=g'} F_g \right|} \quad (3.37)$$

where  $g'$  is the precollision energy group and  $G$  is the lowest energy group, generally the thermal group. Also:

$$D_{kl} = (-1)^l \frac{2l+1}{2} \sum_{g' \rightarrow g}^k P'_k \tilde{\Psi}_{cgl}^* \quad (3.38)$$

$$G_{knl} = \frac{2l+1}{2} \frac{(k-n)!}{(k+n)!} A_{ln} \sum_{g' \rightarrow g}^k P'_{kn} \tilde{\Psi}_{cgl}^* \cos n\varphi' \quad (3.39)$$

$$F_\mu = \sum_{kl}^{KL} D_{kl} P_k P_l + \sum_{kn1}^{Kk} \sum_{l=n}^L G_{knl} P_{kn} P_{ln} \quad (3.40)$$

then, from Eq(2.27): 
$$E(\mu:g) = \gamma \frac{F_\mu}{F_g} \quad (3.41)$$

and: 
$$\mathfrak{S} = \frac{1}{|F_g|} \sum_{q=1}^{N_q} w_q |F_\mu(\mu_q)| \quad (3.42)$$

where  $N_q$  is the order of G-L quadrature,  $w_q$  are the weights and  $\mu_q \in (-1, 1)$  are the Legendre zeros. Finally, define the factors:

$$H_{klm} = \frac{2l+1}{4\pi} A_{lm} \sum_{g' \rightarrow g}^k P'_k P_k P_{lm} \tilde{\Psi}_{cgl}^* \quad (3.43)$$

$$U_{knlm} = \frac{2l+1}{2\pi} \frac{(k-n)!}{(k+n)!} A_{lm} \sum_{g' \rightarrow g}^k P'_{kn} P_{kn} P_{lm} \tilde{\Psi}_{cgl}^* \quad (3.44)$$

$$F_\varphi = \sum_{klm}^{KLl} H_{klm} \cos m\varphi + \sum_{kn1}^{Kk} \sum_{lm}^{Ll} U_{knlm} \cos m\varphi \cos n(\varphi - \varphi') \quad (3.45)$$

from Eq(2.28): 
$$E(\varphi:g,\mu) = \gamma \frac{F_\varphi}{F_\mu} \quad (3.46)$$

$$\mathfrak{S} = \frac{\pi}{|F_\mu|} \sum_{q=1}^{N_q} w_q \left| \sum_{klm}^{KLl} H_{klm} (-1)^m \cos m\pi\varphi_q + \sum_{kn1}^{Kk} \sum_{lm}^{Ll} U_{knlm} (-1)^{n+m} \cos m\pi\varphi_q \cos n(\pi\varphi_q + \varphi') \right| \quad (3.47)$$

where  $N_q$  and  $w_q$  are as defined above and  $\varphi_q \in (-1, 1)$  are the Legendre zeros. The indices  $K$  and  $L$  must be equal otherwise the smallest value prevails for both of them.

### 3.5 Sampling the S and E pdfs

It is apparent now that the expressions for the source and the emission pdfs developed in the previous section (§3.4) are not invertible for direct sampling for the desired random parameter. Instead, the rejection method will be used. The algorithm of the method can be represented by the flow chart shown in Figure 3.4 which requires that the fixed parameters, e.g.,  $H$ ,  $U$  and  $F_\mu$  in the case of Eq(3.46), are known. The first step is to search for the maximum of  $X(x)$  using the method described in §3.3, where  $X$  is any working pdf and  $x$  is the random parameter of interest. Simultaneously, we test whether the pdf is positive definite. If it is not, scaling integral  $\mathfrak{J}$  and  $\gamma$  factor are calculated and

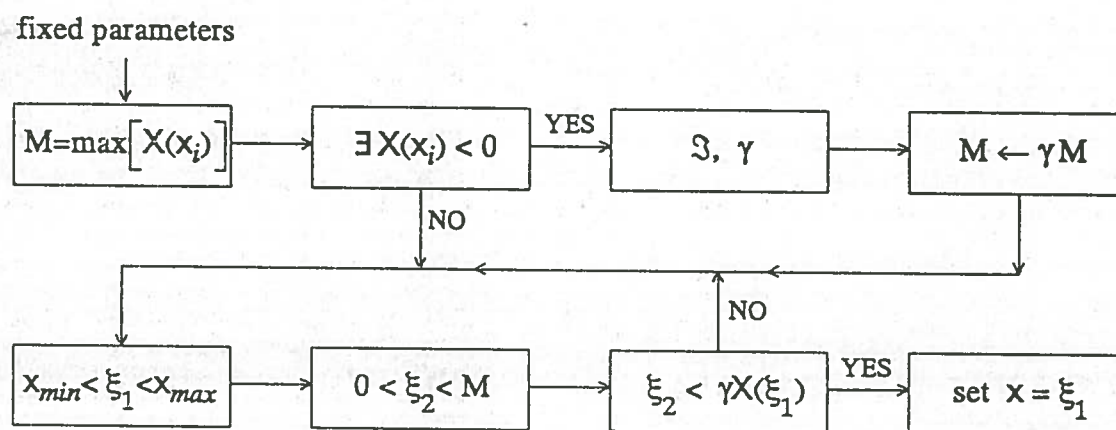


**Figure 3.4.** A flow chart for the sampling of the S and E pdfs represented by  $X(x)$  where  $x$  is a dummy variable which espouses the identity of any of the random variables of S and E.

the maximum  $M$  of  $X$  is scaled with  $\gamma$ . A random number  $\xi_1$  is assigned to  $X$  and a second random number  $\xi_2$  is assigned to  $X$ . Then compare  $\xi_2$  with  $\gamma X(\xi_1)$ . If  $\xi_2 > \gamma X(\xi_1)$ , the test fails. Reject the two random numbers and repeat by selecting another set of two random numbers. When the test succeeds, retain  $\xi_1$  for the desired random parameter and move to the selection of the next random parameter.



## CHAPTER FOUR

### A SHIELDING SAMPLE PROBLEM

#### 4.1 Geometry

A numerical experiment is carried out to test the validity and the effectiveness of the CMC method as formulated in the previous chapters. The object of the experiment is to obtain a boundary crossing response of a detector for a fixed neutron source by the CMC method and by a deterministic method using the two dimensional discrete ordinates DOT code. For that purpose, a concrete orthocylinder (Fig. 4.1) is used for a shield against energetic neutrons emanating from a planar isotropic source placed at the bottom of the cylinder. A thin ring detector is placed at the top of the cylinder to measure a boundary crossing response. The intensity of the source, its extent and the extent of the detector are maintained fixed throughout all the experiment. A cylindrical homogeneous perturbation, coaxial with the cylinder, is placed within the cylinder with its top about half way between source and detector. Its top is maintained fixed and its height of  $H$  centimeters is made variable to analyse the effect of the thickness of the perturbation on the detector response. That way we leave enough room to place the scoring surface at various positions  $h$  centimeters from the top of the perturbation to produce a numerical verification of Williams-Engle's theorem. Dimensions and relative positions of all these components are shown in Figure 4.1.

The spatial discretization of the cylinder for DOT R-Z calculations is shown in Figure 4.2. The first centimeter from all boundaries is divided into four mesh intervals of 0.25 cm in the R and in the Z directions. The remaining space is divided into 1.0 cm mesh in both directions. Each resulting square or rectangular mesh in the R-Z plane is

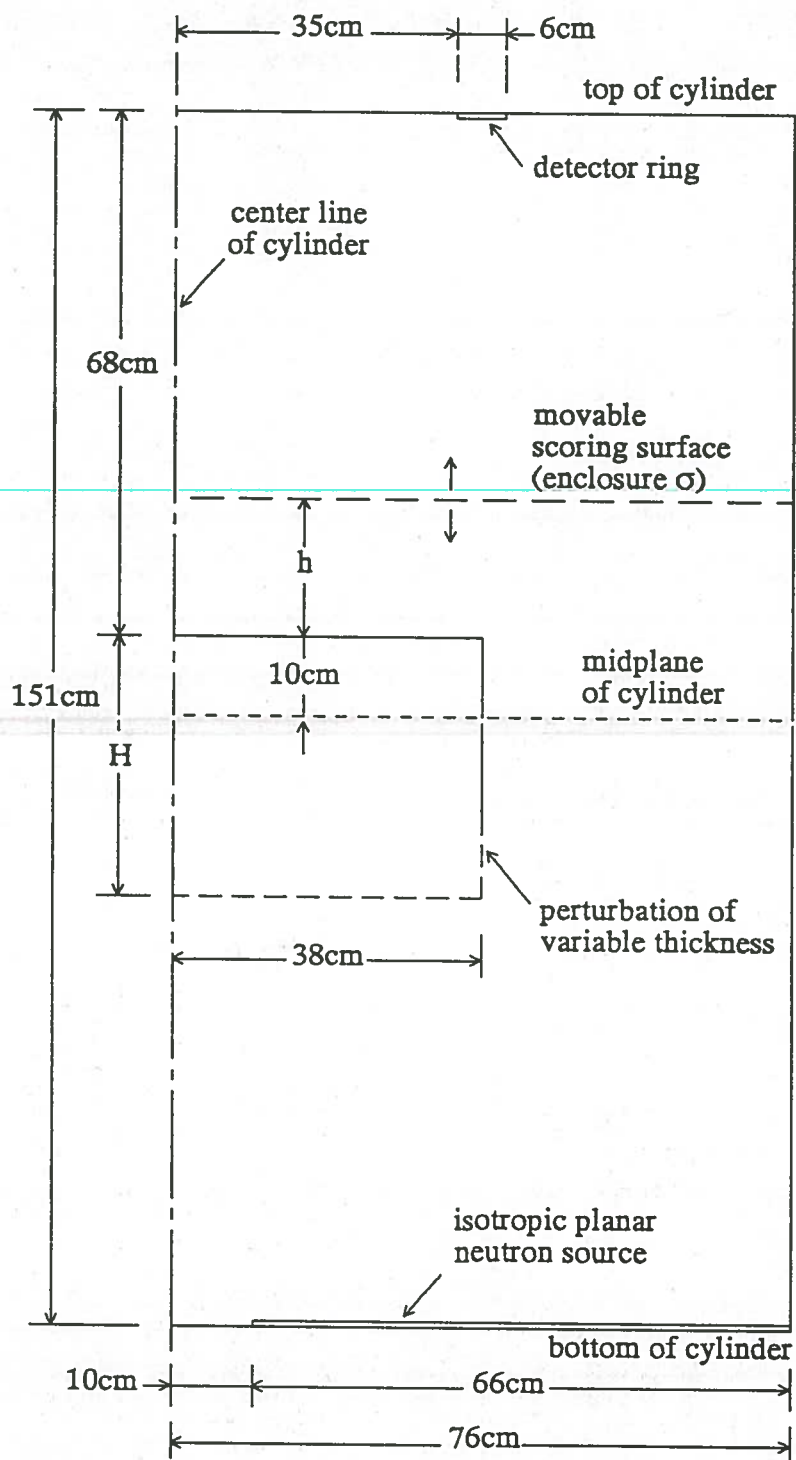


**Figure 4.1.** Cross sectional view in the R-Z plane of the cylindrical shield showing the relative positions of source, detector, perturbation and scoring surface (the enclosure  $\sigma$ ). The thickness  $H$  of the perturbation and the distance  $h$  from top of perturbation to scoring surface are variable.

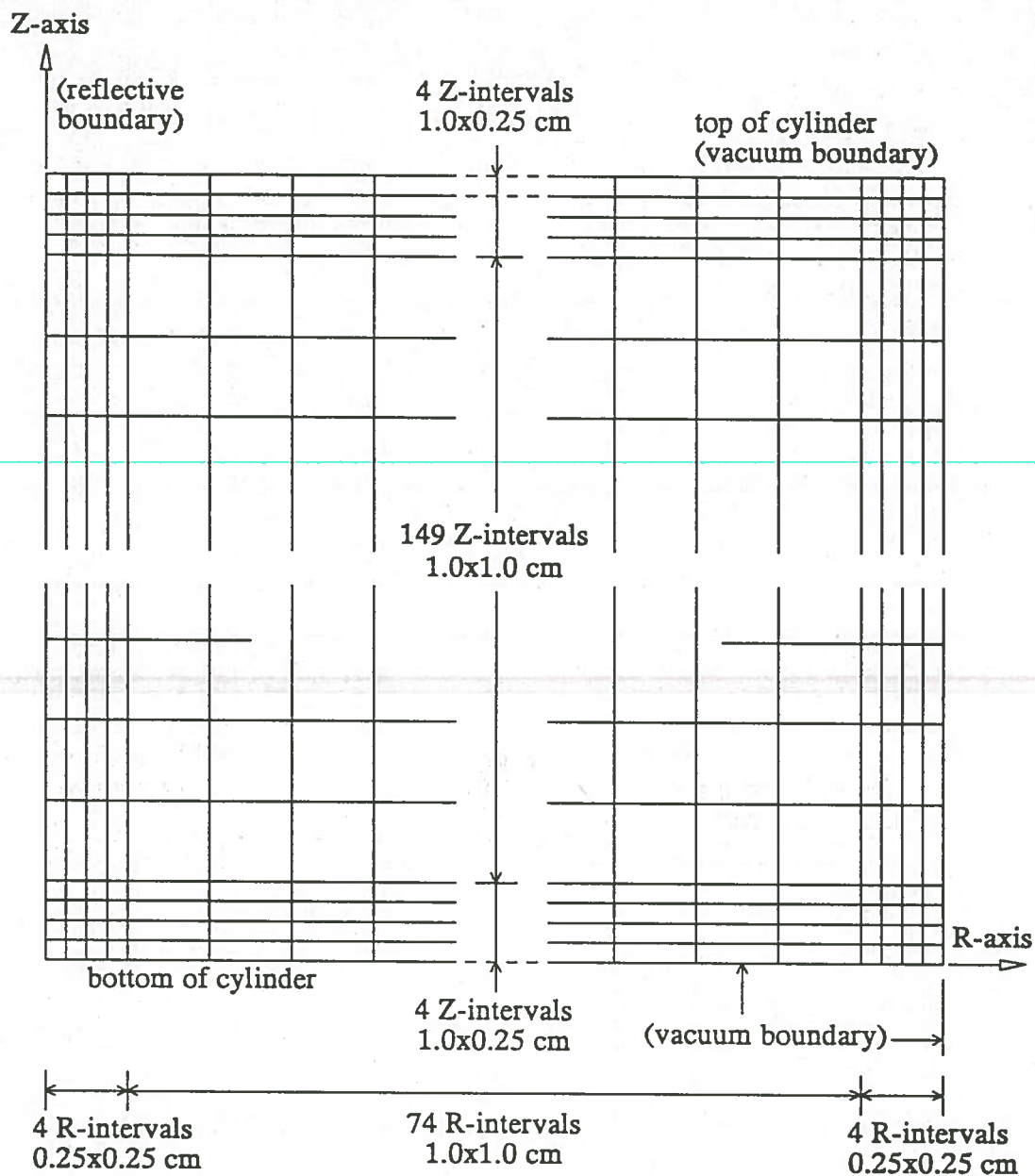


**Figure 4.2.** Discretization of the R-Z plane of the cylinder shield as used in DOT adjoint calculations and in Contribution Monte Carlo calculations. Each rectangle represents of an axisymmetric ring which is a cell in DOT geometry and in Monte Carlo geometry. Field properties and contribution response cross sections are uniform in each cell.

now a *cell*. In CMC geometry, a cell is the annular volume which corresponds to a mesh point in DOT geometry. This discretization results 82 radial intervals and 157 axial intervals resulting a field of 12,874 different cells in both DOT and CMC calculations. Each cell is identified by its *index coordinates* (IR, IZ) where IR is the radial index coordinate and IZ is the axial index coordinate. The first radial index is IR=1 at the center line of the cylinder and the last index is IR=82 at the vacuum boundary of the cylinder. Likewise the first axial index is IZ=1 at the bottom and the last index is IZ=157 at the top of the cylinder. In DOT calculations, vacuum boundary condition is imposed at top, bottom and right boundaries and a reflective boundary condition is imposed on the left boundary which is the center line of the cylinder (Fig. 4.2). The planar source is modeled as a thin disc source at the bottom, IZ=1, extending from the IR=14 to IR=82 inclusive. The detector, placed at the top of the cylinder at IZ=157, extends from the IR=39 to IR=44 inclusive. The perturbation comprises 41 cells in the radial direction from the centerline of the cylinder and a variable number of cells in the axial direction starting from the IZ=86 and counting downward.

#### 4.2 Adjoint and forward DOT calculations

The geometry described in the previous section is used in DOT code to perform adjoint and forward calculations. All calculations are performed in  $S_8$  discrete ordinates and using 10 energy group cross sections collapsed from SAILOR's 47 groups using the COMAND<sup>41</sup> utility code. Energy boundaries and the neutronic cross sections of the 10 groups library are shown in Appendix A. A neutron distributed source  $Q$  is selected arbitrarily to be isotropic and to emit 83% of the neutrons from the first group and 17% from the second group; The adjoint source  $Q^*$  is a 10-group boundary source in  $S_8$  and with magnitude unity in all directions and all energies. The adjoint calculations produce the  $P_3$  moments  $\tilde{\psi}_{lm}^*$  in each cell of the concrete cylinder and store them permanently on

a disk. Four sets of forward calculations are performed to produce the net flow of neutrons through the top of the cylinder. One set of calculations is performed with a plain concrete cylinder and the two other sets are performed with perturbations of two different materials: water and steel. Several runs are made with each type of perturbation material. Each run is for one perturbation thickness represented by the parameter  $H$  shown in Figure 4.1. The ratio of net flow from one run with the perturbation in place to the net flow in a plain concrete cylinder represents the normalized boundary crossing response at the detector. This response is the benchmark data for CMC calculations. DOT adjoint calculations required 8 minutes CPU time on LSU computing facilities, an IBM 3090 main frame system.

### 4.3 Monte Carlo calculations

The CMC method developed in the previous chapters was encoded as a computer program CMC-1 described in Appendix B to solve for the boundary crossing response at the top of a cylinder due to an isotropic boundary source of  $1 \text{ neutron/cm}^2\text{s}$ ; the detector and the geometry of the shield are described in §4.1 supra. The input data needed for the program are the moments  $\tilde{\psi}_{lm}^*$  output from DOT adjoint calculations, the multigroup cross sections, the geometry of the cylinder in the cell field described in §4.2 and shown in Figure 4.2, and the quadrature coefficients and weights needed to evaluate scaling integrals  $\mathfrak{J}$  of Eq(3.11), the thickness  $H$  of the perturbation and the distance  $h$  between the top of the perturbation and the scoring surface  $\sigma$ . Two perturbation materials were used, water and steel. All input data were maintained fixed in all runs except thickness  $H$  which was changed for each run. In one set of calculations  $H$  was maintained fixed and distance  $h$  was changed. The program generates one output point data: the response  $\bar{\mathfrak{R}}$  of the detector and its fractional standard deviation.

## CHAPTER FIVE

### SAMPLE PROBLEM AND ANALYSIS OF THE CMC METHOD

#### 5.1 The $\eta$ -test criterion

It was indicated earlier (§1.4) that the present study is limited to cases with positive emission ratio. For some problems  $\eta$  has a mixed spectrum. The proposed CMC method is not applicable to these problems. For other problems,  $\eta$  has either extended or confined spectra. In the latter case a user may desire to work with analog CMC. In the former case it is required to work with nonanalog CMC, the only option currently available. The  $\eta$ -test criterion is proposed here as a *diagnosis* tool to probe the suitability of the current capabilities of CMC method. It provides information about function  $\eta$  so that users can decide whether this CMC method is suitable for the problem in hand or eventually for the analog CMC. If for a given problem the magnitude of  $\eta$  satisfies condition (1.22) at all points in phase space  $(\mathbf{r}, \tau)$ , the validity of the method is assumed for that perturbation, for the specified shield and type of radiation. If  $\eta$ -test *fails*, the CMC method should be disqualified for the proposed problem, for the time being. A failure of the  $\eta$ -test should be understood in the sense that  $\eta$  is negative over sizable intervals in energy and directions and in relatively large number of cells.

Although the  $\eta$ -test is conceptually a simple criterion, its practical implementation is overwhelmingly tedious in most realistic problems. It will be required to run over 128,000 tests for the sample problem. (Whenever a reference to the sample problem is given, it should be understood the problem of chapter 4.) Instead, a few randomly selected points may be tested by  $\eta$ -test criterion, enough to obtain information

sufficient to the judgement of the user to make a reasonably reliable decision. It is not known at this time how this criterion will work in the case of large positive  $\eta$ .

Emission ratio  $\eta$  is defined by the ratio of  $\bar{\theta}_s$  to  $\bar{\theta}_t$ , which both of them are functions of positional parameters represented by  $r$ , an energy parameter represented by group index  $g$  and directional parameters represented by  $\hat{\Omega}$ . The direction  $\hat{\Omega}$  is usually defined by a directional cosine  $\mu$  and an azimuthal angle  $\varphi$  relative to a polar coordinate system at the collision site as shown in Figure 3.1. All the three parameters  $g$ ,  $\varphi$  and  $\mu$  are incident parameters which make the  $\eta$ -test relatively quick; fix parameter  $g$  and generate a table of data  $\eta(\mu, \varphi)$  then test these values against condition (1.22). The test may be made visually by generating a surface plot of  $\eta(\mu, \varphi)$  which enables quick visual test against condition (1.22). If the test fails, the current CMC method should be determined not suitable for for the problem in hand. A failure of the test should be confirmed by the presence of a pattern characterized by sizable intervals in  $\mu$  and in  $\varphi$  over which  $\eta < 0$ . It should be expected that, when  $\eta$  is close to its lower bound, the test may fail at a few individual scattered points. These are assumed to be aberrations peculiar to the truncation of spherical harmonics series representing coefficients  $\bar{\theta}_s$  and  $\bar{\theta}_t$ . This does not necessarily indicate the failure of the test. If this happens, the prescription of Section 2.2 supra may be followed. On the other hand, when the  $\eta$ -test succeeds at a few positions  $r$ , it is advisable to increase the number of tests as manageably as possible to guarantee a reliable decision on the suitability of the method.

## 5.2 Application of $\eta$ -test to the sample problem

The visual approach is adopted for the analysis of vacuum, steel and water perturbation materials used in the sample problem. Figure 5.1 is a surface plot for a cavity perturbation in concrete and for scattering from group 1 to group 2. It indicates

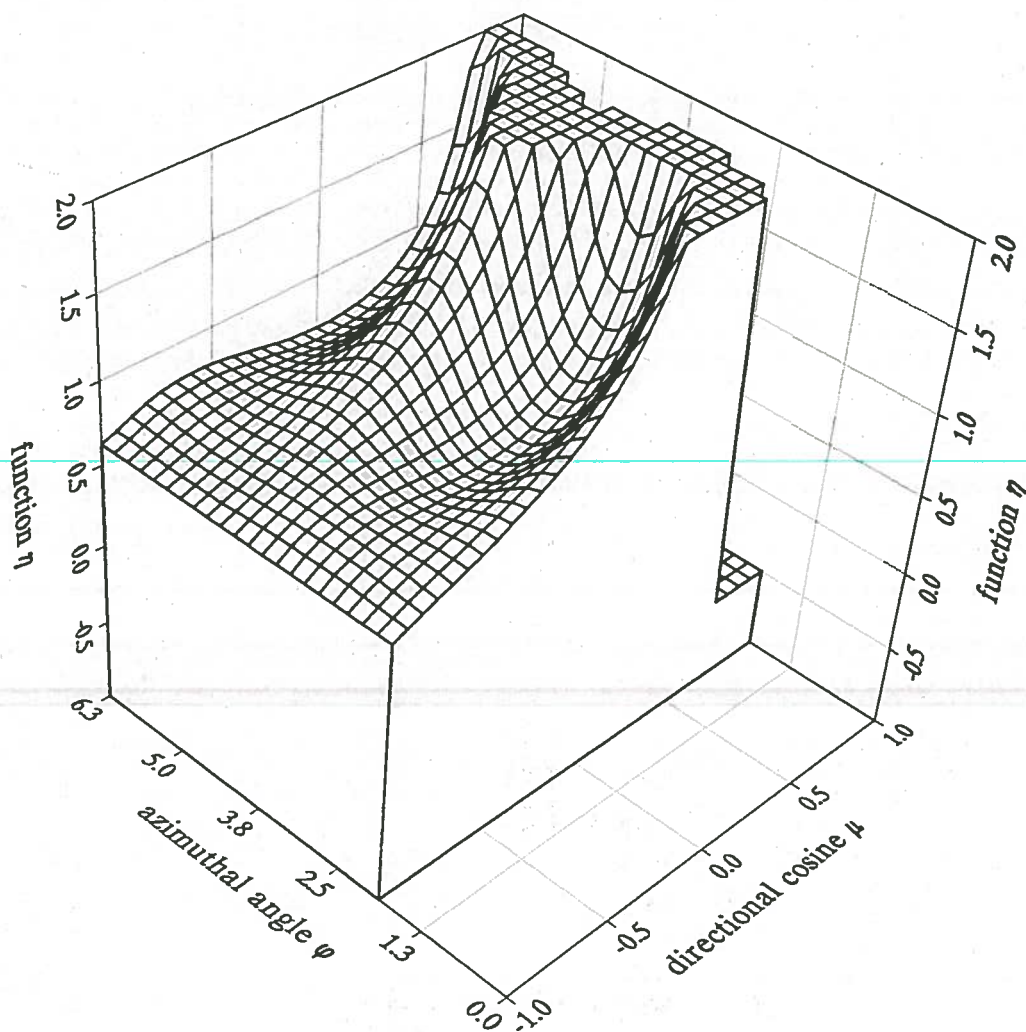


**Figure 5.1.** A surface plot for the emission ratio of vacuum perturbation in concrete shield and a neutron source, for scattering from group 1 to group 2 at cell index (40,53). Angular cosine  $\mu$  and azimuthal angle  $\phi$  (in radians) are incident parameters.



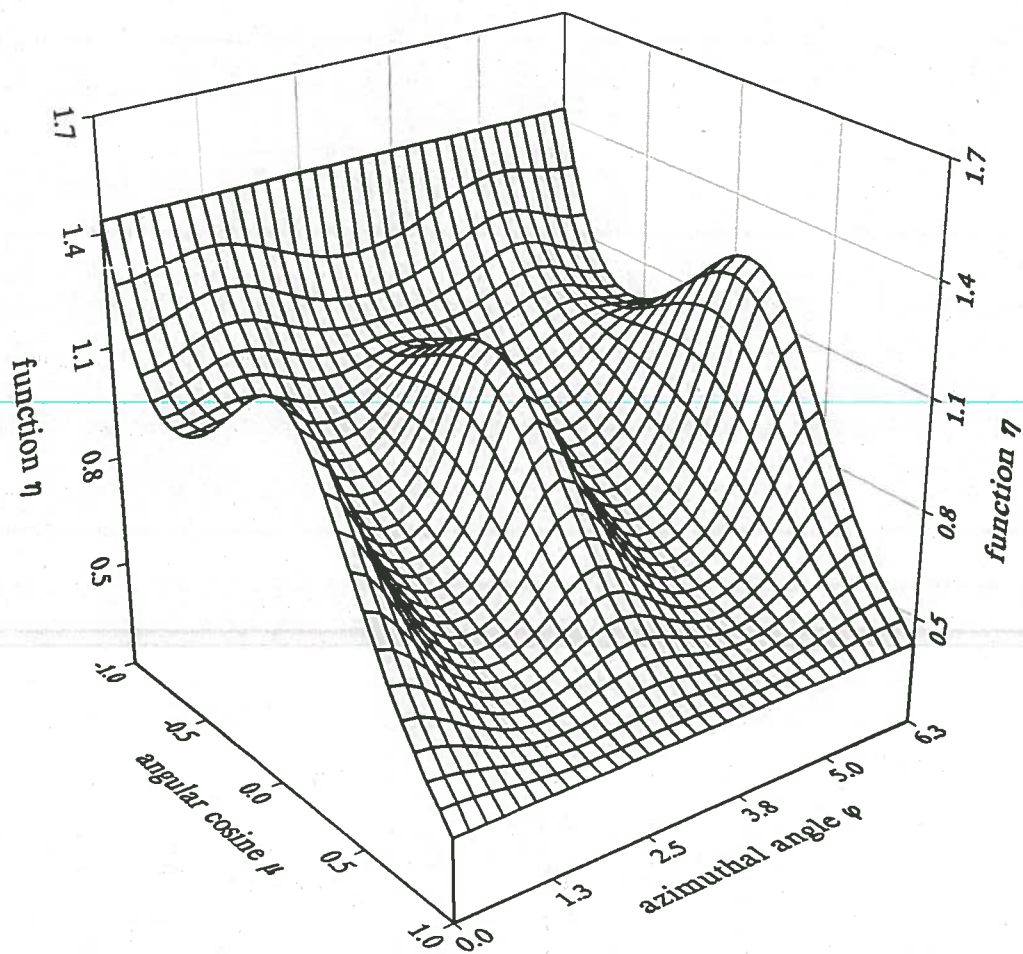
conclusively that the present CMC method is not suitable to this problem. A large interval of directions over which  $\eta < 0$  is distinctly visible. The plateaux at  $\eta = 2$  and  $\eta = -0.5$  are actually chopped peaks of larger magnitudes than 2 or 0.5, up to about 500.

Figure 5.2 is a surface plot for scattering in group 1 and Figure 5.3 is for scattering from group 7 to group 8 in steel perturbations and at the same position in the shield. A quick look at these plots reveals that steel is a regenerative perturbation in concrete medium with a neutron source and for the specified detector. On both figures large intervals of directions over which  $\eta > 1$  are visible. This may not necessarily be the case if gamma rays source is used instead, or if the shield is other than concrete. Nonanalog CMC is the only option at this time to work the sample problem with steel perturbations.

Figure 5.4 is a surface plot for scattering in group 1 in water perturbation, and Figure 5.5 is for scattering from group 1 to group 2 in same perturbation at the same location in the shield. In both cases  $\eta$ -test succeeds with  $\eta$  strictly on the interval  $(0, 1)$ . Several other tests were performed at various locations in the shield and all of them succeeded in the same way. Aberration points were not observed in any of these tests. The conclusion from these observations is that water is a nonregenerative perturbation for the sample problem. Either analog or nonanalog CMC method can be used for the sample problem with this perturbation material. This conclusion may not necessarily be true if a gamma rays source is used instead of a neutron source in the sample problem.

### 5.3 Analysis of source pdfs in CMC

There are two features which make CMC an efficient method: the small number of source particles to be sampled and the effectiveness of its pdfs. For the first part, the



**Figure 5.2.** A surface plot for the emission ratio of steel perturbation in concrete shield and a neutron source, for scattering in group 1 at cell index (40,53). Angular cosine  $\mu$  and azimuthal angle  $\phi$  (in radians) are incident parameters.

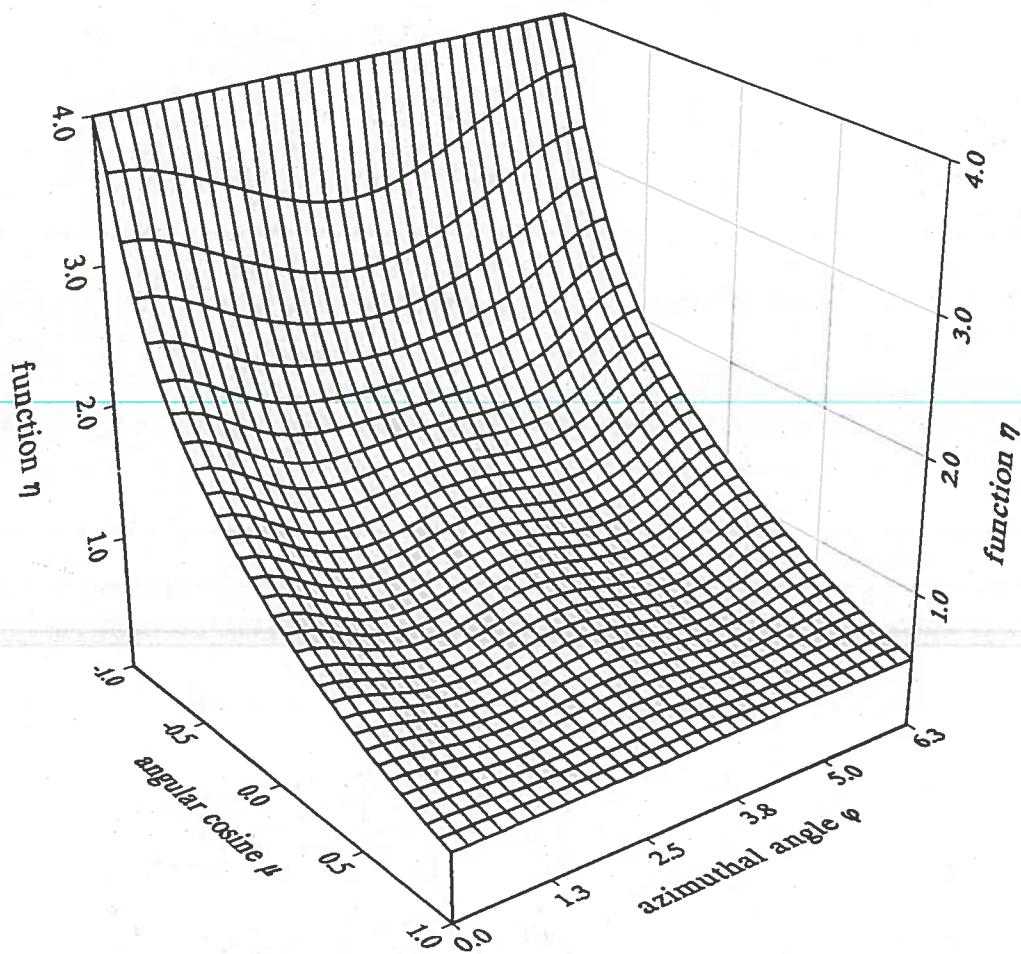


**Figure 5.3.** A surface plot for the emission ratio of steel perturbation in concrete shield and a neutron source, for scattering from group 7 to group 8 at cell index (40,53). Angular cosine  $\mu$  and azimuthal angle  $\phi$  (in radians) are incident parameters.

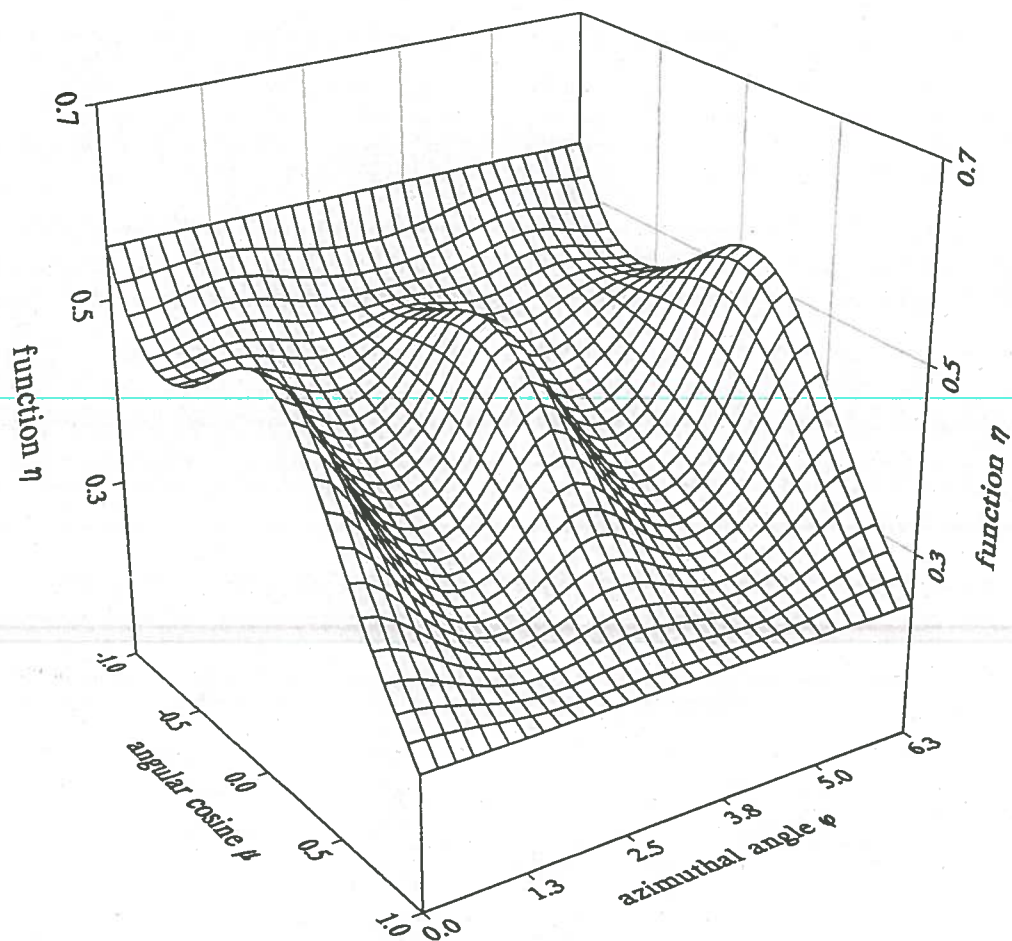


**Figure 5.4.** A surface plot for the emission ratio of water perturbation in concrete shield and a neutron source, for scattering in group 1 at cell index (40,53). Angular cosine  $\mu$  and azimuthal angle  $\phi$  (in radians) are incident parameters.

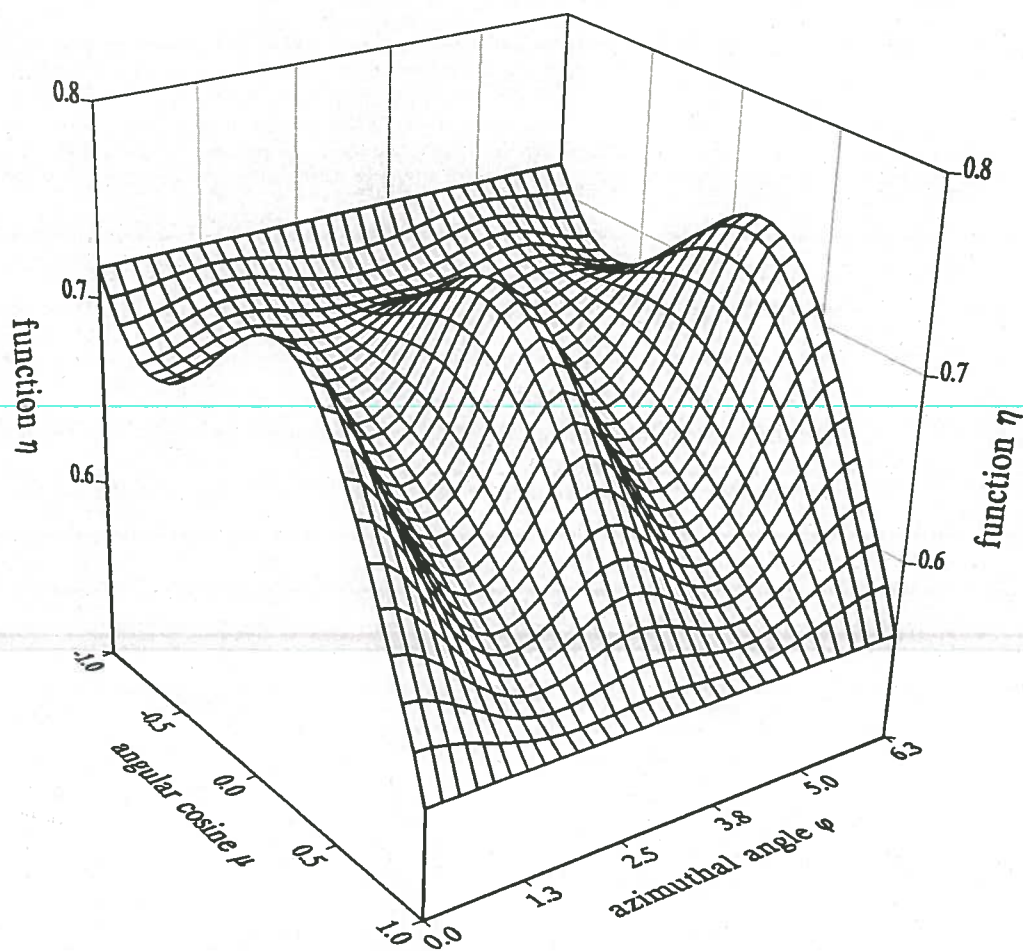


**Figure 5.5.** A surface plot for the emission ratio of water perturbation in concrete shield and a neutron source, for scattering from group 1 to group 2 at cell index (40,53). Angular cosine  $\mu$  and azimuthal angle  $\phi$  (in radians) are incident parameters.

reduction of source particles should not be offset by coarsening the fractional standard deviation. This undesirable effect is well taken care of by the fact that a response particle progresses in the unperturbed region without depleting its response value and without escaping from the system. In contribution Monte Carlo this is the natural random walk of response particles, inherent to contribution response theory; in conventional Monte Carlo methods, the closest to this random walk is introduced by way of biasing against leakage at the expense of reducing the weight of the particle. With such a random walk of contribution Monte Carlo, it should be expected that one to two thousands source particles should produce nearly exact answers. On the other hand, reducing the number of source particles that way should not be made at the expense of excessive computational labor, that is, a source emitted particle or an emergent particle from a collision should be directed naturally to follow the Shortest POSSible RAndom Walk (sporaw) to reach the detector. Analysis of CMC pdfs is expected to provide information about how effective these probability functions are to make a response particle to follow a sporaw.

A response particle is first selected from source  $c$ -pdf expressed by Eq(3.22). Figure 5.6 shows that the most probable emission location of source response particles is cell 45, almost right underneath the detector favoring a first flight sporaw. By contrast, the same isotropic neutron source emits its particles at the most probable cell just 1cm from the free surface boundary. A first flight path from this position is almost a sporaw to a detector 150cm away, but emission from this position increases the probability for the neutron to escape from the system to almost a certainty.

The selection of the energy of emitted neutrons is performed from a discrete pdf with 87% probability emission from group 1 and 17% probability from group 2 (§4.2 supra) from any source cells. Response particles pdf of Eq(3.24) changes these figures to 99.5% and 0.5% respectively and virtually for all source cells, on the average. The most probable emission is still from group 1, but emission from the second group is practically

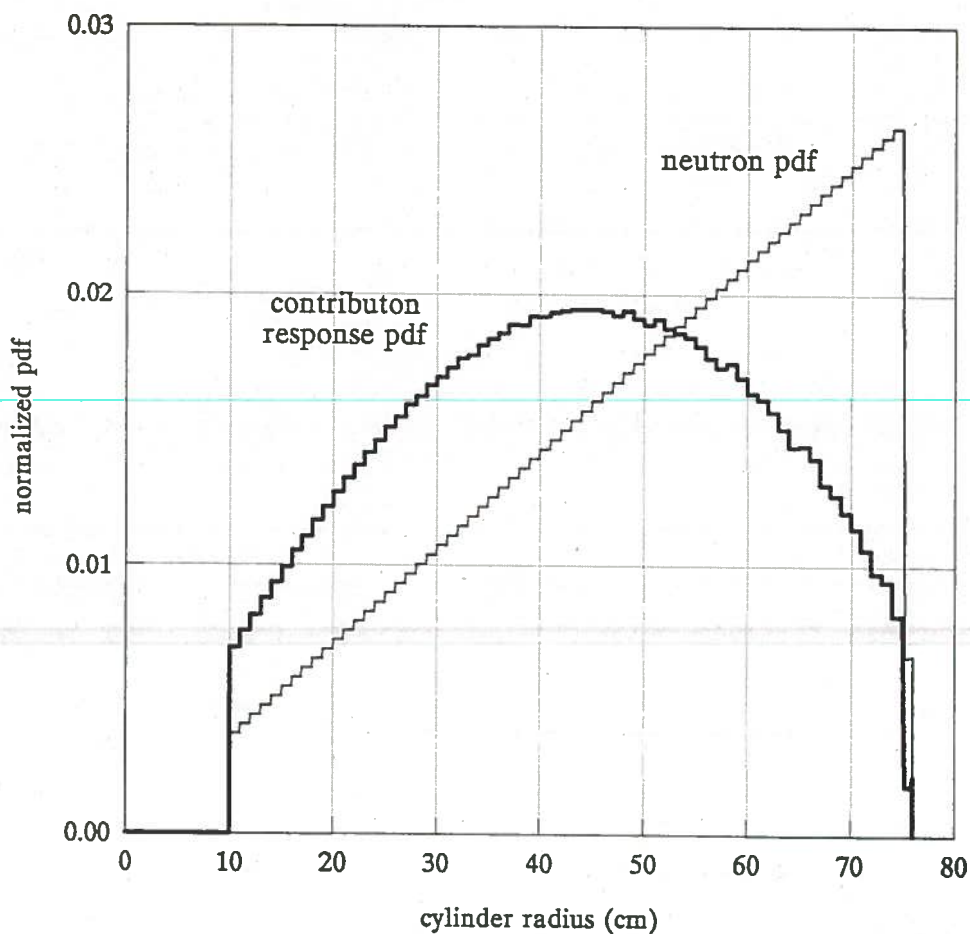


**Figure 5.6.** Graphs for contribution response pdf (thick line) for the selection of emission cell, due to a plane isotropic neutron source and a ring detector of sample problem. The neutron source pdf is shown in thin line. The source is at the bottom of the concrete cylinder with inner radius of 10cm and outer radius of 76cm.

eliminated. Favoring emission from group 1 is functionally equivalent to favoring a sporaw path since essentially only high energy source neutrons can reach a detector through 150cm concrete shield.

The polar direction characterized by angular cosine  $\mu$  of an emitted neutron is selected from an isotropic pdf as shown in Figure 5.7 (thin solid line at 0.5). A response particle is emitted in a direction selected from a source  $\mu$ -pdf expressed by Eq(3.26) and shown in Figure 5.7 as two thick lines for groups 1 and 2. While neutron directions are equally probable on the interval  $\mu \in (-1, 1)$ , response particles are solely selected in upward directions toward the detector, about half of them are within an angle of  $40^\circ$  from the Z-direction, and with a most probable direction parallel to Z-axis. Clearly, these directions favor a sporaw.

The complete direction of an emitted source particle is determined by selecting the azimuthal angle  $\varphi$ . Neutron azimuthal directions are selected from the isotropic pdf  $1/2\pi$  shown as a dotted line circle (curve d) in polar coordinates system of Figure 5.8. The pole of this coordinates system coincides with the emission site and the axis along  $180^\circ$ - $0^\circ$  coincides with a radius of the cylinder in the outward direction. Three other curves, solid lines a, b and c, representing response particles  $\varphi$ -pdfs of Eq(3.29) are also shown on the same graph. They correspond to directions  $\mu=0.1, 0.5$  and  $0.9$  respectively. These curves exhibit most probable  $\varphi$ -directions leading toward the inside of the cylinder. The significance of this tilting of directions is that the current emission site is at a radial position farther than the outer radius of the detector thus favoring a sporaw path toward the detector.



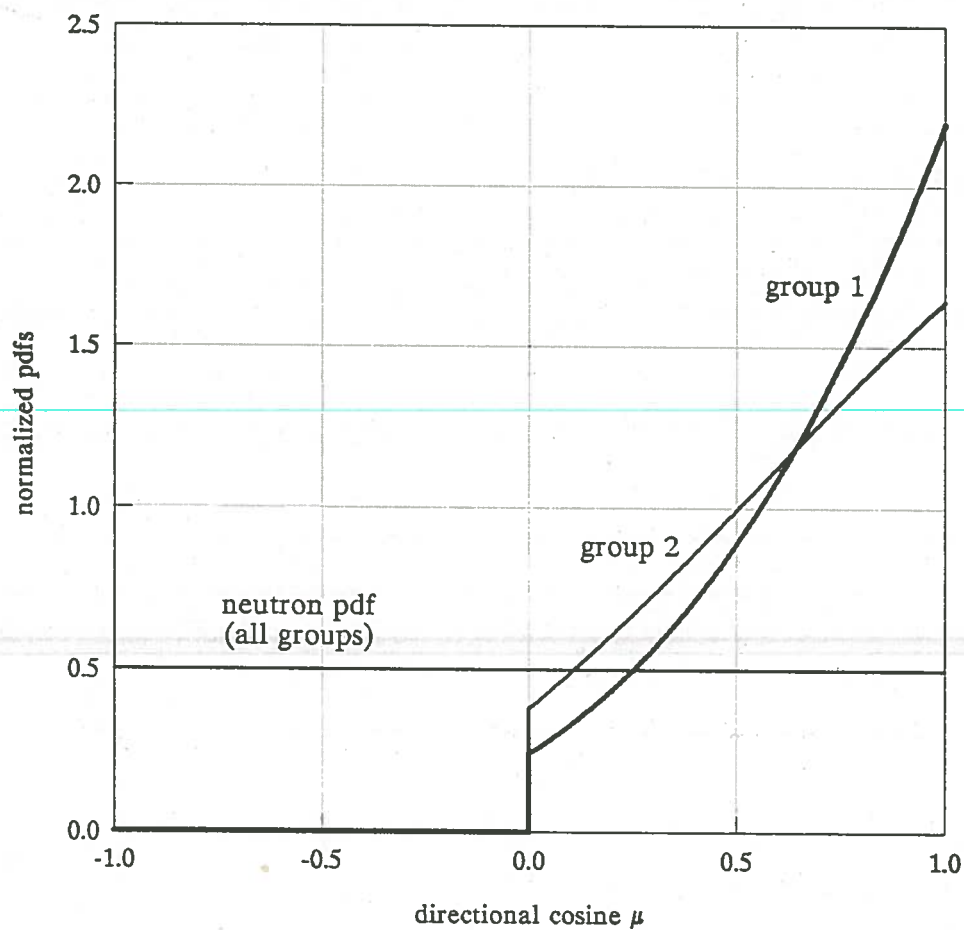


**Figure 5.7.** Graphs for contribution response pdfs (thick lines) for the selection of the angular cosine  $\mu$ , of an emitted response particle from source radial cell 41 and for groups 1 and 2. The isotropic pdf for selection of source neutron is shown at 0.5 (thin line). The neutron source and the ring detector are those of the sample problem in concrete shield.

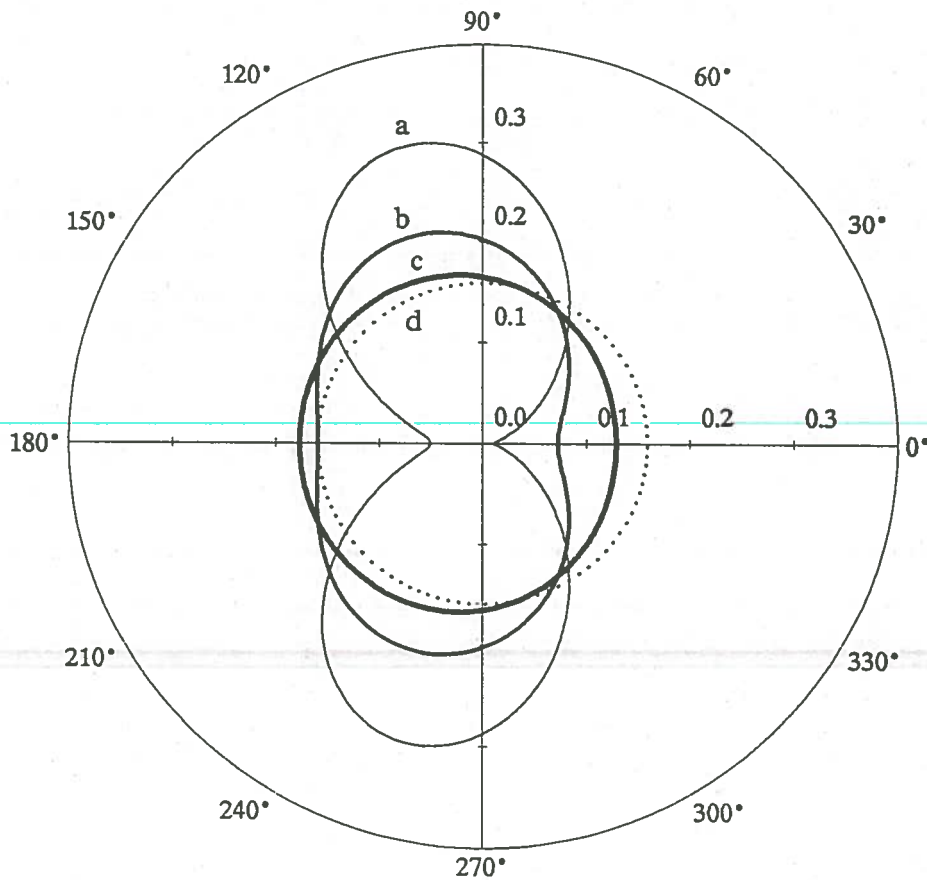
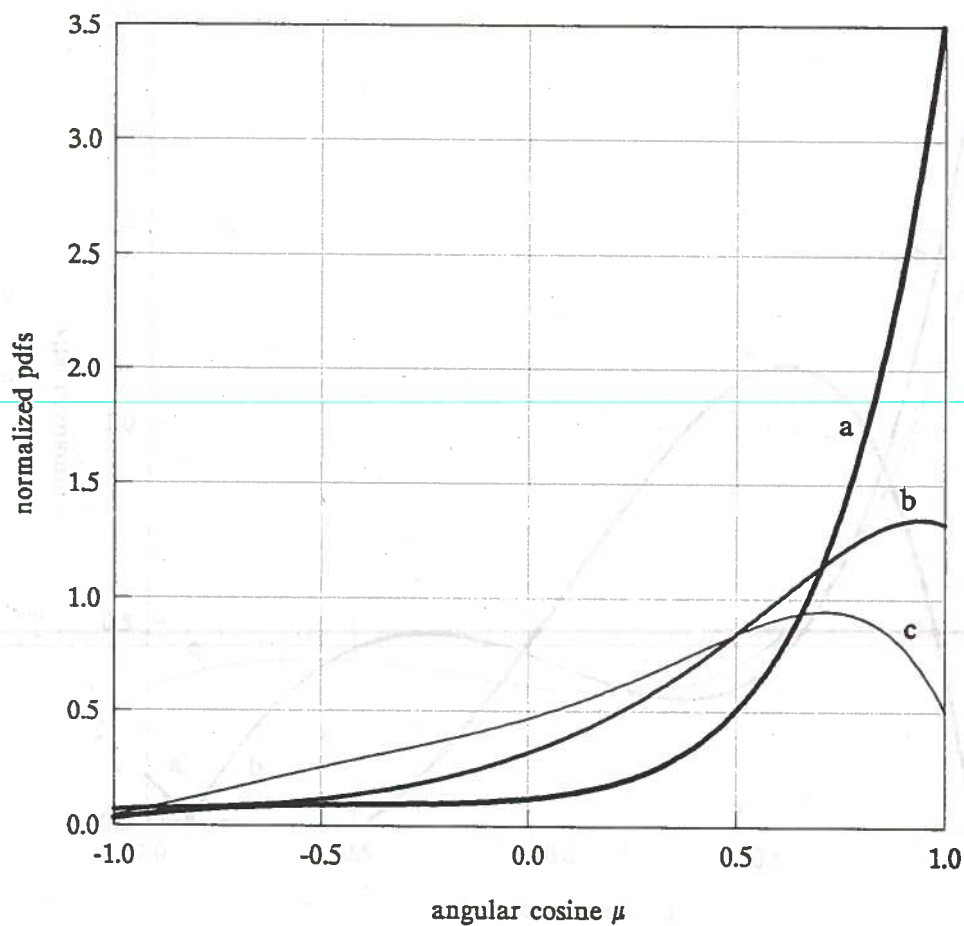


**Figure 5.8.** Polar graphs for response particles pdfs (solid lines curves) for the selection of the azimuthal angle  $\varphi$  of an emitted response particle from response source radial cell 41 and for group 1. Curves a, b, c correspond to emergent directional cosines  $\mu=0.1, 0.5, 0.9$  respectively. Dotted line circle (curve d) is the isotropic pdf for neutron emission.

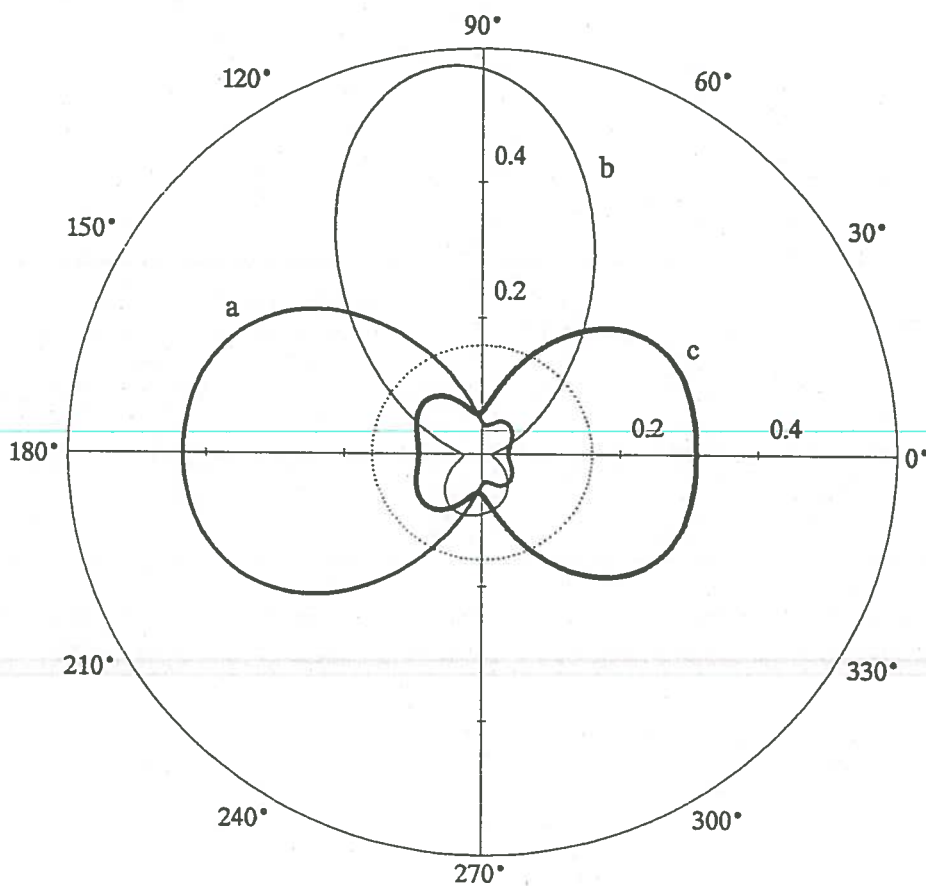


Figure 5.9 illustrates scattering  $\mu$ -pdfs of Eq(3.41) at cell (40,53) for scattering in group 1, incident azimuthal direction  $\varphi'=\pi/4$  and for different incident directions  $\mu'$ . It is apparent that for this scattering most of the emergent directions  $\mu$  are narrowly clustered in the vertical direction upward favoring a sporaw path. Figure 5.10 illustrates the emergent azimuthal directions  $\varphi$ -pdf of Eq(3.46) within same cell (40,53), same energy group and for incident directions  $\mu'=0.3$  and  $\varphi'=\pi, \pi/2$  and 0 (curves a, b and c respectively). The emergent azimuthal angles  $\varphi$  are clustered within an angle of about  $60^\circ$  centered around the incident direction in all three cases. The case of down scatter from group 7 to group 9 at the same location is also examined at the same cell location. Figure 5.11 represents the  $\mu$ -pdf of Eq(3.41) for incident directions  $\varphi'=\pi/4$  and  $\mu'=0.1, 0.5$  and  $0.9$  (curves a, b and c respectively). The effect of scaling factor  $\gamma$  (see §3.2) on curves *a* and *b* is distinctly visible. In the case of curve *b*, a small interval  $\delta$  is removed from the domain  $\mu=[-1, 1]$  while in the case of curve *a* almost 25% of the interval is removed. Despite the most probable direction is peaked upward in all cases, backscatter is about 40% of all possible  $\mu$ -directions for most incident  $\mu'$ -directions. This is expected in this energy range ( $\sim 5\text{eV}$  for group 7) where relatively small energy loss per collision gets the particle to almost thermal equilibrium with the medium where scattering is close to isotropic. The wavy shape of the curves is most likely attributable to low order  $P_3$  expansion cross sections and adjoint functions  $\tilde{\psi}^*$ .

One case of scattering near the free surface boundary is also examined. Figure 5.12 illustrates scattering from group 6 to group 6 at cell (78,100), which is 1cm from the free surface boundary and slightly above the midplane of the cylinder. Two sets of curves are shown for the same incident azimuthal direction  $\varphi'=\pi$ . Dotted line curves correspond to  $\mu'<0$  and solid line curves correspond to  $\mu'>0$  where  $|\mu'|=0.9, 0.5$  and  $0.1$  (curves a, b and c respectively).



**Figure 5.9.** Graphs for response particles scattering pdfs in concrete shield, for the selection of emergent directional cosines  $\mu$ , from group 1 to group 1 scattering, at cell index (40,53) and for incident azimuthal angle  $\varphi' = \pi/4$  and incident directional cosines  $\mu' = 0.9, 0.5, 0.1$  corresponding to curves a, b and c respectively. Neutron source and ring detector are those of sample problem.



**Figure 5.11.** Graphs for response particles scattering pdfs in concrete shield, for the selection of emergent directional cosines  $\mu$ , for scattering from group 7 to group 9, at cell index (40,53), for incident azimuthal angle  $\varphi'=\pi/4$  and for incident directional cosines  $\mu'=0.9, 0.5, 0.1$  corresponding to curves a, b and c respectively. Neutron source and ring detector are those of sample problem.

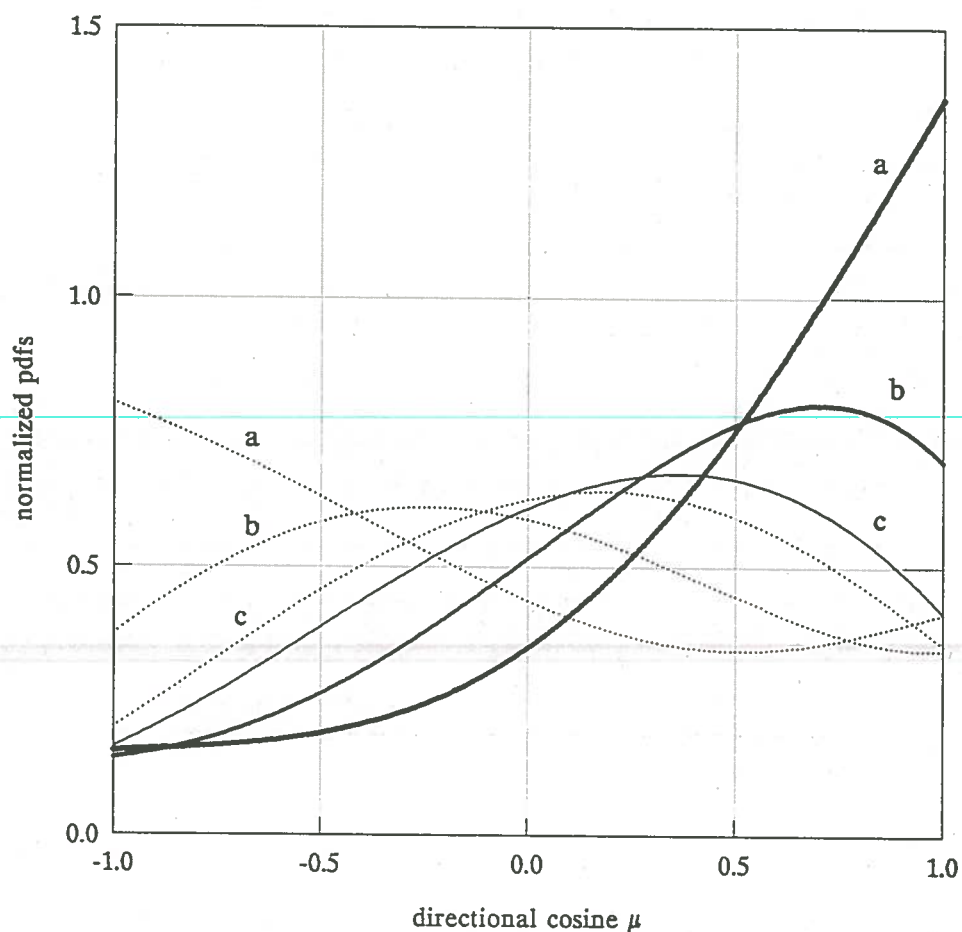


**Figure 5.12.** Graphs for response particles scattering pdfs in concrete shield, for the selection of emergent directional cosines  $\mu$ , for scattering in group 6, at cell index (78,100), for incident azimuthal direction  $\varphi'=\pi$  and for two sets of incident directional cosines:  $\mu'<0$  (dotted lines) and  $\mu'>0$  (solid lines) of values  $|\mu'|=0.9, 0.5, 0.1$  corresponding to curves a, b and c respectively.

At the top of the cylinder the particles are most expected to be in their lowest energy group. Figure 5.13 shows the graphs of  $\mu$ -pdfs at cell (40,148) 1cm just underneath the detector and for group 10 scattering. If the particle is moving downward,  $\mu' < 0$ , the emergent direction is selected with almost equal probability from dotted line curves a, b, and c and in any direction on the interval  $\mu = [-1, 1]$ . If the particle is moving upward,  $\mu' > 0$ , the most probable emergent direction is tilted upward but the probability that the particle scatters back downward away from the detector is still sizable (solid line curves a, b and c).

---



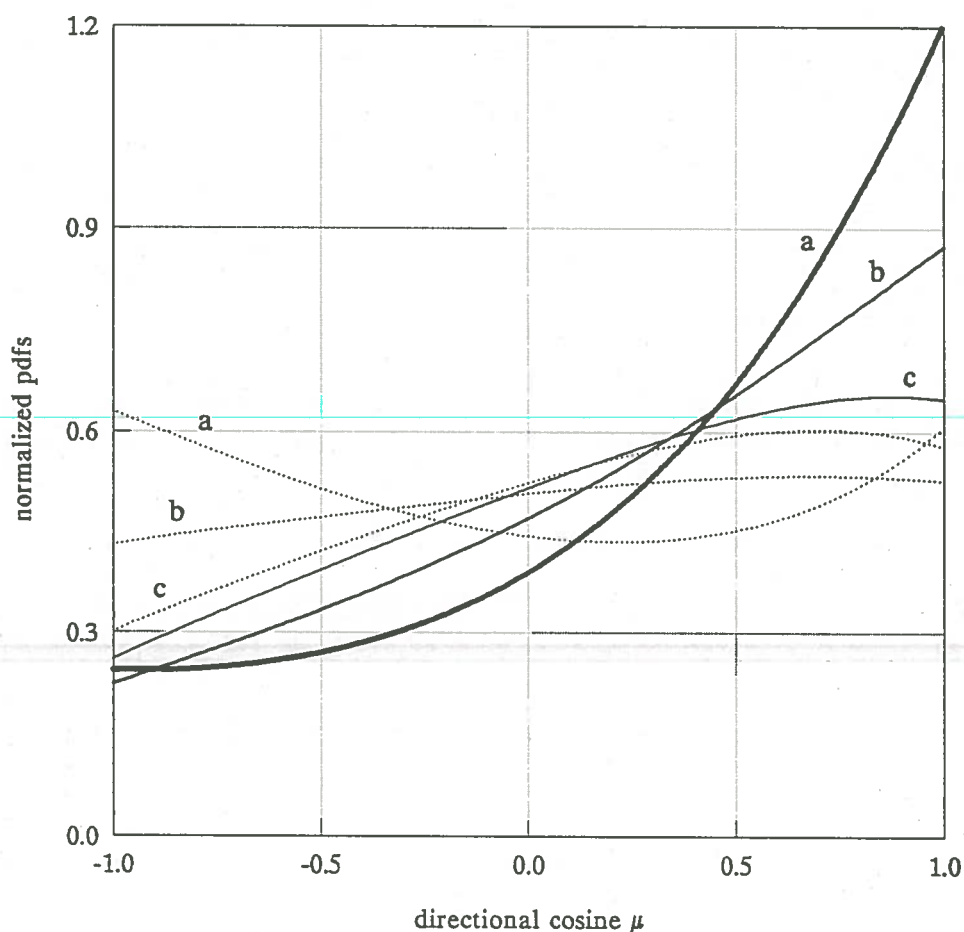


**Figure 5.13.** Graphs for response particles scattering pdfs in concrete shield, for the selection of emergent directional cosines  $\mu$ , for scattering in group 10, at cell index (40,148), for incident azimuthal direction  $\varphi'=\pi$  and for two sets of incident directional cosines:  $\mu'<0$  (dotted lines) and  $\mu'>0$  (solid lines) of values  $|\mu'|=0.9, 0.5, 0.1$  corresponding to curves a, b and c respectively.

## CHAPTER SIX

### RESULTS FROM CMC CALCULATIONS AND RECOMMENDATIONS

#### 6.1 Results

The results from  $\eta$ -tests discussed in the previous chapter were used to select the appropriate calculation mode with CMC-1 code. A steel perturbation in a concrete shield causes the emission ratio to span an extended positive spectrum with upper limit substantially larger than 1. Nonanalog CMC is the only option available at this time for this type of perturbation and the algorithm developed in §2.2 supra is used. An  $\eta$ -test for a water perturbation in a concrete shield indicates that the spectrum of  $\eta$  is confined. Both analog and nonanalog CMC options can be and are used in this case. The spectrum of the emission ratio is mixed in the vacuum perturbation. Various algorithms were tested for this spectrum but none were successful. No further considerations will be given to this problem in this Section.

The results from calculations with a steel perturbation are shown in table 6.1 and results with a water perturbation are shown in table 6.2. The nonanalog calculations in both tables are shown in columns with the header "biased". A numerical verification of Williams-Engle's theorem was carried out with a water perturbation, an axisymmetric water cylinder, 76cm in diameter and 20cm high, coaxial with the concrete cylinder. The results are shown in table 6.3 with scoring surface placed at different positions from the perturbation. All CMC results are obtained from sampling only 1000 source particles!

The responses calculated with the CMC-1 program are compared with those obtained from DOT calculations for same perturbations. While these results are explicitly

**TABLE 6.1.** Comparison of detector response calculated with nonanalog CMC and with DOT code for steel perturbation of variable thickness H. The ratio of Monte Carlo to DOT calculations is also shown. The fractional standard deviations and the CPU time are for Monte Carlo calculations only. Scoring surface is h=10cm above perturbation.

H (cm)	DOT (ru)	$\bar{R}$ CMC (ru)		$\bar{R}$ CMC/DOT		fsd (%)		CPU minutes	
		biased	analog	biased	analog	biased	analog	biased	analog
2	0.906	0.908	-	1.00	-	0.8	-	4.6	-
4	0.860	0.871	-	1.01	-	1.1	-	4.8	-
8	0.806	0.838	-	1.04	-	1.6	-	5.2	-
12	0.776	0.817	-	1.05	-	1.7	-	5.4	-
16	0.795	0.793	-	1.00	-	1.9	-	5.2	-
20	0.750	0.786	-	1.05	-	1.9	-	4.8	-
25	0.748	0.802	-	1.07	-	1.9	-	5.1	-
30	0.751	0.786	-	1.05	-	1.9	-	4.9	-
40	0.765	0.788	-	1.03	-	2.1	-	5.2	-

**TABLE 6.2.** Comparison of detector response calculated with nonanalog and with analog CMC and with DOT code for water perturbation of variable thickness H. The ratio of Monte Carlo to DOT calculations is also shown. The fractional standard deviations and the CPU time are for Monte Carlo calculations only. Scoring surface is h=10cm above perturbation.

H (cm)	DOT (ru)	$\bar{R}$ CMC (ru)		$\bar{R}$ CMC/DOT		fsd (%)		CPU minutes	
		biased	analog	biased	analog	biased	analog	biased	analog
2	0.892	0.864	0.878	0.97	0.98	0.5	1.2	5.7	4.7
4	0.819	0.822	0.806	1.00	0.98	0.6	1.6	5.1	4.6
8	0.717	0.721	0.714	1.00	1.00	0.8	2.0	5.0	4.2
12	0.648	0.657	0.640	1.01	0.99	1.0	2.4	5.4	3.8
16	0.594	0.612	0.602	1.03	1.01	1.1	2.6	5.7	3.7
20	0.552	0.558	0.551	1.01	1.00	1.2	2.9	5.6	3.7
25	0.510	0.527	0.529	1.03	1.04	1.3	3.0	5.9	3.4
30	0.475	0.494	0.494	1.04	1.04	1.4	3.2	5.3	3.2
40	0.423	0.435	0.431	1.03	1.02	1.6	3.6	6.0	2.5

**TABLE 6.3** Numerical verification of Williams-Engle's theorem where the scoring surface (enclosure) is placed  $h$  centimeters from the top of the perturbation. The detector response is calculated with analog CMC for 20cm water perturbation.

$h$ (cm)	$\bar{R}$ CMC (ru)	$\bar{R}$ CMC/DOT	fsd (%)	CPU minutes
10	0.551	1.00	2.9	3.7
20	0.553	1.00	2.5	7.1
30	0.568	1.03	2.4	8.4
40	0.578	1.05	2.4	10.1
50	0.567	1.03	2.4	13.9

shown in the captioned tables, it was found that the ratio of the response from CMC-1 to the response from DOT is more instructive a comparison. In all of the cases reported in these tables, this ratio is just 1.0 within a few percent due to statistical fluctuations inherent to Monte Carlo calculations; DOT calculations are also associated with some round off and other errors characteristics to finite difference. It is difficult in this case to tell which set of these calculations is more precise. The compatibility of DOT calculations with CMC calculations associated with relative errors (fsd) of the order of 3% or less is indicative of the effectiveness of the proposed contribution CMC method. Judging by its performance in the sample problem, the CMC method is promising and should be attempted on more complicated geometries with various types and shapes of perturbation materials and shield materials. The user may choose either the analog or the nonanalog option for perturbations with confined  $\eta$ -spectra; the method is currently limited to the nonanalog option for perturbations with extended  $\eta$ -spectra.

Additional observations of merits can be made from tables 6.1 and 6.2. The thin perturbation disk and the thick perturbation cylinder deserve some attentions. The thin disk is 2 cm thick in a shield of 151 cm high, that is, the perturbation is barely 1.3% of

the thickness of the host medium, the concrete cylinder in this case. It is not recorded anywhere in the Monte Carlo literature that one thousand source particles ever did anything with this special case of problems, with a detector less than 8% of the cross-sectional area of the top of the concrete shield, and impressively when analog Monte Carlo is considered, save the unresolved complications associated with deep penetration problems. By way of comparison, MORSE-CG code was run analog for the same sample problem. One million source particles were sampled, none of them made it to the detector!

The other extreme is the 40 cm high perturbation. This height is nearly the third of the height of the host medium. The diameter of this perturbation is 76 cm, that's half the diameter of the concrete shield, and its volume slightly exceeds 1/4 of the volume of the host medium. It hardly can be characterised as a perturbation, yet Williams' perturbation equation (1.18) demonstrated high performance in this extreme case as well.

The foregoing observations cannot be ignored or be taken lightly regardless of what future modifications or improvements will be introduced to the proposed CMC method. The success of this numerical experiment, however small or big it may be, demonstrates a great flexibility of Williams-Engle's contribution response theory, and in particular, Williams' perturbation model, to address various types of intractable shielding problems.

## 6.2 Recommendations for further investigations

The results from CMC calculations are very encouraging to justify further investigations to establish a strong confidence in the performance of the method in different shielding situations and in other engineering design problems in radiation transport. Most pressing are the following items.

(a) Emission ratios of many perturbations are extended spectra. Steel is an illustration in the sample problem. The analog Monte Carlo did not work for the steel perturbation of the sample problem. The decision to terminate or to survive the particle at a collision was made by one criterion: test a random number  $\xi$  against  $\eta < 1$ . This is the conventional Russian Roulette. Naturally, when  $\eta > 1$  the particle always survives. It is the contention of the author that, in an analog CMC with extended  $\eta$ -spectra, more than one criterion must be satisfied concurrently before a decision on the fate of the particle can be made. This requires to devise a conceptually different game than the Russian Roulette. Such an  $\eta$ -game could be a probabilistic generalization of the currently used Roulette. The suggestion is to devote the efforts toward developing this  $\eta$ -game so that it can be used for both confined and extended spectra as demanded by the random walk.

Another question associated with the extended  $\eta$ -spectrum and pertaining to the nonanalog CMC is the update of the response value of the particle by regeneration. The underlying hypothesis and its implementation performed successfully in the sample problem with steel perturbation. It is required to demonstrate the validity of this model in the general case of any perturbation material of extended spectra, and to develop its theoretical justification. This will require further exploration of the understanding of the regeneration problem and its sensitivity to the order of truncation of the expansion of spherical harmonics series. Extensive analysis and experimental verifications may be needed before ascertaining the validity of the model in the general case.

(b) With respect to the definition of the function  $\bar{\theta}_a$  expressed by Eq(1.20), it was suggested<sup>42</sup> to modify the representation of this coefficient by ascribing to it the physical significance of a net difference between the absorption and the emission coefficients. A negative value of  $\bar{\theta}_a(r, \tau)$  means that more response is being emitted than being absorbed

at phase space point  $(r, \tau)$ , leading to response amplification. It follows that the total cross section of Eq(1.19) will have to be redefined as  $\bar{\theta}_t = \bar{\theta}_a + \bar{\theta}_s - \bar{\theta}_e$  where  $\bar{\theta}_s$  is defined by Eq(1.10) in the approximate geometry,  $\bar{\theta}_e$  a response emission coefficient and  $\bar{\theta}_a$  a response absorption coefficient unrelated to Eq(1.20), and all of the three coefficients are positive. By this representation for the total cross section, the interpretation of the emission coefficient is that when  $\eta < 1$  absorption dominates and when  $\eta > 1$ , or when  $\eta < 0$ , emission dominates. However, neither of the coefficients  $\bar{\theta}_a$  or  $\bar{\theta}_e$  is known. It is worth the efforts to find explicit expressions for these coefficients, or at least to develop an algorithm to implement them in contribution Monte Carlo calculations. The expectations of the author of this amplification model is that it will result a more effective treatment to the update of the response value of a particle emerging from a collision than the regeneration model.

(c) The proposed algorithms appear to work very well for perturbations with confined and extended emission ratios spectra. The method is still not operational in mixed spectra. This problem is very important in shielding design since in many cases the shield itself contains cavities and various types of pipings which have mixed spectra. It is expressly demanded that this problem be investigated to develop the appropriate algorithm for the CMC method with mixed  $\eta$ -spectra.

(d) The  $\eta$ -test criterion worked well with two perturbation materials of the sample problem, water and steel. It is not clear how it will work with other materials. A preliminary investigation to find a substitute to this criterion suggests that a criterion utilizing the moderating ratio  $\xi \Sigma_s / \Sigma_a$  of the perturbation material could be used to decide whether a perturbation is regenerative or nonregenerative. Further investigation to validate the usefulness of this criterion may be worth the efforts.

(e) It was observed during the testing of the CMC-1 program that, when scoring was performed at the detector without a scoring surface, most particles spend too much time moving around the detector before they interact with it and terminate there. The CPU times shown in table 6.3 are quantitative illustrations to this phenomenon. This observation can be explained in light of the analysis of the scattering pdfs in the immediate neighborhood of the detector. It was indicated in §5.4 supra that a particle just underneath the detector has almost equal probability to emerge from a collision with any direction  $\mu \in (-1, 1)$  for all incident directions  $\mu' \in (-1, 1)$  (Fig. 5.13). It will be worthwhile to investigate the possibility of devising a technique which could remedy this inconvenience without sacrificing the effectiveness of the method.



## REFERENCES

1. Williams M.L., "*Generalized Contribution Response Theory*", Nuc. Sc. Eng., **108**, 355-383 (1991)
2. Kahn H., "*Application of Monte Carlo*", USAEC Report AECU-3259, April 1954
3. Coveyou R.R., Cain V.R., Yost K.J., "*Adjoint and Importance in Monte Carlo Applications*", Nuc. Sci., Eng., **27**, 219-234 (1967)
4. Goertzel H., Kalos M.H., "*Monte Carlo Methods in Transport Problems*", Progress in Nuclear Energy, Physics and Mathematics, Series I, Vol. 2, p. 315, Pergamon press (1958)
5. Burgart C.E., Stevens P.N., "*A general Method of Importance Sampling The Angle of Scattering in Monte Carlo Calculations*", Nuc. Sci. Eng., **42**, 306-323, (1970)
6. Bendall D.E., McCracken A.K., "*McBend-A Prototype Code Utilizing Both Removal-Diffusion and Monte Carlo Methods*", Proc. Int. Conf. on the Physics of Problems of Reactor Shielding, September 26-29, 1967
7. Cain V.R., Franz K.D., "*Comparison of Monte Carlo Calculations With Measurements of Fast Neutron Dose Transmitted from a Beam Source Through a SNAP-2 LiH Shield*", USAEC Report ORNL-TM-2423, December 1968
8. Schmit F.A.R., Straker E.A., Cain V.R., "*Applications of Adjoint Flux Calculations to Monte Carlo Biasing*", USAEC Report ORNL-TM-2454, December 1968
9. Tang J.S., Hoffman T.J., Stevens P.N., "*Monte Carlo Shielding Calculations Using Event-Value Path-Length Biasing*", Nuc. Sci. Eng., **62**, 617-626 (1977)
10. Tang J.S., Hoffman T.J., "*Monte Carlo Shielding Analysis Using Automated Biasing Procedure*", Nuc. Sci. Eng., **99**, 329-342 (1988)
11. Rhodes W.A., Childs R.L., "*An Update Version of DOT-4 One- and Two-Dimensional Neutron/Photon Transport Code*", ORNL-5851, July 1982

12. Cramer S.N., "*Discrete Angle Biasing in Monte Carlo Radiation Transport*", Nuc. Sci. Eng., **98**, 279-298 (1988)
13. Vergnaud T et. al., "*Biasing Technique in the TRIPOLI-2 System*", Proc. Int. Mtg. Advances in Nuclear Engineering Computational Methods, Knoxville, Tennessee, April 9-11 (1985); Also available as RSIC Computer Code Package CCC-272, ORNL (1980)
14. Kalos M.H., "*Importance Sampling in Monte Carlo Shielding Calculations*", Nuc. Sci. Eng., **16**, 227-234 (1963)
15. MORSE-CG, "*General Purpose Monte Carlo Multigroup Neutron and Gamma Ray Transport Code With Combinatorial Geometry*", ORNL/RSIC-CCC-203
16. Carter L.L., McCormick N.J., "*Coupled Sampling with Monte Carlo Method in Neutron Transport Calculations*", Nuc. Sci. Eng., **39**, 296 (1970)
17. Hoogenboom J.E., "*A Practicle Monte Carlo Adjoint Technique for Fixed Source and Eigenfunction Neutron Transport Problem*", Nuc. Sci. Eng., **78**, 357-373 (1981)
18. Williams M.L., Engle W.W. Jr., "*The Concept of Spatial Channel Theory Applied to Reactor Shielding Analysis*", Nuc. Sci. Eng., **62**, 92-104 (1977)
19. Dubi A., Gerstl S.A.W., Dudziak D.J., "*Monte Carlo Aspect of Contributions*", Nuc. Sci. Eng., **68**, 19-30 (1978)
20. Lewins J., "*Importance: The Adjoint Function*", Pergamon Press, Oxford (1978)
21. Abu-Shumays I.K., Selva R.J., Shure K., "*Refinements for Spatial Channel Computations*", Proc. Comp. Mtd. in Nuc. Eng., Williamsburg, Virginia, April 23-25, 1979, Am. Nuc. Sct. (1979)
22. Bell G.I., Glasstone S., "*Nuclear Reactor Theory*", Krieger, Huntington, New York (1979)
23. Henry A.F., "*Nuclear Reactor Analysis*", The MIT Press, (1975)
24. Case K.M., De Hoffmann F., Placzek G., "*Introduction to the Theory of Neutron Diffusion*", Los Alamos Scientific Laboratory, 1953.

25. Davison B., "*Neutron Transport Theory*", Oxford University Press, 1958
26. Case K.M., Zweifel P.F., "*Existence and Uniqueness Theorems for the Neutron Transport Equation*", J. Math. Phys., 4, 1376-1385 (1963)
27. Olhoeft J.E., "*The Doppler Effect for Non-Uniform temperatures*", University of Michigan Ph.D. thesis (1962)
28. Case K.M., Zweifel P.F., "*Linear Transport Theory*", Addison-Wesley, (1967)
29. Lewis E.E., Miller W.F., "*Computational Methods of Neutron Transport*", Wiley (1984)

---

30. Williams M.M.R., "*Mathematical Methods in Particle Transport Theory*", Wiley (1971)
31. Duderstadt J.J., Martin W.R., "*Transport Theory*", Wiley (1979)
32. Arfken G., "*Mathematical Methods for Physicists*", 2nd ed., Academic press (1970)

---

33. Carter L.L., Cashwell E.D., Taylor W.M., "*Monte Carlo Sampling with Continuously Varying Cross Sections Along Flight Paths*", Nuc. Sci. Eng., 48, 403-411 (1972)
34. Carter L.L., Cashwell E.D., "*Particle Transport Simulation with the Monte Carlo Method*", USERDA, TID-26607, (1975)
35. "*SAILOR, Coupled, Self-shielded, 47 Neutron, 20 Gamma-Ray, P<sub>3</sub>, Cross Section Library for Light Water Reactors*", RSIC Data Library Collection, ORNL, DLC-76 (1983)
36. Coveyou R.R., "*A Monte Carlo Technique for Selecting Neutron Scattering Angles from Anisotropic Distributions*", Nuc. Sci. Eng., 21, 260 (1965)
37. Irving D.C., Freestone R.M. Jr., Kam F.B.K., "*O5R, A General Purpose Monte Carlo Transport Code*", ORNL-3622 (1965)
38. Cramer S.N. et al, "*ESP, A General Monte Carlo Reactor Analysis Code*", TM-3164, ORNL (1972)
39. Davis P., Rabinowitz P., "*Methods of Numerical Integration*", 2nd Ed., Academic Press (1984).

40. Brockmann H., "*Treatment of Anisotropic Scattering in Numerical Neutron Transport Theory*", Nuc. Sci. Eng., 77, 377-414 (1981)
41. "*AMPX-II, Modular Code System for Generating Coupled Multigroup Neutron-Gamma-ray Cross Section Libraries From Data in ENDF Format*", RSIC Computer Code Collection, PSR-63, ORNL (1978)
42. Williams M.L., Louisiana State University, personal communication, 1992, unpublished work.

## VITAE

The author was born in Beirut (Lebanon) in 1943, and was naturalized U.S. citizen in 1992. After his secondary education in Lebanon, he earned his degree *Ingenieur en Energie Atomique* (IEA) from the *Institut Technique Professionnel* (France). In Lebanon, he taught physics and mathematics in secondary schools and he authored two physics textbooks. In 1976, he fled Lebanon as a result of the civil war and resided in Grenoble (France) where he worked at the Nuclear Studies Center. In 1977, he moved to the U.S. and earned his Masters degree in Nuclear Engineering from the University of Cincinnati. He was nominated and served as a reviewer to the journal *Nuclear Technology/Fusion* until 1982. He participated in various research and development projects sponsored by NASA and by the EPRI at the University of Cincinnati and at the University of Missouri-Rolla. He taught mathematics and nuclear engineering science and technology at Saint Louis University, the University of Cincinnati and with the American Technical Institute. In 1989, he joined the Interdepartmental Program in Engineering at Louisiana State University.

*Vivere Vixie Victum*